UNCLASSIFIED

Copy 274
RM E56G13a

3545

NACA RM E56G13a

NACA CASE FILE COPY

RESEARCH MEMORANDUM

DEVELOPMENT OF FLOW DISTORTIONS IN A FULL-SCALE NACELLE INLET AT MACH NUMBERS 0.63 AND 1.6 TO 2.0

By Thomas G. Piercy and Bruce G. Chiccine

Lewis Flight Propulsion Laboratory
Cleveland, Ohio

Classification Changed
To UNCLASSIFIED
By Authority of R. A. #11 Date 12-1-59

CLASSIFIED DOCUMENT

This material contains information affecting the National Defense of the United States within the meaning of the espionage laws, Title 18, U.S.C., Secs. 793 and 794, the transmission or revelation of which in any manner to an unauthorized person is prohibited by law.

NATIONAL ADVISORY COMMITTEE
FOR AERONAUTICS

WASHINGTON

October 22, 1956

UNCLASSIFIED

UNCLASSIFIED

NATIONAL ADVISORY COMMITTEE FOR AERONAUTICS

RESEARCH MEMORANDUM

DEVELOPMENT OF FLOW DISTORTIONS IN A FULL-SCALE NACELLE INLET AT MACH NUMBERS 0.63 AND 1.6 TO 2.0

By Thomas G. Piercy and Bruce G. Chiccine

SUMMARY

A typical full-scale nose inlet was tested at Mach numbers 0.63 and 1.6 to 2.0 to determine the nature of flow-distortion development throughout the subsonic diffuser. Inlet design variables studied included 14° and 17° internal cowl-lip angles, conical compression surfaces with and without boundary-layer removal slots, and cone tip translation. Angles of attack to -8° were investigated at Mach 2.0.

At zero angle of attack, changes in cowl angle or compression-surface bleed had little effect on the distortion at the diffuser exit, this value being fairly well predicted by calculations of the turbulent-flow profile. Operation at other angles of attack, however, consistently produced diffuser-exit distortions larger than the calculated values.

Flow distortion in the subsonic diffuser generally decreased from the inlet throat to the diffuser exit. This decrease was particularly true when the distortion at the throat was larger than the calculated pipe-flow values. When distortions less than the pipe-flow values occurred near the inlet throat, the distortion either remained constant or increased with diffuser length until a value higher than that of pipe flow was attained. The distortion then decreased toward the pipe-flow value at the diffuser exit.

At zero angle of attack the use of centerbody bleed improved the over-all pressure recovery a maximum of only 2 percent over comparable no-bleed inlets. However, at other angles of attack, bleed generally reduced the pressure recovery. Maximum pressure recovery, as well as minimum flow distortion, was obtained when the compression-surface shocks were positioned ahead of the inlet lip.

UNCLASSIFIED

INTRODUCTION

The performance of a turbojet engine is adversely affected by nonuniform air distribution at the compressor (ref. 1). In order to determine the characteristics of a particular air-inlet-duct combination, rake instrumentation is usually placed at the diffuser exit in a location simulating the compressor inlet. Such instrumentation provides a basis for numerically defining the flow distortion and for obtaining velocity or total-pressure profiles. Frequently this instrumentation is supplemented with flow-survey rakes near the inlet throat. Relatively little, however, is known about the character of the flow between the inlet throat and the diffuser exit or the influence of the physical characteristics of the subsonic diffuser on this flow development.

The primary purpose of this investigation was to determine the development of flow distortion through the diffuser of a typical full-scale axisymmetric nose inlet. Variables studied include the effect of oblique-shock location relative to the cowl lip, the internal cowl-lip angle, and bleed from the centerbody near the inlet throat.

The development of the flow distortion in the diffuser duct was determined using total-pressure survey rakes located near the inlet throat, the diffuser exit, and at two intermediate positions. These distortion data constitute the major portion of this report. Performance charts of the over-all diffuser pressure recovery and mass flow are presented for completeness.

Tests were conducted at Mach numbers 0.63, 1.6, 1.8, and 2.0, with emphasis placed on Mach 2.0 operation, in the 8- by 6-foot supersonic wind tunnel at the NACA Lewis laboratory. At Mach 2.0, angles of attack to -8° were investigated.

SYMBOLS

A	area
C	pertaining to inlet cowl
H	radial distance between centerbody and cowl, in.
h	radial distance measured along H (see fig. 4)
M	Mach number
m	mass flow
P	total pressure

UNCLASSIFIED

ΔP	numerical difference between maximum and minimum total pressure at rake station
$\Delta P/P_{av}$	total-pressure distortion parameter
p	wall static pressure
r	radius, in.
S	pertaining to inlet centerbody
α	angle of attack, deg
θ_l	spike-tip-position parameter, deg (see table I)

Subscripts:

av	average
b	bleed centerbody
d	design
ds	double shock
l	local
s	smooth centerbody
0	free stream
1	rake station 7
2	rake station 19
3	rake station 41
4	rake station 58
5	mass-flow station 122.5
14	pertaining to cowl with 14° internal lip angle
17	pertaining to cowl with 17° internal lip angle

UNCLASSIFIED

APPARATUS AND PROCEDURE

Basic Inlets

The basic model tested was a full-scale axisymmetric nose inlet (fig. 1). External compression was provided by a translating 25° half-angle cone. Inlet variations included cowls with 14° or 17° internal lip angles and compression surfaces with or without bleed slots in the region of the inlet throat. Inlet configurations are designated by the combination of letters CS. For example, $C_{17}S_b$ represents the inlet with a 17° internal-lip-angle cowl and with provisions for bleed on the compression surface. Coordinates of the various cowls and centerbodies are presented in table I.

Sketches of the various inlet configurations are presented in figure 2. The double-shock inlet configuration was obtained by fitting a 15° cone onto the tip of the 25° cone (fig. 2(c)).

Details of the bleed slot are shown in figure 2(d). Bleed air was dumped into a plenum chamber and was then metered by four calibrated venturi tubes. Bleed air then passed through the centerbody interior (fig. 1) to struts and then out the base annulus. A remote-controlled bleed valve was used to vary the bleed-flow rate.

Area distributions in the subsonic diffuser are presented in figure 3 for the two cowls investigated for several values of the spike-tip-position parameter θ_l. The rate of initial area expansion was reduced considerably with the 14° cowl. Changes in the area distribution due to the bleed slots are neglected in these charts.

Instrumentation

Total-pressure rakes were located at diffuser stations 7, 19, 41, and 58, the last representing the compressor-inlet station. Orientation of the tubes composing these rakes is shown in figure 4. Each rake was composed of five spokes spaced at 45° intervals around the annulus. Flow in only half the duct was surveyed. In order to maintain flow symmetry, dummy rakes were installed in the other duct half. At stations 7 and 19, six total-pressure tubes were located in each spoke, whereas eight tubes per spoke were used at stations 41 and 58. Locations of tubes are given as percentages of the duct height H. All tubes were spaced to give approximately equal area weighting.

At station 7 the total-pressure rake was split, with half the tubes mounted to the cowl and the other half to the cone surface. This split was necessary to prevent binding of the rakes when the cone tip was translated. The rake was alined for values of $\theta_l = 42.6°$ for the

UNCLASSIFIED

single-shock inlets (or $\theta_l = 33.8^\circ$ for the double-shock inlet). Because of the change of diffuser area near the throat for the two cowls investigated, spacing of the tubes at station 7 was altered somewhat depending upon the cowl being used.

Static-pressure orifices were spaced on both vertical and horizontal centerlines of the diffuser on both cowl and centerbody back to diffuser station 60. In addition, orifices were located at the base of each of the total-pressure rakes.

The bleed plenum and venturi meters were instrumented with static-pressure orifices in order to determine the bleed-mass-flow rate. Inlet mass flow was determined from the static pressure measured at diffuser station 122.5 assuming a choked exit, the area of which was determined from a calibrated exit plug. At free-stream Mach number 0.63, for which the exit was not choked, mass flow was determined from pressure measurements at station 58.

Dynamic pressure pickups were located at diffuser stations 36.5 and 58 to aid in determining inlet stability limits.

Test Procedure

Pressure recovery, mass flow, and total-pressure distortion at each rake station were determined for each inlet configuration at Mach numbers 1.6, 1.8, and 2.0. At Mach number 2.0, angles of attack to -8° were investigated. (Negative angles of attack have been indicated inasmuch as the nose of the inlet was lowered by the action of the strut mechanism (fig. 1)).

Values of the spike-tip-position parameter θ_l were scheduled such that, for each Mach number, the oblique compression shock would fall on, ahead of, and inside the inlet lip. The value of θ_l for which the oblique shock falls on the lip is designated $\theta_{l,d}$, values of which are given in the following table:

Free-stream Mach number, M_0	Design spike-tip-position parameter, $\theta_{l,d}$, deg	
	25° Cone	15°-25° Cones
2.2	40.0	31.3
2.0	42.6	33.8
1.8	46.0	37.3
1.6	51.0	42.0

UNCLASSIFIED

Because of limits on spike-tip travel, values of θ_l were limited to the range of 38.9° to 51.6° for the single-shock inlets and from 31.0° to 39.4° for the double-shock inlet. Hence, at Mach number 1.6, the oblique compression shock could not be made to fall appreciably inside the inlet.

Limited data were also obtained for Mach number of 0.63 at zero angle of attack.

5007

DISCUSSION OF RESULTS

Inlet Performance Summary

Inlet-total-pressure recovery and total-pressure distortion at station 58 are plotted as functions of diffuser-mass-flow ratio in figures 5 to 10 for all configurations investigated. Values of the flow-discharge Mach number are also indicated.

It will be noted that the supercritical inlet-mass-flow ratio was less than 1 for the cases of oblique "shock-on-lip" ($\theta_l = \theta_{l,d}$). Part of this discrepancy was due to slight misalinement of the spike tip and because the inlet cowls were somewhat out-of-round. Occasionally at Mach numbers of 1.8 and 1.6 the inlet terminal shock could not be swallowed because of a limit of the diffuser-plug exit area. When this condition occurred, only subcritical operation of the inlets could be determined.

The minimum stable operating points were not always determined in these tests. Dynamic pressure pickups in conjunction with schlieren equipment were used to define the onset of instability, and the minimum stable points that were determined are indicated by tailed symbols.

For the inlets incorporating bleed, two performance curves are usually shown. These correspond to the maximum bleed rate and a throttled, or reduced, bleed rate. In a few instances, data were obtained for zero bleed flow. Maximum bleed varied from about 8 to 10 percent of the maximum capture mass flow at zero angle of attack.

For each configuration, total-pressure recovery increased and distortion at the diffuser exit decreased as θ_l was decreased. Typically, total-pressure recovery decreased and distortion increased with angle of attack.

The variation of distortion with mass flow was somewhat irregular for the bleed configurations. Frequently, minimum distortion was attained with some degree of supercritical operation. This is probably

UNCLASSIFIED

associated with the interaction of the inlet terminal shock and the boundary layer in the neighborhood of the bleed slot. Flow distortion generally decreased with decreased mass flows (subcritical inlet operation), but exceptions occurred for values of $\theta_l > \theta_{l,d}$, for which the distortion at first increased with subcritical operation because of the formation of a vortex sheet at the inlet face (ref. 1). With the no-bleed inlets, distortion increased rapidly during supercritical operation. This increase was less noticeable, however, with the inlets incorporating bleed.

Increasing the amount of bleed for the bleed configurations increased the peak pressure recovery and generally reduced the distortion. As in reference 2, however, bleed from the centerbody reduced the stable subcritical mass-flow range in comparison with the no-bleed inlets.

The oblique shocks of the $C_{14}S_{s,ds}$ inlet configuration coalesced outside the inlet lip at Mach 2.0. When this inlet was run subcritically, two vortex sheets entered the inlet. This partially accounts for the large distortions with subcritical inlet operation of this inlet (fig. 9(a)).

Subsonic performances of three of the inlet configurations are presented in figure 10. Total-pressure recovery varied considerably for the different configurations, although the distortion was essentially independent of configuration. The total-pressure recovery for the bleed configuration was as much as 0.05 lower than those obtained with the smooth-cone inlets.

Comparison of the performances of the various inlet configurations is made in figure 11 for peak-pressure-recovery inlet operation. Unless otherwise stated, maximum bleed was used with the bleed configurations. In figure 11(a) for Mach number 2.0, maximum pressure recovery at zero angle of attack was attained with the $C_{17}S_b$ inlet. The largest increase in pressure recovery due to bleed was about 2 percent, occurring at zero angle of attack for $\theta_l < \theta_{l,d}$. At other angles of attack, however, the bleed inlets generally attained lower recoveries than the comparable no-bleed inlets, one exception being the $C_{14}S_b$ inlet at $\theta_l = 40.0^\circ$. Pressure recovery at other angles of attack decreased most rapidly for the $C_{17}S_b$ inlet.

Although the effects were small, somewhat lower distortions were obtained with the bleed inlets for $\theta_l \leqslant \theta_{l,d}$ in comparison with the no-bleed inlets at zero angle of attack. At other angles of attack the effect of bleed was inconsistent and dependent upon the cowl-lip angle and value of θ_l. The largest effect of bleed noted was detrimental;

UNCLASSIFIED

that is, for the $C_{17}S_b$ inlet at $\theta_l = 40^\circ$, 22.5 percent flow distortion was measured at -8° angle of attack in comparison with 14.9 percent for the no-bleed $C_{17}S_s$ inlet.

The variation of peak pressure recovery and distortion at the diffuser exit with free-stream Mach number for the condition of shock-on-lip is summarized in figure 11(b). The maximum spread in peak pressure recovery was less than 2 percent for all configurations tested, whereas the spread in total-pressure distortion at the diffuser exit was usually about 3 percent. Data for shock-on-lip conditions at Mach numbers 1.8 and 1.6 for the double-shock inlet were not obtained. Extrapolation of the data of figure 9, however, to the higher values of θ_l indicates that pressure recoveries comparable to the single-shock inlets would be obtained. The distortions, however, would be considerably larger than those for the single-cone inlets.

5007

The flow distortion as well as peak pressure recovery decreased with increased free-stream Mach numbers. Slightly lower distortions were obtained with bleed throughout the Mach number range.

Distortion at Critical Inlet Operation

The remaining data of this report were obtained for critical inlet operation. This mode of operation occurs when the terminal shock is located at the inlet lip. In figures 5, 6, and 9 for the no-bleed configurations this point is well defined by the knee in the pressure-recovery - mass-flow curves. With the bleed configurations, however, critical operation was determined by schlieren observation inasmuch as the action of the bleed slot caused a slanting of the pressure-recovery - mass-flow curves when the terminal shock was in the neighborhood of the bleed slot. Estimated critical operation points are indicated in figures 5 to 10 by arrows.

A summary of the pressure recoveries and flow distortions at the diffuser exit for critical inlet operation is presented in figure 12. As was previously discussed for peak-pressure-recovery operation, the distortion spread at zero angle of attack was rather small for all configurations. At other angles of attack, the distortion increased as did the spread between different configurations.

Typical total-pressure contours at the various rake stations are presented in figures 13 to 15. These contours represent cross sections of the flow such as would be seen by an observer looking downstream through the diffuser. In order to avoid confusion, it should be remembered that negative angles of attack were tested. In the following discussion, description of portions of the duct refers to the duct as installed in the tunnel.

UNCLASSIFIED

Contours plotted are isobars, defined by $\left(\frac{P_l}{P_{av}} - 1\right)$ expressed in percent. For example, lines labeled 5 indicate an isobar 5 percent above the average pressure. Similarly, negative numbers indicate pressures lower than the average pressure. Wall-static-pressure ratios are likewise presented. At each total-pressure rake the maximum as well as the minimum local total-pressure ratios are shown. The total-pressure distortion quoted herein for each contour is then the numerical sum of the maximum and minimum values.

Figure 13 presents total-pressure contours at the diffuser exit for Mach number 2.0 and $\theta_l = \theta_{l,d}$. At angle of attack the flow distortion increases because the absolute values of both the positive and negative total-pressure ratios increase. Also the shapes of the isobars shift from nearly concentric at zero angle of attack to a condition where the low-total-pressure air fills the upper portion of the duct and the high-pressure core is moved only slightly downward. Although highly distorted flows were encountered, no flow separation at the diffuser exit was noted.

The total-pressure contours presented in figure 14 at diffuser station 7 were obtained simultaneously with those of figure 13 for the diffuser exit. A comparison of the distortions at the inlet throat with those at the diffuser exit reveals that the exit distortions are considerably smaller. This result is due to the mixing which occurs in the diffuser.

The large flow distortions near the inlet throat are due to nonuniform compression and boundary-layer effects (ref. 1). In figure 14, the increase of distortion at angle of attack is due primarily to the effects of low-total-pressure-ratio regions (boundary-layer effects). Generally these regions occurred on the upper cowl surface, although at -8° angle of attack the minimum-total-pressure region was located at the centerbody surface for the smooth-cone inlets. Hence, bleed from the inlet throat was rather ineffective, particularly at angles of attack other than zero, because the lower-pressure regions were located at the cowl rather than at the compression surface.

Comparison of the contours for smooth-cone and bleed-cone inlets in most cases indicates larger distortions in the region of the inlet throat for the bleed-cone inlet because of lower total pressures next to the cowl surface. This effect is similar to results obtained with short diffusers employing suction on one wall, where it has been noted that suction can separate the boundary layer of the opposite diffuser wall (ref. 3). This effect was most noticeable with the 17° cowl, presumably because of its relatively greater area expansion and, hence, greater tendency to separate because of the larger pressure gradient. In at

UNCLASSIFIED

least one case, however, bleed appreciably reduced the distortion. This occurred with the C_{14} inlets at -8° angle of attack, presumably because the bleed slot removed the low-total-pressure air next to the centerbody surface.

At zero angle of attack the total-pressure contours were not quite symmetrical, attesting to the slight misalinement and asymmetry of the inlet previously mentioned. Generally, the high-pressure core shifted toward the bottom of the inlet at other angles of attack. No separation at the throat station was observed.

Typical developments of the flow distortion through the subsonic diffuser are presented in figure 15. Total-pressure contours are plotted consecutively for stations 7, 19, 41, and 58. Figures 15(a) and (b) present typical data for the $C_{14}S_s$ inlet at Mach number 2.0 at angles of attack 0° and -8°, respectively, while data for the $C_{17}S_s$ inlet at Mach number 1.8 are given in figure 15(c).

In figures 15(a) and (c) for zero angle of attack, the static pressure was nearly uniform about the circumference at each rake station, and the total-pressure contours remained nearly concentric through the duct. At -8° angle of attack, however, there was considerable static-pressure variation about the duct circumference at stations 7 and 19, with the lowest static pressures occurring near the top of the duct. Thus, low-energy air on both centerbody and cowl surface begins to move towards the upper portion of the duct, accounting for the accumulation of low-pressure air in this region as previously noted.

In figure 15(a) the total-pressure distortion increased slightly between stations 7 and 19, then decreased to the final value at station 58. In figure 15(b) for -8° angle of attack, the distortion decreased continually through the diffuser; this is the expected result of mixing due to length and the reduction of flow Mach number (refs. 1 and 4). In figure 15(c) for Mach 1.8, a large increase of distortion occurred between stations 7 and 19 although no separation was evident. Between these two stations, the absolute values of both the positive and negative pressure ratios increased. Behind station 19 the distortion again decreased with length.

At this point, the question of rake interference may arise. As previously discussed, the spokes of each rake were directly downstream of the preceding rake element. Although there was obviously an aggregated total-pressure loss across each rake station, these losses are believed to be quite small, inasmuch as the present pressure-recovery data agree with previous data for the same inlet where only a diffuser-exit rake was used (ref. 2). There may also be some question on the effect of the wake of one rake on the distortion measured at the following rake.

UNCLASSIFIED

(Such interference effects would apply most directly to the distortions measured at station 19.) There are few, if any, data available for wakes in diverging channels at high subsonic speeds. An attempt, however, was made to determine the order of magnitude of these effects. From the equations for the wake behind a flat plate in incompressible flow from reference 5, a maximum error of 0.04 in total-pressure recovery was calculated for the case of zero diffusion, corresponding to a maximum velocity-ratio decrement of 0.1 in the wake. With diffusion, two limiting solutions were considered: (1) the flow completely mixed, between stations 7 and 19, or (2) the velocity-ratio decrement 0.1 persisted at station 19. The first assumption would, of course, give zero interference effect. The second assumption yielded an interference corresponding to a 0.025 decrement in total-pressure ratio. The interference effect is probably between these limits (i.e., about 1 percent).

Distortion data as a function of diffuser station for all configurations are summarized in figures 16 to 20. The distortion at station 7 is presented only for the value of θ_l at which the two sections of the survey rake were alined. For the bleed configurations, data are shown for the maximum bleed rate and a reduced bleed of approximately one-half the maximum bleed.

Increased distortion at angle of attack is seen to persist throughout the diffuser. The mixing process reduces the large distortions at station 7 to considerably lower values; nevertheless, the mixing is inadequate to overcome completely the initially higher throat distortions with the fixed mixing length between the throat and the diffuser exit. Consequently, the distortions at the diffuser exit increase with angle of attack.

The increase of distortions with larger values of θ_l is again noted. An example of this effect is shown in figure 21 for the $C_{17}S_s$ inlet at zero angle of attack. Here distortion is plotted as a function of the decrement of the shock angle from the shock-on-lip value. The increase of distortion with larger values of θ_l for the present data is due to two effects: (1) The larger values of distortion may be traced to larger distortions at the inlet throat; and (2) as indicated in figure 21, increasing the value of θ_l increases the value of the discharge Mach number to maintain critical inlet operation. (As indicated in a later section of this report, increasing the discharge Mach number tends to increase the distortion.)

An example of (1) is illustrated in figure 22. In figure 22(a) total-pressure profiles obtained at station 7 are presented as functions of θ_l for the $C_{17}S_b$ inlet. At $\theta_l = 40^\circ$ (oblique shock ahead of lip) the flow was fairly uniform across the inlet except for a rather thick

UNCLASSIFIED

boundary layer next to the cowl surface. At $\theta_l = 42.6^\circ$, distortion increased because of a thickening of the centerbody boundary layer. Finally at $\theta_l = 46^\circ$, with the shock inside the lip, the total-pressure profiles indicated a sizeable discontinuity in total pressure about midway between the cowl and centerbody surfaces. This discontinuity is due to the vortex sheet originating at the intersection of the oblique and normal shocks.

Typical total-pressure profiles at the diffuser exit are presented in figure 22(b) for the same conditions. This example was chosen to show not only the change in distortion with oblique-shock position but also to indicate the change in shape of the profiles. In this example, the high-pressure core shifted toward the hub at the higher values of θ_l while the total pressure decreased at the tip. In the present investigation the shape of the profiles is dependent upon θ_l, the presence of bleed, angle of attack, and to a lesser extent on free-stream Mach number and cowl angle.

The data presented for the bleed configurations up to this point have been primarily for a maximum and a reduced bleed rate. While increasing the bleed rate consistently increased the pressure recovery, the effects on distortion were seen to be somewhat inconsistent. Typical effects of a continuous variation of bleed ratio from zero to the maximum value on pressure recovery and distortion at the diffuser exit are presented in figures 23(a) and (b), respectively.

As indicated in figure 23(a), increasing the bleed rate to the maximum value increased the recovery. With the 14° cowl inlet, pressure recoveries with maximum bleed slightly exceeded those of the smooth-cone inlet. With the 17° cowl inlet, however, pressure recoveries with the bleed inlet never equalled those of the smooth-cone inlet.

In figure 23(b) distortions at both stations 7 and 58 are considered. At station 7 the cone surfaces incorporating bleed slots increased the distortion above the smooth-cone values at zero bleed. Increasing the bleed flow rate reduced these distortions, especially at -8° angle of attack. With the maximum amount of bleed, the distortion at station 7 was reduced about 2 percent in comparison to the smooth-cone inlet with 14° cowl. For the 17° cowl, however, the distortion even with the optimum amount of bleed was still 7 percent higher than for the smooth-cone inlet. This effect may be due to the greater tendency for separation at the cowl surface with the 17° cowl, as was previously noted.

At station 58, bleed had relatively little effect on the distortion level at zero angle of attack. Minimum distortion with the $C_{17}S_b$ inlet was obtained with about 75 percent of the maximum bleed rate, but

UNCLASSIFIED

this value was only slightly better than that of the smooth-cone inlet. In spite of rather large differences in distortion at station 7, the distortion at the diffuser exit was rather insensitive to both bleed rate and cowl angle.

Mixing in subsonic diffuser. - The data of figures 16 to 20 indicate that the distortion generally decreased as it passed through the diffuser. Some data, particularly at Mach numbers 1.8 and 1.6, however, exhibit a considerable increase of distortion between stations 7 and 19. The total-pressure contours, such as figures 15(a) and (c), reveal that this increase is caused by increases in the absolute values of both the positive and negative total-pressure ratios defining the distortion number. There was no evidence of separation unless it occurred between the two measuring stations and became reattached before station 19.

In figure 24(a), the variation of distortion through the diffuser is repeated for the double-shock inlet for Mach numbers 2.0, 1.8, and 1.6. Added to these data, however, are the values of distortion associated with a one-seventh power velocity profile in a pipe (ref. 6). The pipe-flow values were determined as follows: At each rake station the average flow Mach number was computed from the measured pressures at that station and the diffuser mass flow. The variation of total pressures associated with the theoretical velocity profile was then computed across the duct to the outermost tube at each rake station (these radius ratios given in fig. 4). The distortion number was then computed as before.

At Mach 2.0 the distortion at station 7 was higher than the pipe-flow value. The change in distortion due to mixing in the diffuser was then fairly well predicted by the variation of the pipe-flow curve. At Mach numbers 1.8 and 1.6 the distortion at station 7 was less than the pipe-flow values, and for these cases the distortion increased downstream of station 7 until distortions higher than the pipe-flow values occurred; the distortion then decreased toward the pipe-flow value at the distortion exit.

Similar data are presented in figure 24(b) for the $C_{14}S_s$ inlet at Mach 2.0. At angles of attack other than zero, the entering distortion was larger than pipe-flow values, and the change in distortion due to mixing was again fairly well predicted by the shape of the pipe-flow curve. (Pipe-flow values in this example are shown as a narrow band because of small changes in flow Mach number over the angle-of-attack range.) At zero angle of attack, however, the distortion at station 7 was less than pipe flow, and the distortion again increased slightly downstream until the distortion was larger than pipe-flow values.

UNCLASSIFIED

In order to understand these variations of distortion through the diffuser, it is well to review the factors affecting flow mixing. The distortion at any station in the diffuser depends upon the amount of distortion entering the inlet and upon the amount of mixing that occurs in the diffuser ahead of the particular station. Mixing, in turn, is dependent upon the distortion level, the length available for mixing, the average flow Mach number, and so forth. In regard to the first of these, a highly distorted flow will mix faster than a less distorted flow. In the region of the inlet throat, mixing is reduced because of the rather high flow Mach numbers unless the flow is highly distorted (such as at angles of attack other than zero). Actually, when the distortion entering the inlet throat is quite low, normal boundary-layer growth may increase the distortion level more rapidly than mixing can reduce it. An example of this is the development of turbulent flow in a smooth constant-area pipe. In figure 24(b) two examples of this development are shown; (1) the development of distortion in a smooth pipe at flow Mach number 0.32, which corresponds to the diffuser-exit Mach number, and (2) a portion of the development for flow Mach number 0.588, which corresponds to the Mach number at station 7. These curves were derived from the data of reference 7.

If the flow were at Mach 0.32 throughout the diffuser length, the normal rate of boundary-layer growth would yield distortions which would approach (asymtotically) the turbulent pipe-flow value from the lower side. At the higher flow Mach number the rate of increase of distortion is much larger, and the distortion curve is approximately parallel to the data curve for zero angle of attack.

The difference in distortion between the actual data and the development curve is primarily due to the contribution of distortion of the terminal shock. It would appear that for any distortion level greater than the development value, but less than the pipe-flow value, the distortion will increase downstream to values greater than the pipe-flow value and then approach the pipe-flow value asymtotically at the diffuser exit. Likewise, for any distortion level considerably less than the development value, the distortion should remain, ideally at least, less than pipe-flow values and should approach the pipe-flow value asymtotically from the lower side.

Because the area of the diffuser is increasing and the flow is distorted because of shock - boundary-layer interactions, the analogy of flow development should not be carried too far. The data of figure 24(a) for Mach number 1.6 indicate that, even for very low entering distortion (less than the development value), the distortion increases to above pipe-flow values. This is probably the result of the adverse pressure gradient of the diffuser. It should not be expected that the distortion development in an actual diffuser without special features will ever yield distortions at the diffuser exit less than that

5007

UNCLASSIFIED

associated with a fully developed turbulent profile. One such special feature, for example, is the diffuser which is overexpanded area-wise and then rapidly converged at the diffuser exit (ref. 6).

It was previously believed that lower distortions at the diffuser exit could be achieved by reducing the distortion entering the inlet (ref. 4). The foregoing brief analysis indicates a limit to available distortion reduction, that being the turbulent profile value near the inlet throat. Any reduction of distortion near the throat below the pipe-flow value would still yield near-turbulent profile values at the diffuser exit.

Correlation of distortion data with fully developed turbulent flow. Flow distortion at the diffuser exit of the $C_{17}S_s$ inlet is plotted in figure 25(a) as a function of the diffuser-exit Mach number. Data points again represent critical inlet operation. Also indicated are distortions computed for fully turbulent pipe flow (three-dimensional) and channel flow (two-dimensional). Distortions at the diffuser exit less than pipe-flow values were measured herein (see also figs. 24(a) and (b)) and in reference 6 for a similar centerbody configuration. However, as might be expected, the two-dimensional distortion values appear to provide a more realistic lower limit, as least for the case of the centerbody inlet. The variation of distortion with oblique-shock location previously noted is again observed. Previous results indicated a reduction of distortion with increase in free-stream Mach number (see fig. 11(b)). When the inlets are compared at the same diffuser-discharge Mach number, however, distortion increases at the higher Mach numbers. This result is probably due to larger distortions caused by the terminal-shock - boundary-layer interaction at the higher Mach numbers.

Similar data are presented in figure 25(b) for all configurations tested. The results again indicate that the two-dimensional turbulent profile represents a better distortion-limit reference than do the three-dimensional values for centerbody inlets.

SUMMARY OF RESULTS

A typical full-scale nose inlet having four total-pressure rakes in the subsonic diffuser was tested at Mach numbers 0.63 and 1.6 to 2.0 to determine the nature of flow-distortion development in the subsonic diffuser. Inlet parameters included 14° and 17° internal cowl-lip angles, conical compression surfaces with and without boundary-layer removal slots, and cone tip translation. At Mach 2.0, angles of attack to -8° were investigated. The results of this investigation are summarized as follows:

1. Bleed from the centerbody near the inlet throat improved the peak total-pressure recovery a maximum of 2 percent at zero angle of

UNCLASSIFIED

attack but generally reduced the recovery at other angles of attack. Bleed was generally ineffective because low-pressure regions were located near the cowl surface rather than the cone surface.

2. Pressure recovery was improved and total-pressure distortion was decreased for oblique shocks positioned ahead of the inlet lip. This oblique-shock location is beneficial because of reduced duct Mach numbers and absence of vortex sheets into the inlet.

3. At zero angle of attack, changing the cowl from a 14° to a 17° internal lip angle, or changes in the centerbody bleed configuration near the inlet, had little effect on the distortion at the diffuser exit. This value may be predicted fairly closely by calculation of the turbulent-profile value at the diffuser exit.

4. As angle of attack increased, the distortion increased throughout the diffuser, and the distortions at the diffuser exit were considerably larger than those associated with turbulent-profile values.

5. Decreasing the distortion at the inlet throat reduced the distortion at the diffuser exit until the throat distortion was reduced to about the pipe-flow value. For this condition, flow distortion throughout the length of the diffuser was predicted by turbulent-profile calculations. When the throat distortion was less than the pipe-flow value, the distortion at the exit remained at the turbulent-profile value.

6. For inlets incorporating centerbodies, two-dimensional, or channel, flow provided a better lower distortion limit at the diffuser exit than did pipe, or three-dimensional, flow.

Lewis Flight Propulsion Laboratory
National Advisory Committee for Aeronautics
Cleveland, Ohio, August 2, 1956

REFERENCES

1. Piercy, Thomas G.: Factors Affecting Flow Distortions Produced by Supersonic Inlets. NACA RM E55L19, 1956.

2. Kremzier, Emil J., and Wise, George A.: Effect of Centerbody Boundary-Layer Removal Near the Throat of Three Conical Nose Inlets at Mach Number 1.6 to 2.0. NACA RM E55H16a, 1955.

3. Woollett, Richard R.: Preliminary Investigations of Short Two-Dimensional Subsonic Diffusers. NACA RM E56C02, 1956.

5007

UNCLASSIFIED

4. Piercy, Thomas G., and Klann, John L.: Experimental Investigation of Methods of Improving Diffuser-Exit Total-Pressure Profiles for a Side-Inlet Model at Mach Number 3.05. NACA RM E55F24, 1955.

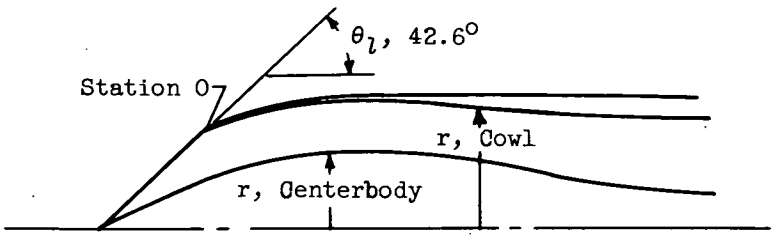
5. Schlichting, H.: Lecture Series "Boundary Layer Theory." Pt. I - Laminar Flows. NACA TM 1217, 1949.

6. Sterbentz, William H.: Factors Controlling Air-Inlet Flow Distortions. NACA RM E56A30, 1956.

7. Deissler, Robert G.: Analytical and Experimental Investigation of Adiabatic Turbulent Flow in Smooth Tubes. NACA TN 2138, 1950.

UNCLASSIFIED

TABLE I. - COWL AND CENTERBODY COORDINATES (RADII)



Station, in.	Centerbody radius, in.		Cowl radius, in.	
	25° Spike	15°-25° Spike	17° Cowl	14° Cowl
-12.880	-	0	(Lip radius, 0.03")	(Lip radius, 0.06")
-9.380	0	15° Conical		
	25° Conical			
-4.710	2.190	2.190		
0	4.375	4.375 25°	8.625	8.625
1.000	4.845	4.845 Conical	8.930	8.875
1.290	4.980	4.980		
2.0	5.300	5.300	9.230	9.125
4.0	6.145	6.145	9.780	9.620
6.0	6.865	6.865	10.290	10.085
8.0	7.480	7.480	10.720	10.505
10.0	8.000	8.000	11.080	10.895
12.0	8.370	8.370	11.400	11.260
14.0	8.650	8.650	11.675	11.600
16.0	8.845	8.845	11.900	11.880
18.0	8.960	8.960	12.075	12.070
20.0	9.000	9.000	12.200	12.195
22.0	9.000	9.000	12.275	12.275
24.0	8.900		12.300	
26.0	8.900	Same as	12.300	Same as
28.0	8.850	25° spike	12.275	17° cowl
30.0	8.675		12.210	
32.0	8.400		12.120	
34.0	8.080		12.000	
36.0	7.700		11.830	
38.0	7.250		11.650	
40.0	6.775		11.460	
42.0	6.280		11.290	
44.0	5.800		11.125	
46.0	5.330		10.960	
48.0	4.910		10.820	
50.0	4.550		10.700	
52.0	4.270		10.600	
54.0	4.075		10.530	
56.0	3.950		10.500	
58.0	3.875		10.500	
60.0	3.830		10.500	

UNCLASSIFIED

5007

CR-3 back

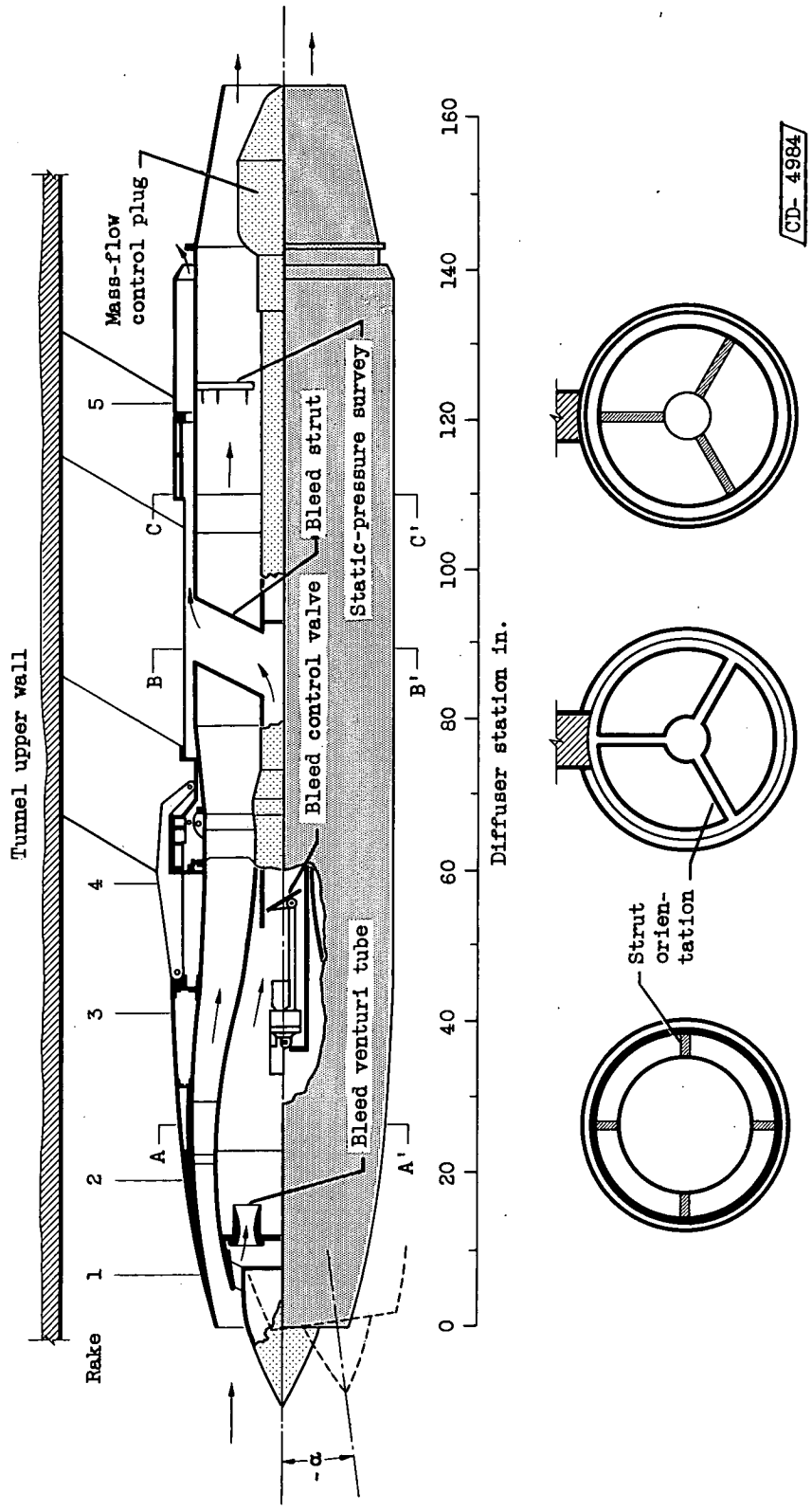
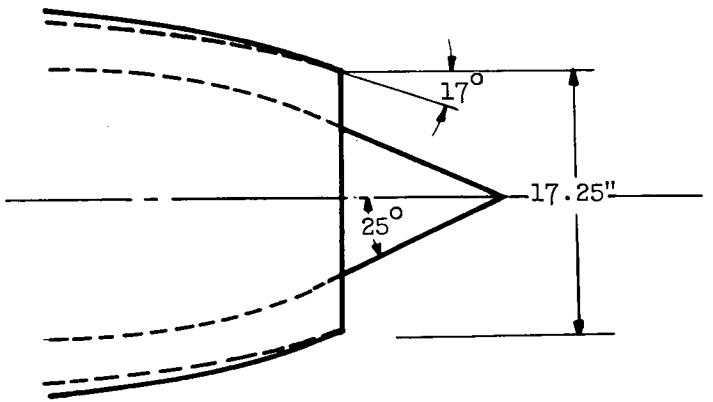
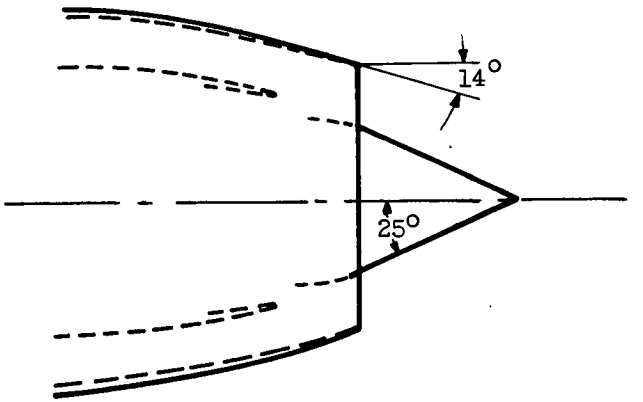


Figure 1. - Schematic drawing of model investigated.

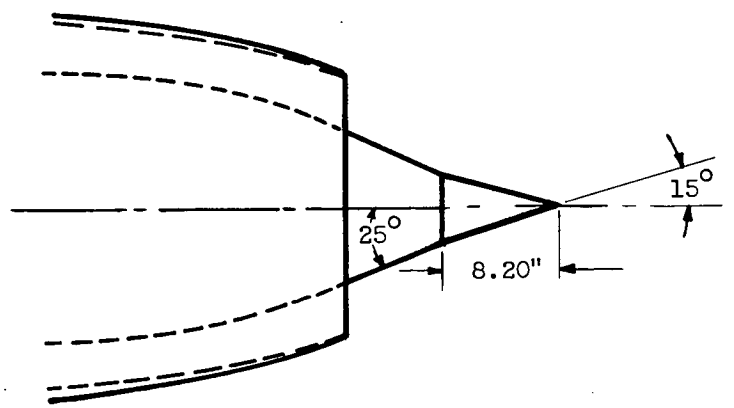
CONFIDENTIAL



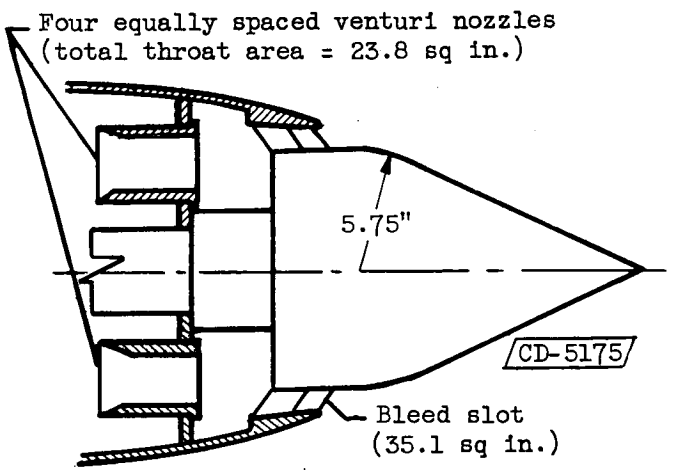
(a) Inlet $C_{17}S_s$.



(b) Inlet $C_{14}S_b$.



(c) Inlet $C_{14}S_{s,ds}$.



(d) Details of bleed slot.

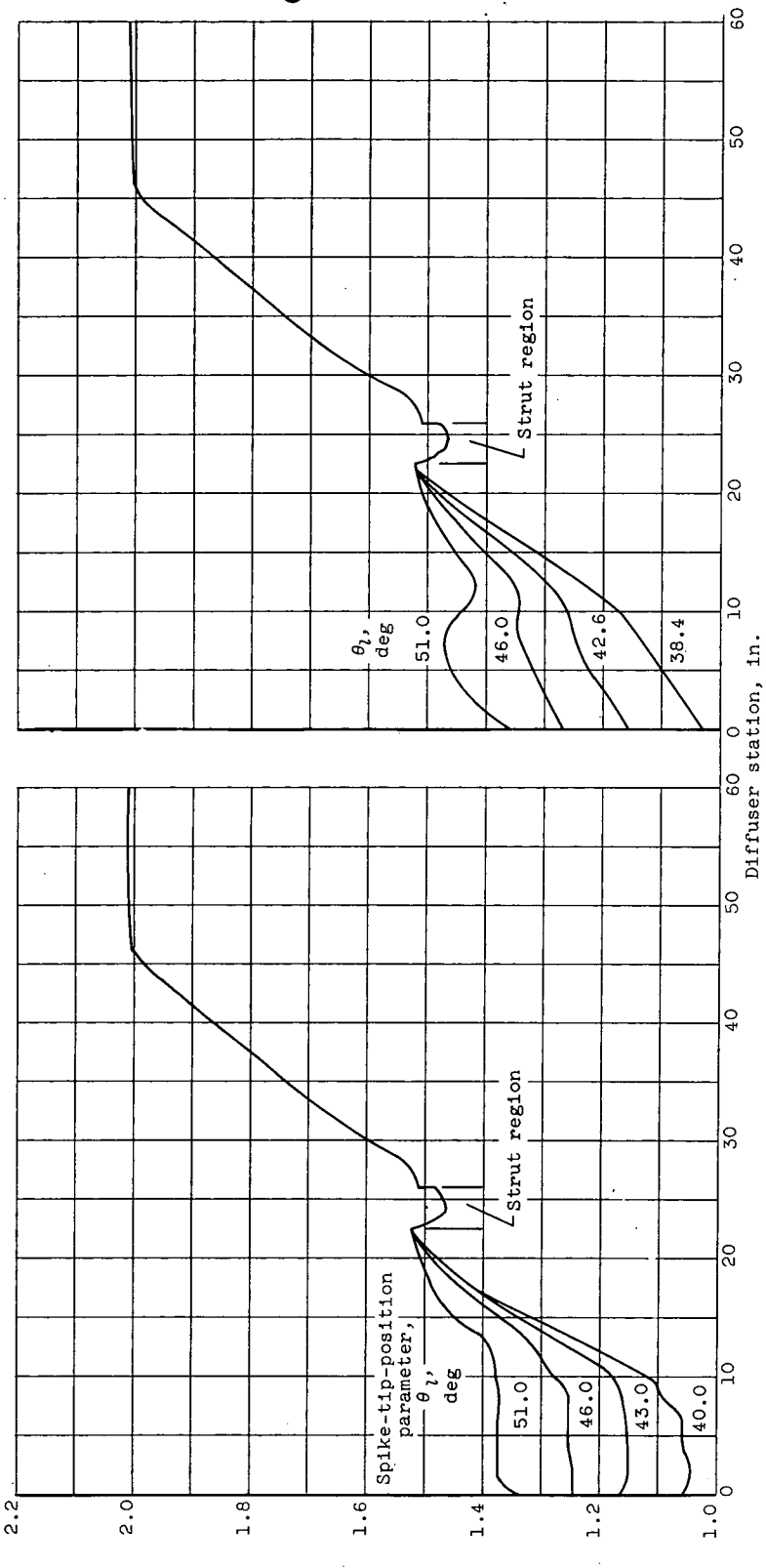
Figure 2. - Inlet configurations.

UNCLASSIFIED

CONFIDENTIAL

UNCLASSIFIED

5007

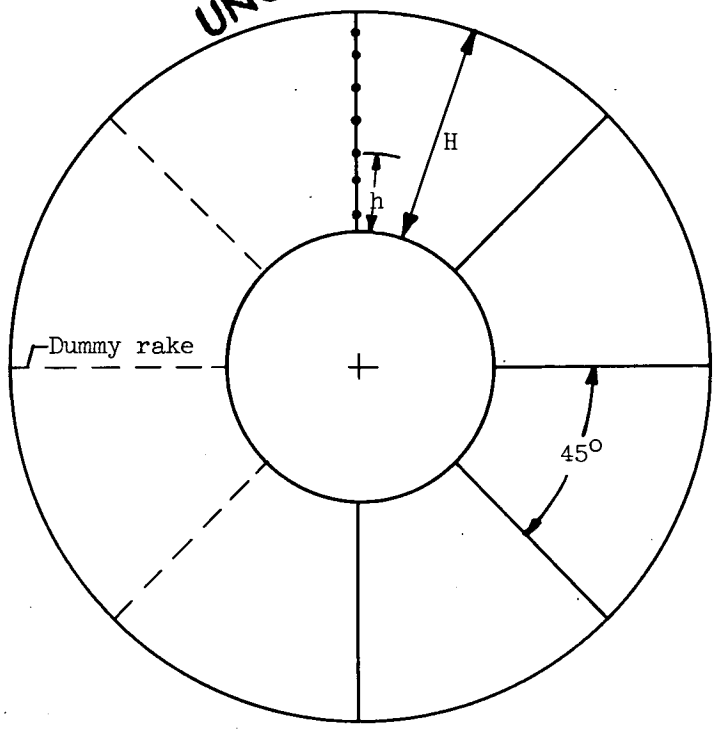


(a) Inlet series C_{14}. (b) Inlet series C_{17}.

Figure 3. - Subsonic diffuser area variations.

UNCLASSIFIED

5007



Tube	Station, in.					
	7		19		41	58
	Diffuser passage height, H, in.					
	3.21[a]	3.10[b]	3.15[a]	3.22[b]	4.85	6.62
	Tube location, h/H					
1	0.11	0.10	0.14	0.14	0.08	0.11
2	.30	.30	.31	.31	.23	.28
3	.49	.47	.48	.48	.38	.43
4	.61	.62	.64	.64	.50	.55
5	.77	.78	.80	.80	.62	.67
6	.92	.93	.94	.94	.74	.77
7	---	---	---	---	.84	.87
8	---	---	---	---	.96	.96

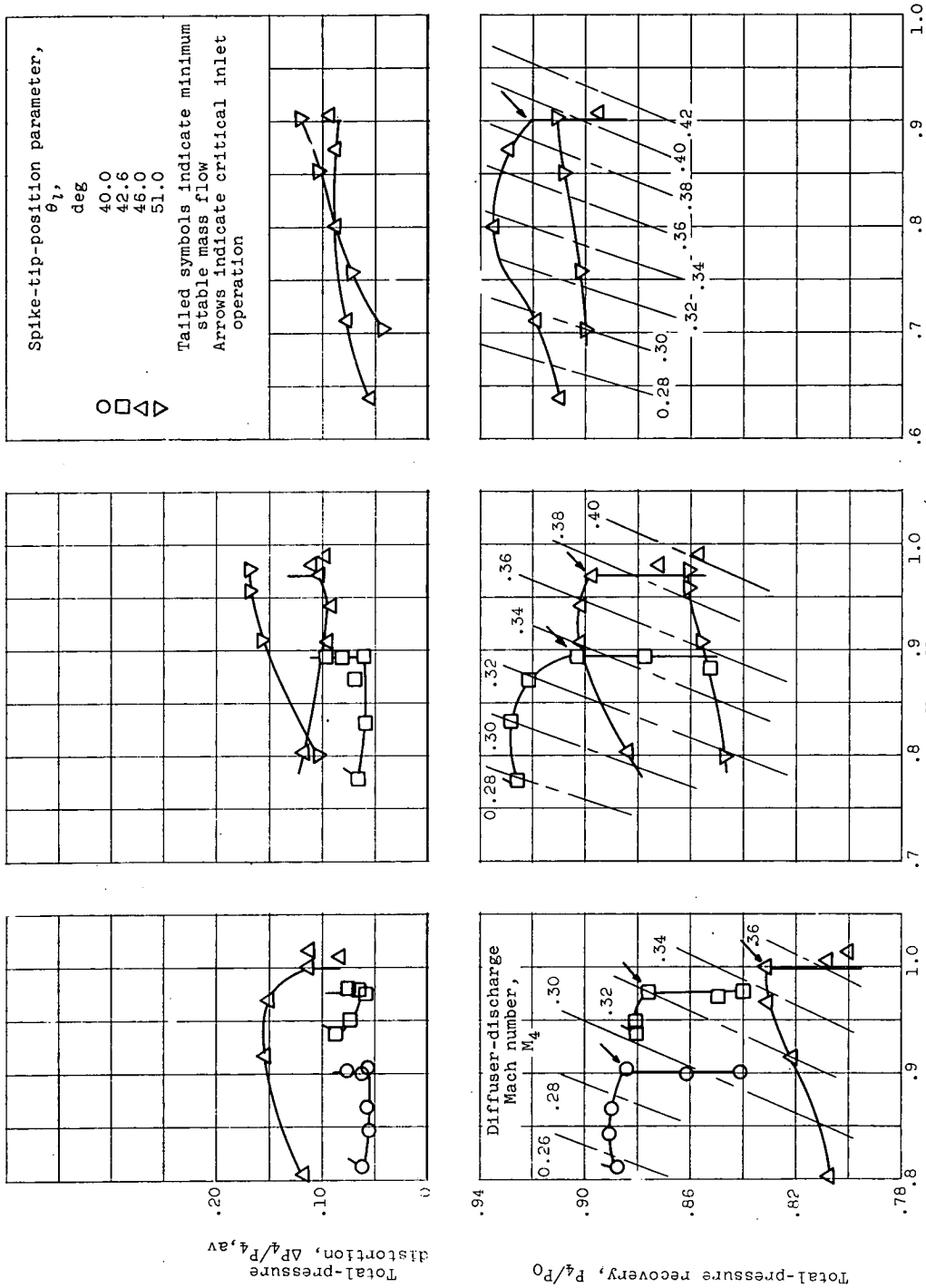
[a] 17° Cowl.

[b] 14° Cowl.

Figure 4. - Total-pressure-tube locations.

UNCLASSIFIED

5007



(a) Angle of attack, 0°; free-stream Mach number, 2.0.

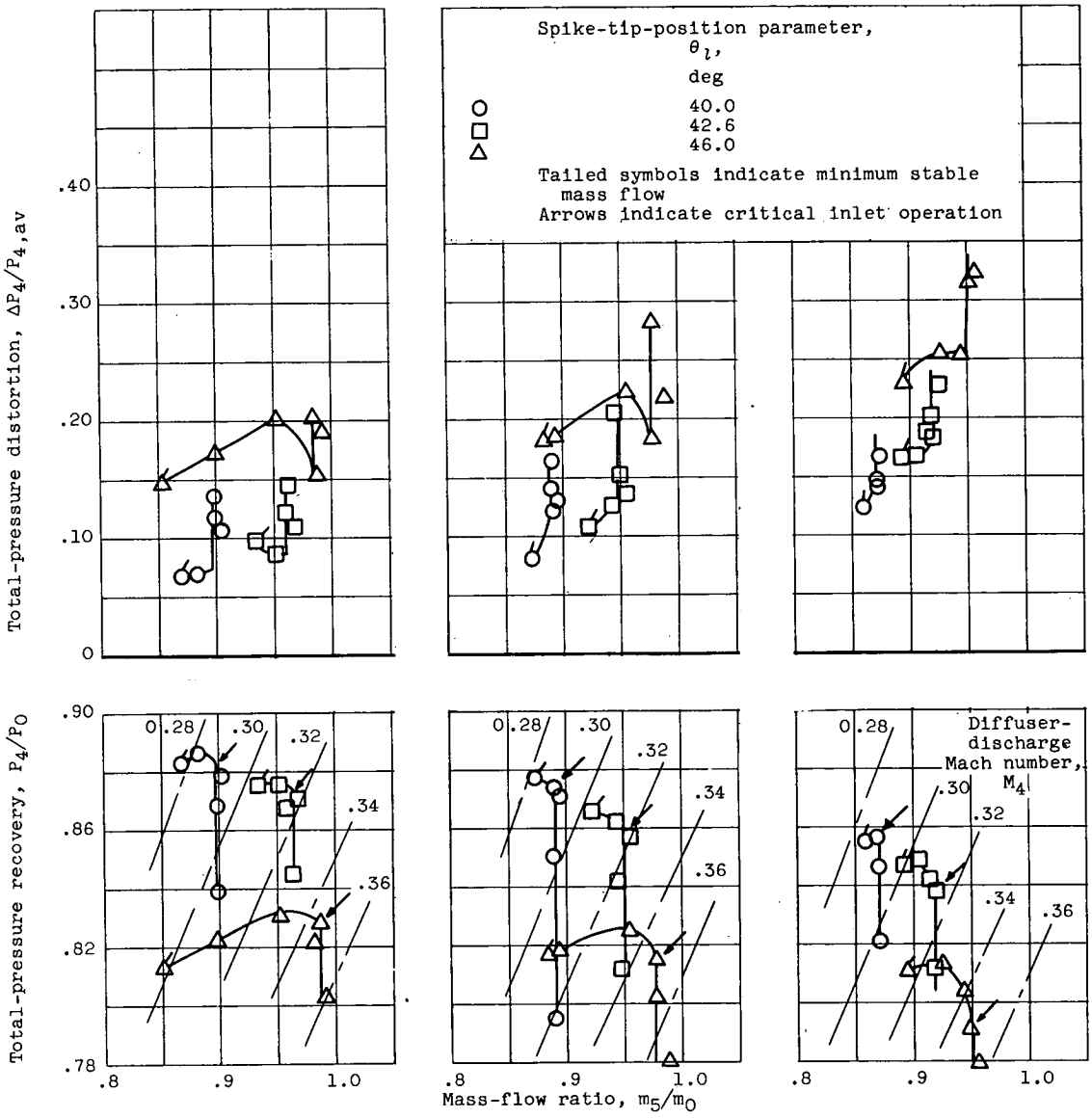
(b) Angle of attack, 0°; free-stream Mach number, 1.8.

(c) Angle of attack, 0°; free-stream Mach number, 1.6.

Figure 5. - Performance of inlet $C_{14}S_8$.

UNCLASSIFIED

5007



(d) Angle of attack, -3°; free-stream Mach number, 2.0.

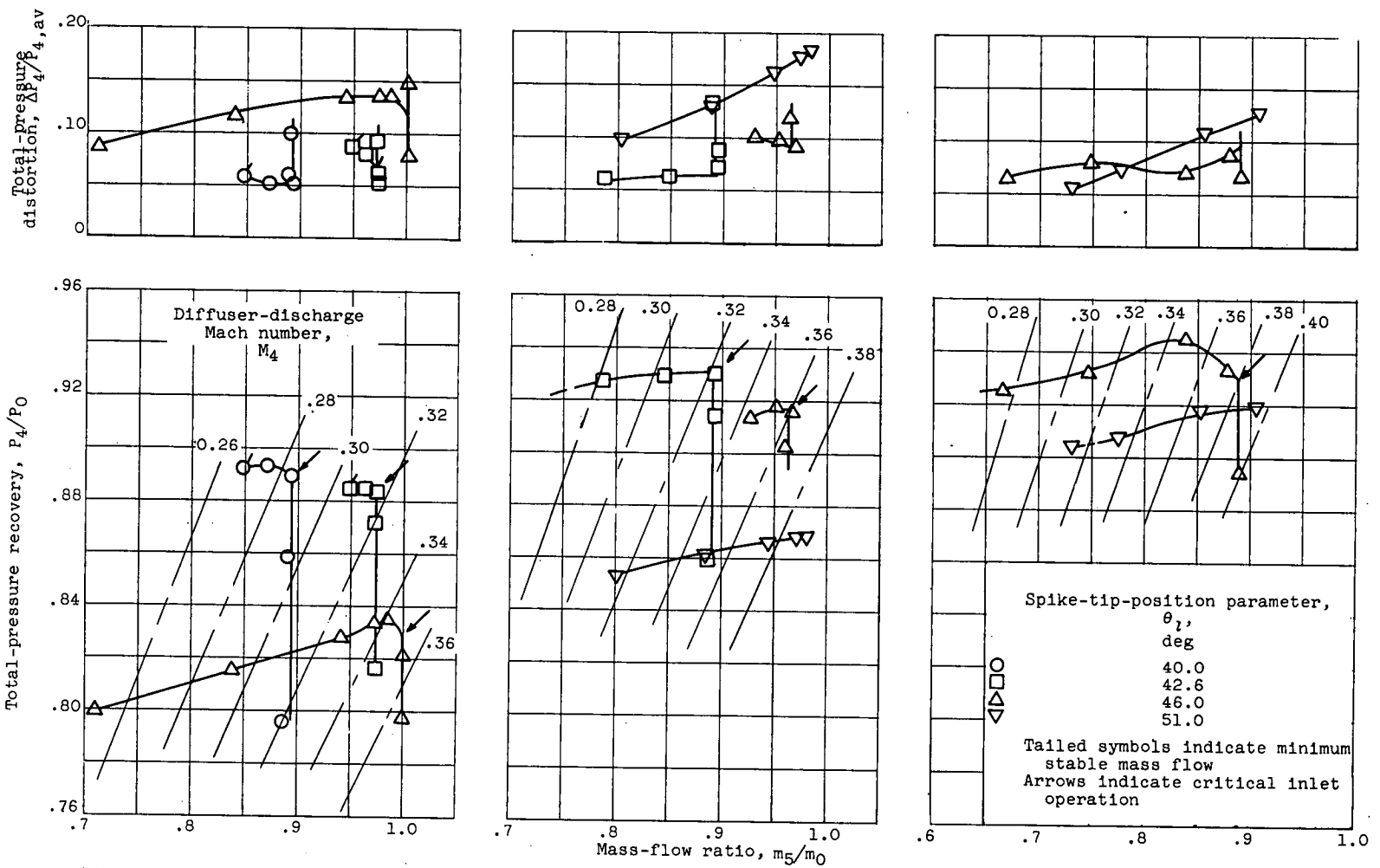
(e) Angle of attack, -5°; free-stream Mach number, 2.0.

(f) Angle of attack, -8°; free-stream Mach number, 2.0.

Figure 5. - Concluded. Performance of inlet $C_{14}S_8$.

CONFIDENTIAL

CONFIDENTIAL
UNCLASSIFIED



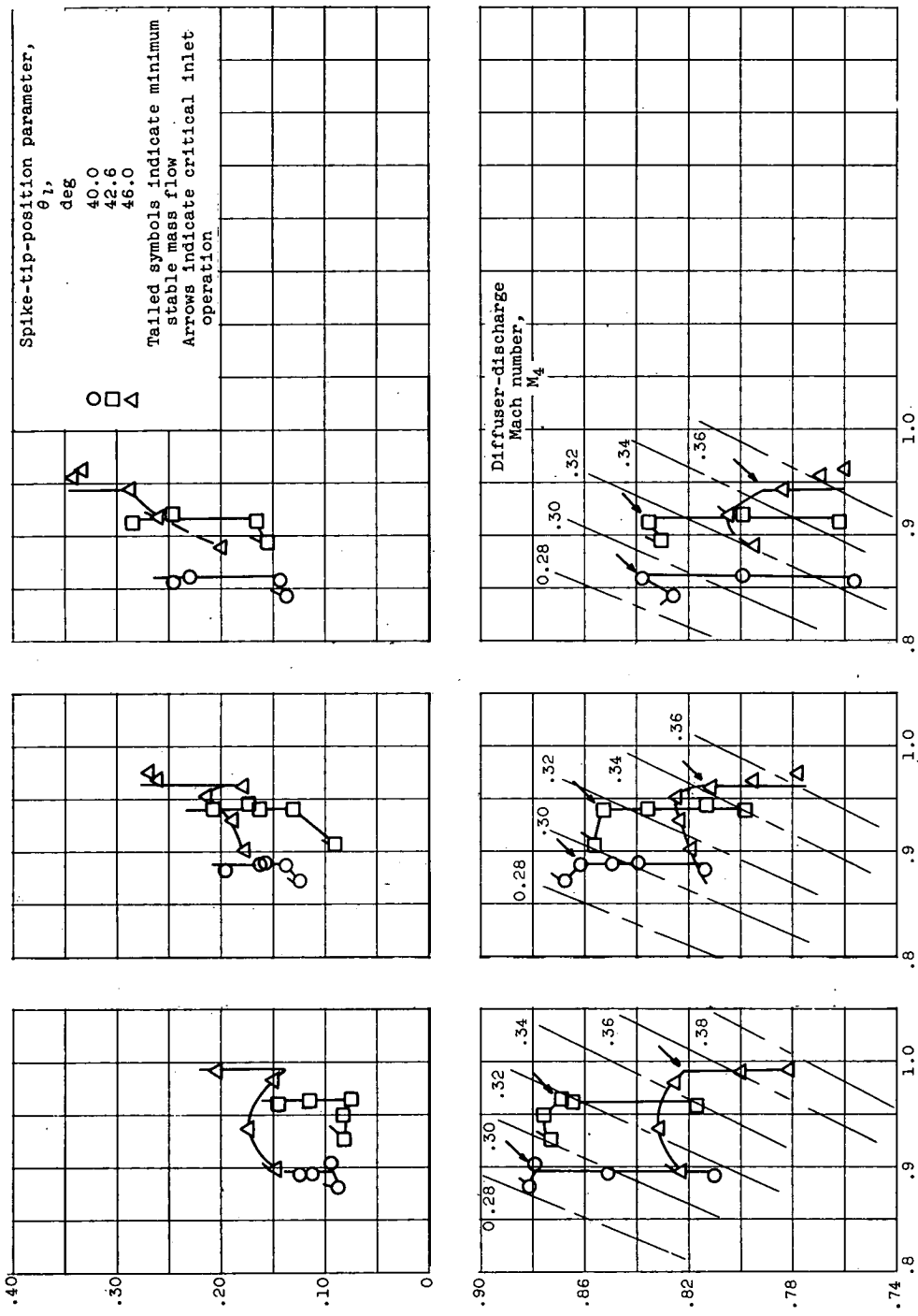
(a) Angle of attack, 0°; free-stream Mach number, 2.0.

(b) Angle of attack, 0°; free-stream Mach number, 1.8.

(c) Angle of attack, 0°; free-stream Mach number, 1.6.

Figure 6. - Performance of inlet $C_{17}S_s$.

UNCLASSIFIED



(d) Angle of attack, -3°; free-stream Mach number, 2.0.

(e) Angle of attack, -5°; free-stream Mach number, 2.0.

(f) Angle of attack, -8°; free-stream Mach number, 2.0.

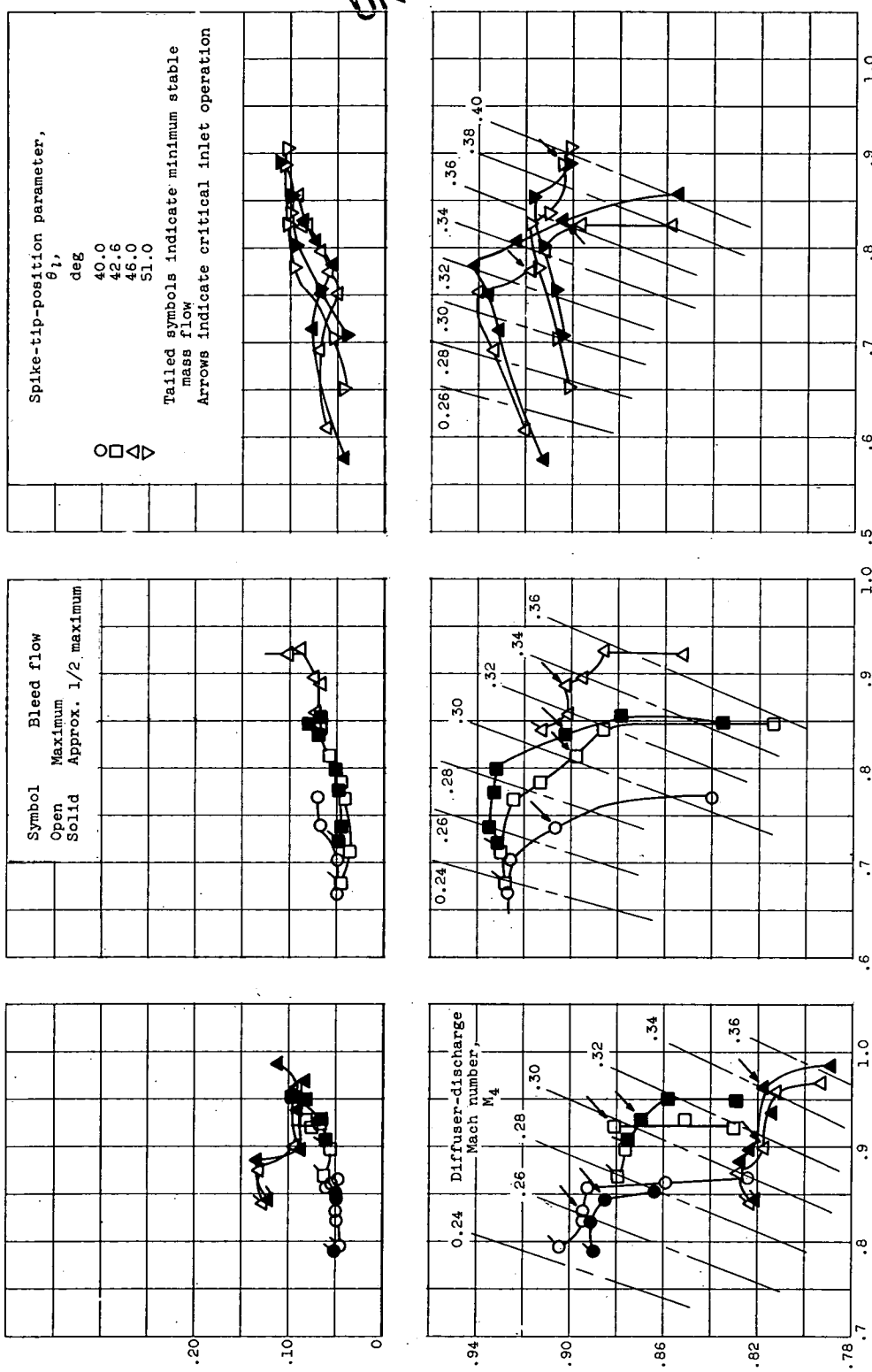
Figure 6. - Concluded. Performance of inlet $C_{17}S_s$.

5007

UNCLASSIFIED

5007

CR-4 back



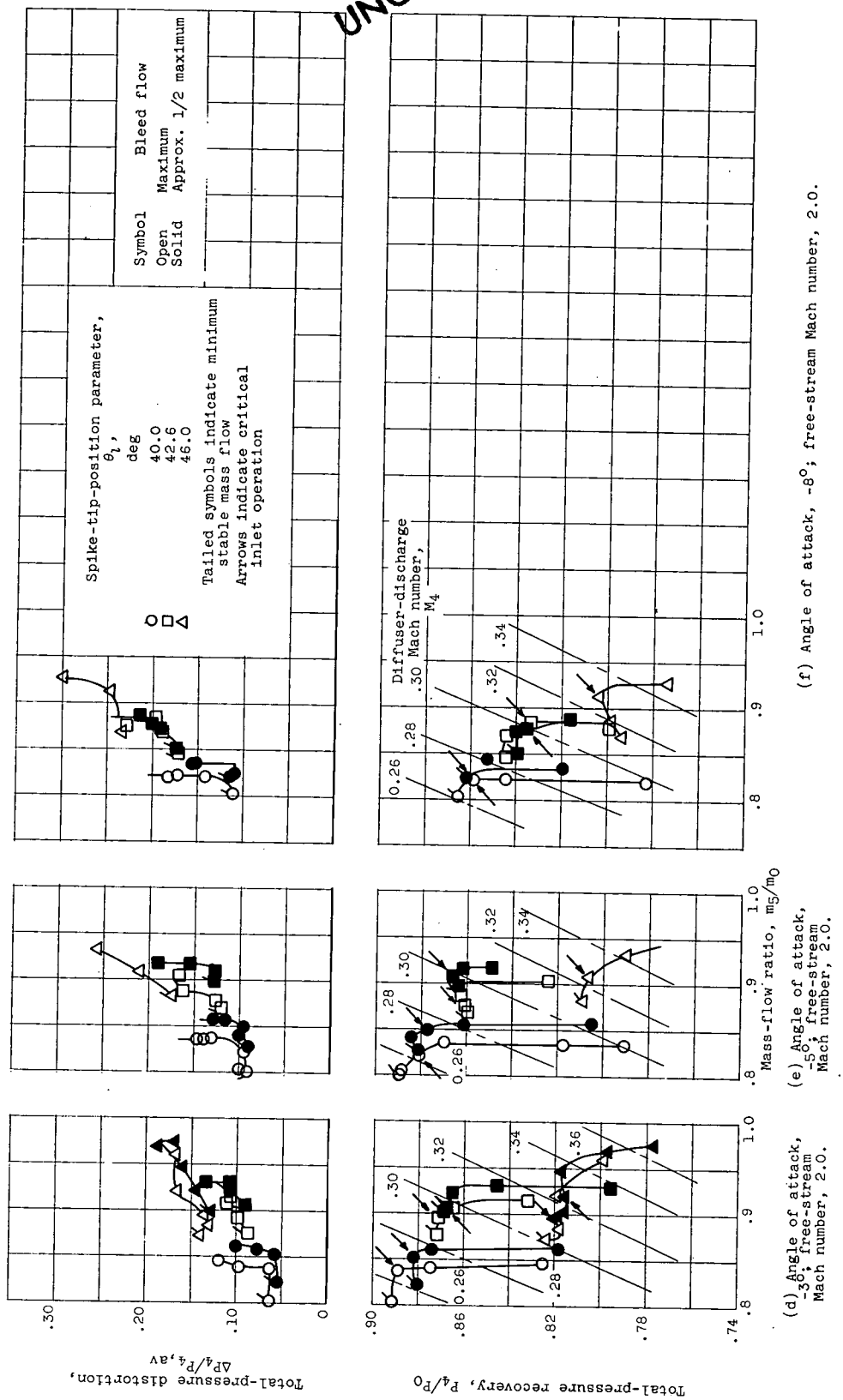
(a) Angle of attack, 0°; free-stream Mach number, 2.0.

(b) Angle of attack, 0°; free-stream Mach number, 1.8.

(c) Angle of attack, 0°; free-stream Mach number, 1.6.

Figure 7. - Performance of inlet $C_{14}S_b$.

UNCLASSIFIED



(d) Angle of attack, -3°; free-stream Mach number, 2.0.

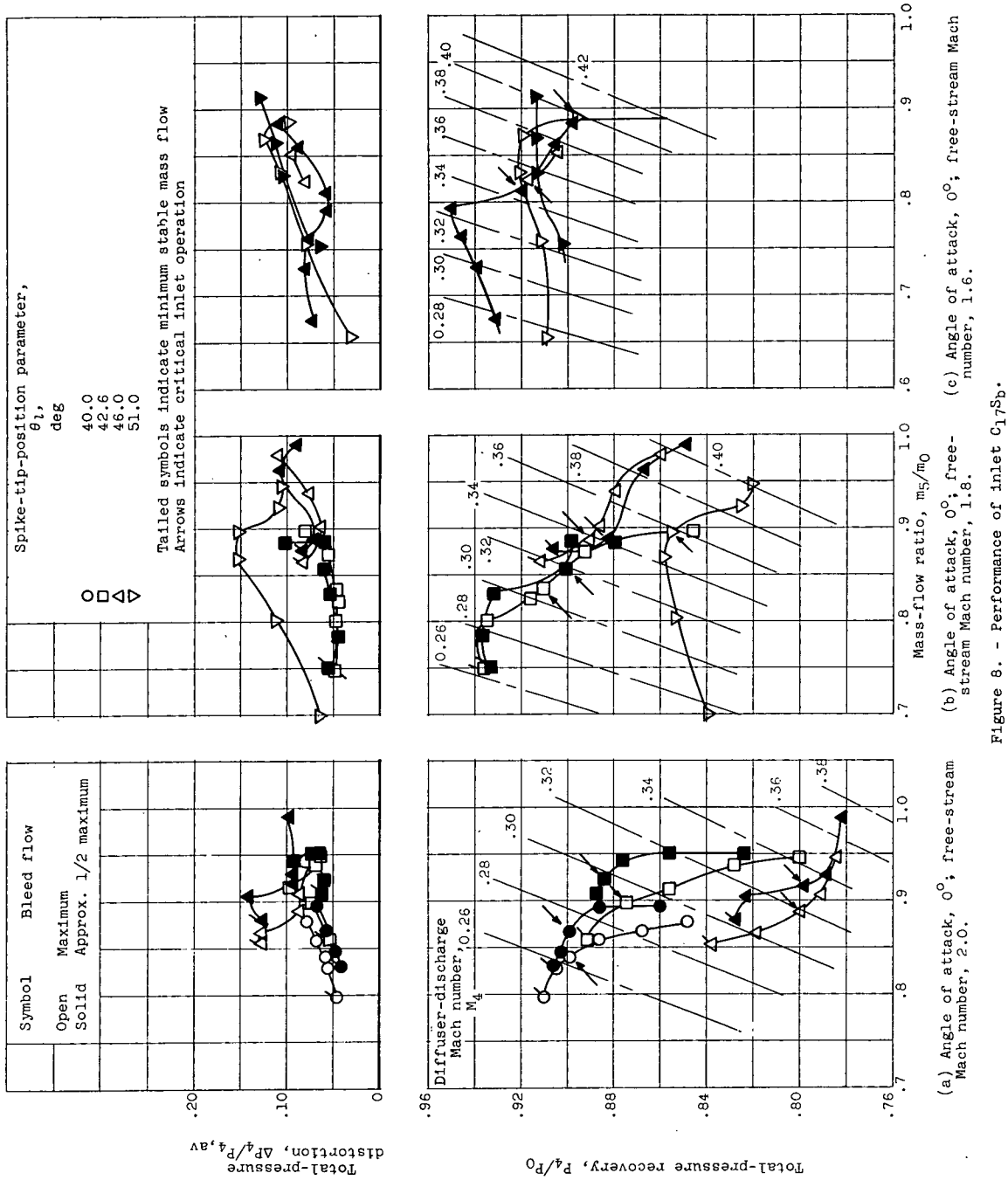
(e) Angle of attack, -5°; free-stream Mach number, 2.0.

(f) Angle of attack, -8°; free-stream Mach number, 2.0.

Figure 7. - Concluded. Performance of inlet $C_{14}S_b$.

5007

CONFIDENTIAL UNCLASSIFIED



(a) Angle of attack, 0°; free-stream Mach number, 2.0.

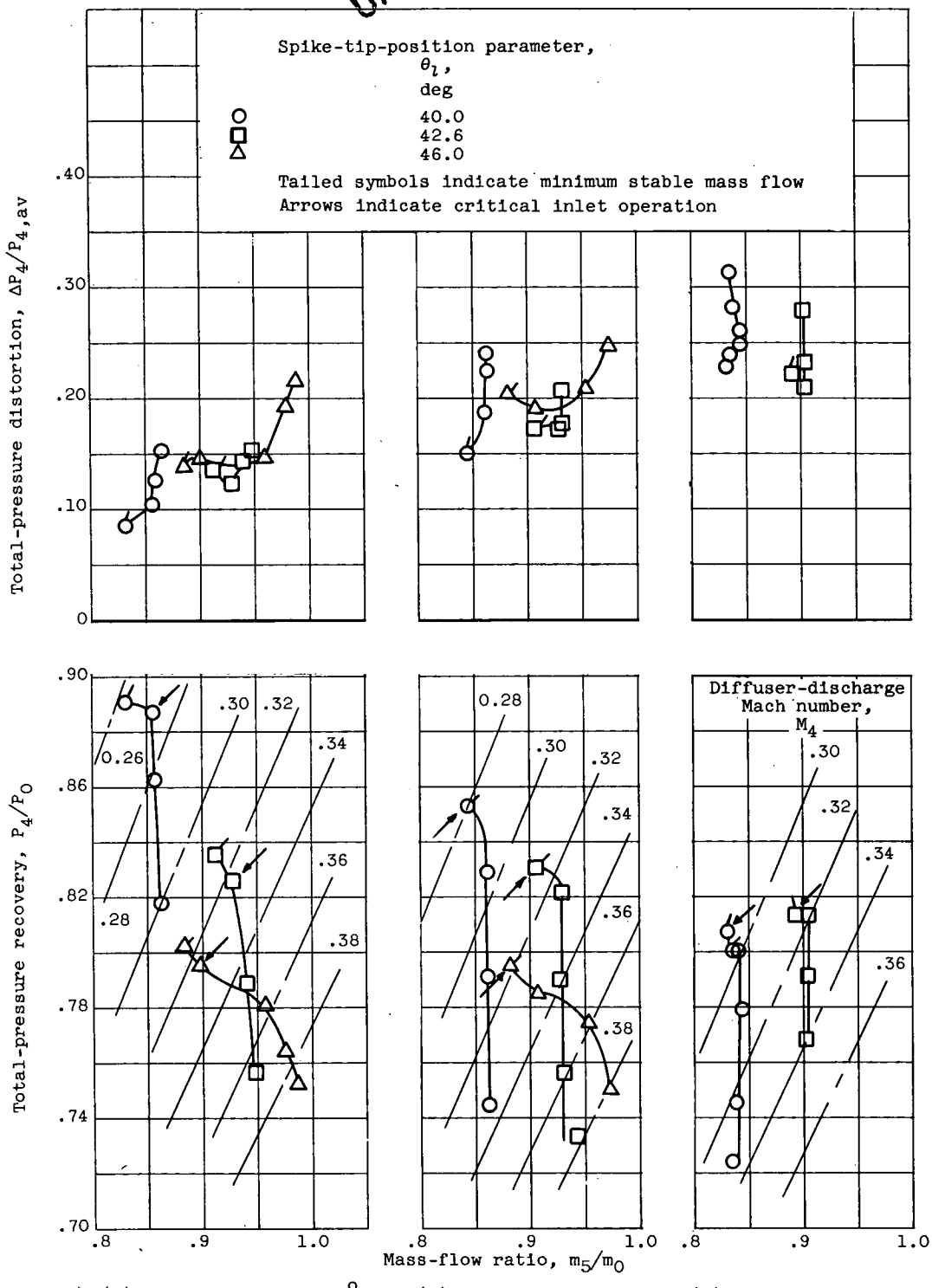
(b) Angle of attack, 0°; free-stream Mach number, 1.8.

(c) Angle of attack, 0°; free-stream Mach number, 1.6.

Figure 8. - Performance of inlet $C_{17}S_b$.

UNCLASSIFIED

5007



(d) Angle of attack, -3°; free-stream Mach number, 2.0.

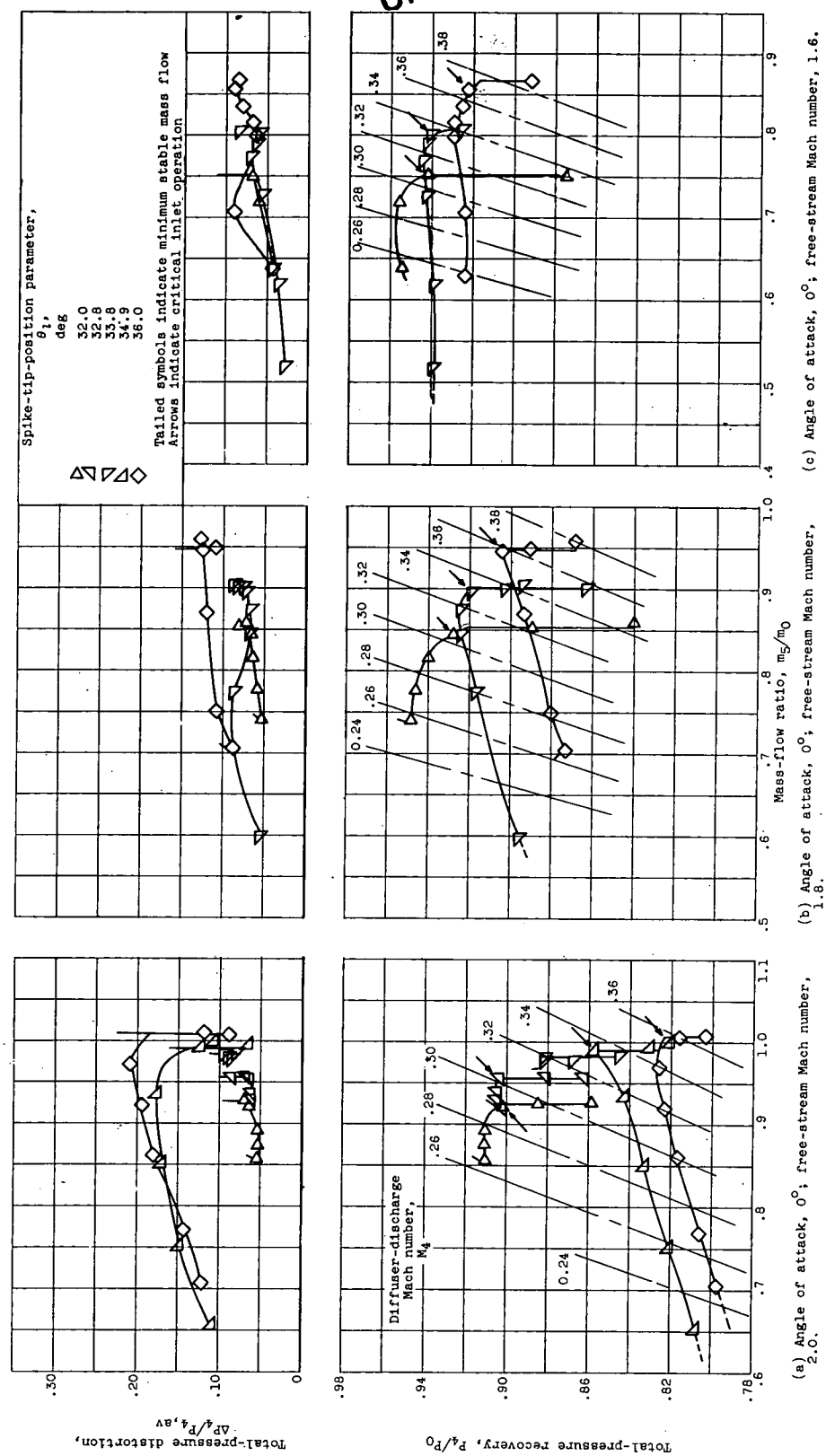
(e) Angle of attack, -5°; free-stream Mach number, 2.0.

(f) Angle of attack, -8°; free-stream Mach number, 2.0.

Figure 8. - Concluded. Performance of inlet $C_{17}S_b$.

UNCLASSIFIED

5007



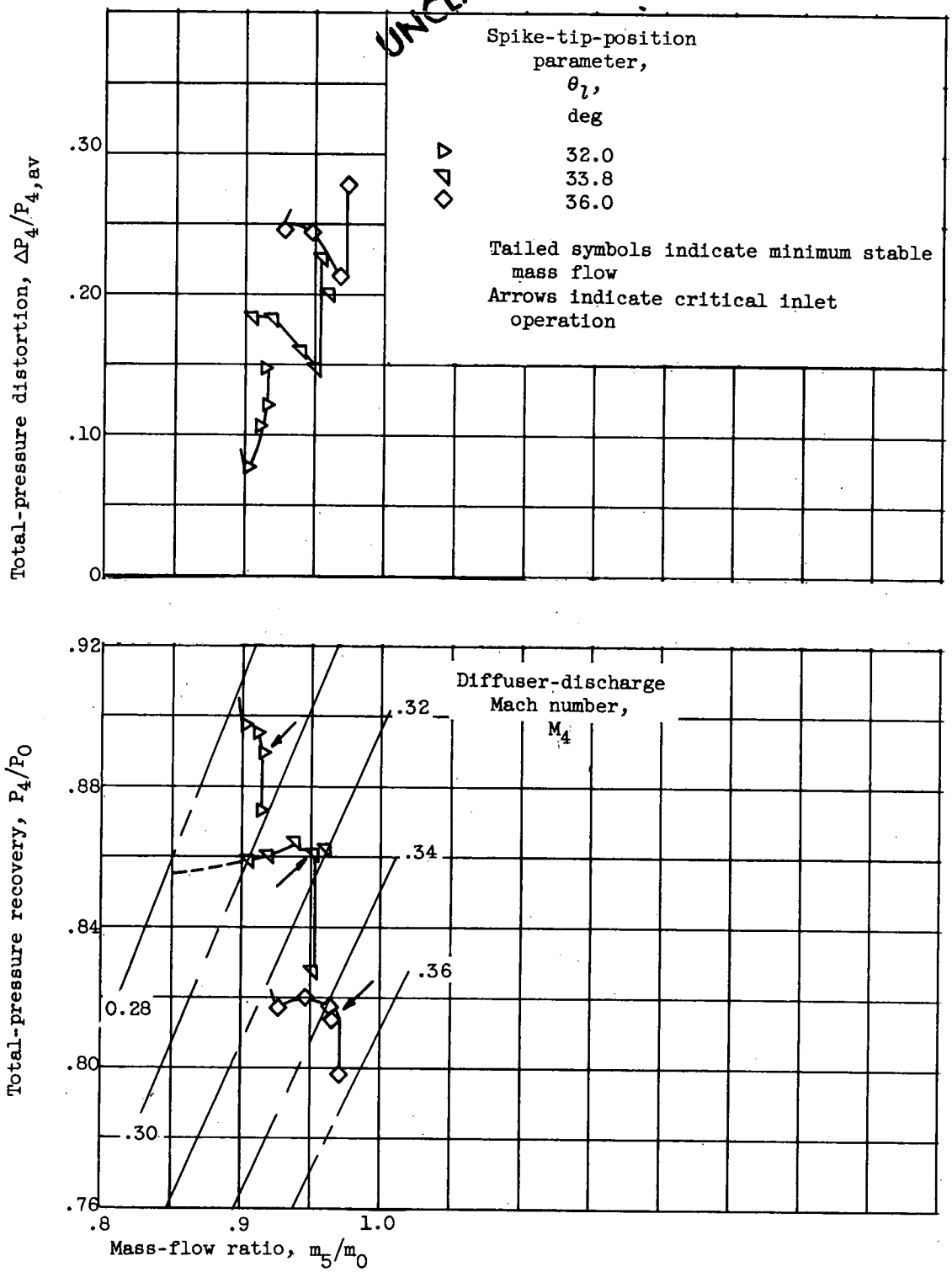
(a) Angle of attack, 0°; free-stream Mach number, 2.0.

(b) Angle of attack, 0°; free-stream Mach number, 1.8.

(c) Angle of attack, 0°; free-stream Mach number, 1.6.

Figure 9. - Performance of double-shock inlet $C_{14}S_{s,ds}$.

UNCLASSIFIED



(d) Angle of attack, -5°; free-stream Mach number, 2.0.

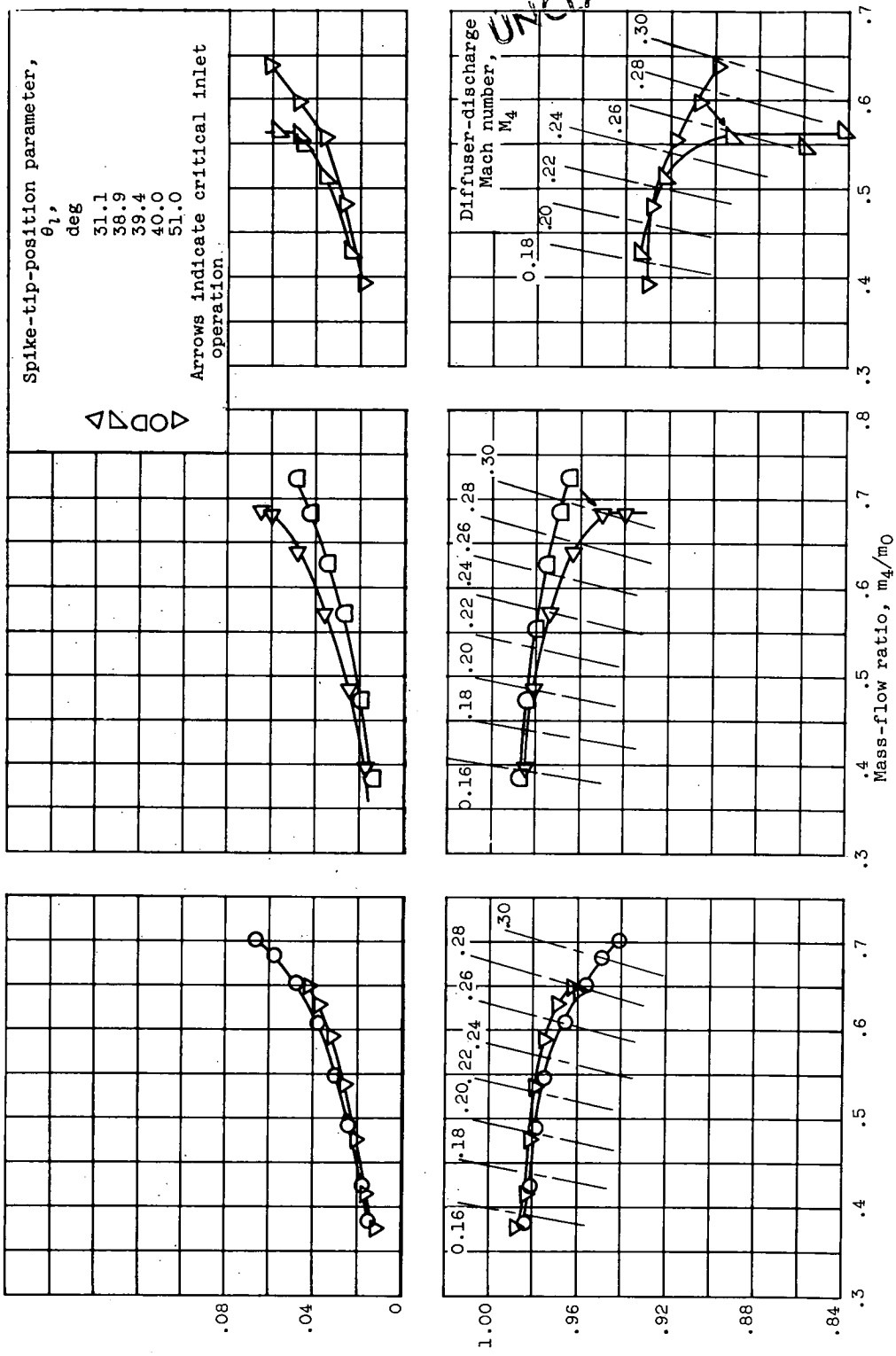
Figure 9. - Concluded. Performance of double-shock inlet $C_{l4}S_{s,ds}$.

5007

UNCLASSIFIED

5007

CR-5



(a) Inlet $C_{17}S_s$.

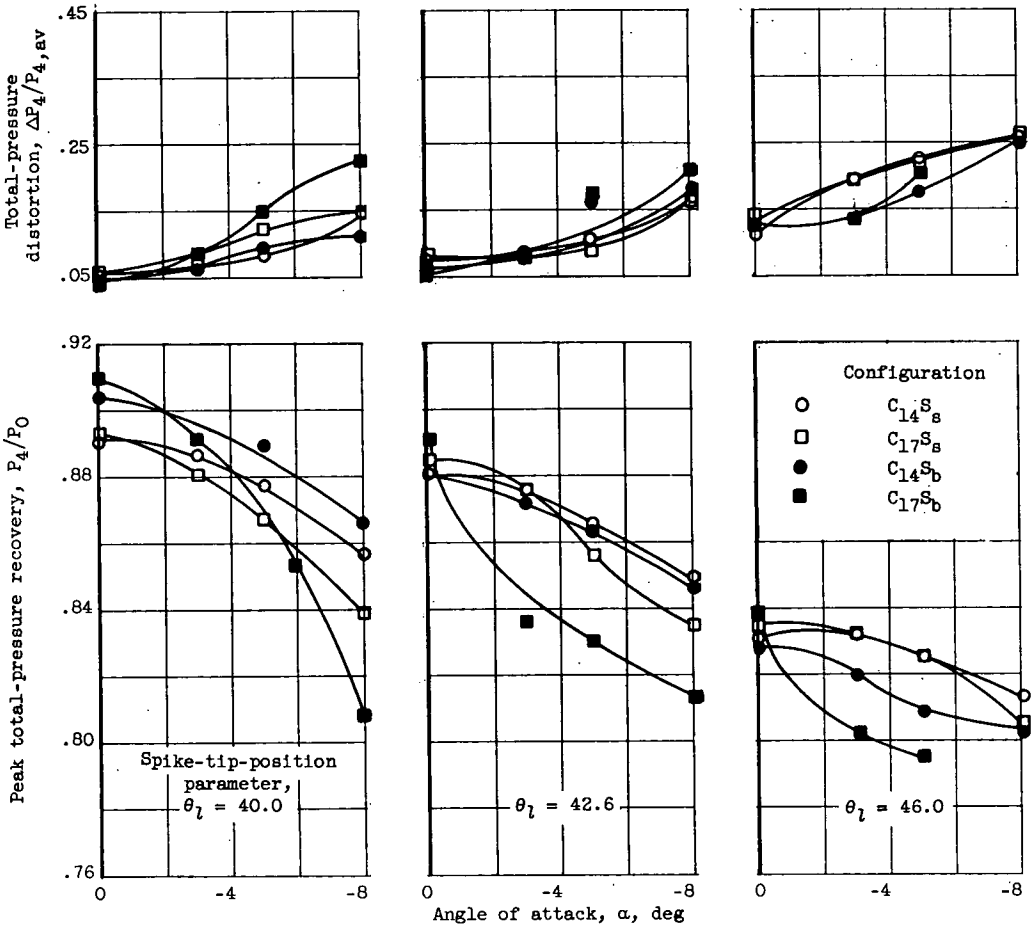
(b) Inlet $C_{14}S_s$,ds.

(c) Inlet $C_{14}S_b$.

Figure 10. - Subsonic performances of several inlets. Free-stream Mach number, 0.63.

UNCLASSIFIED

5007



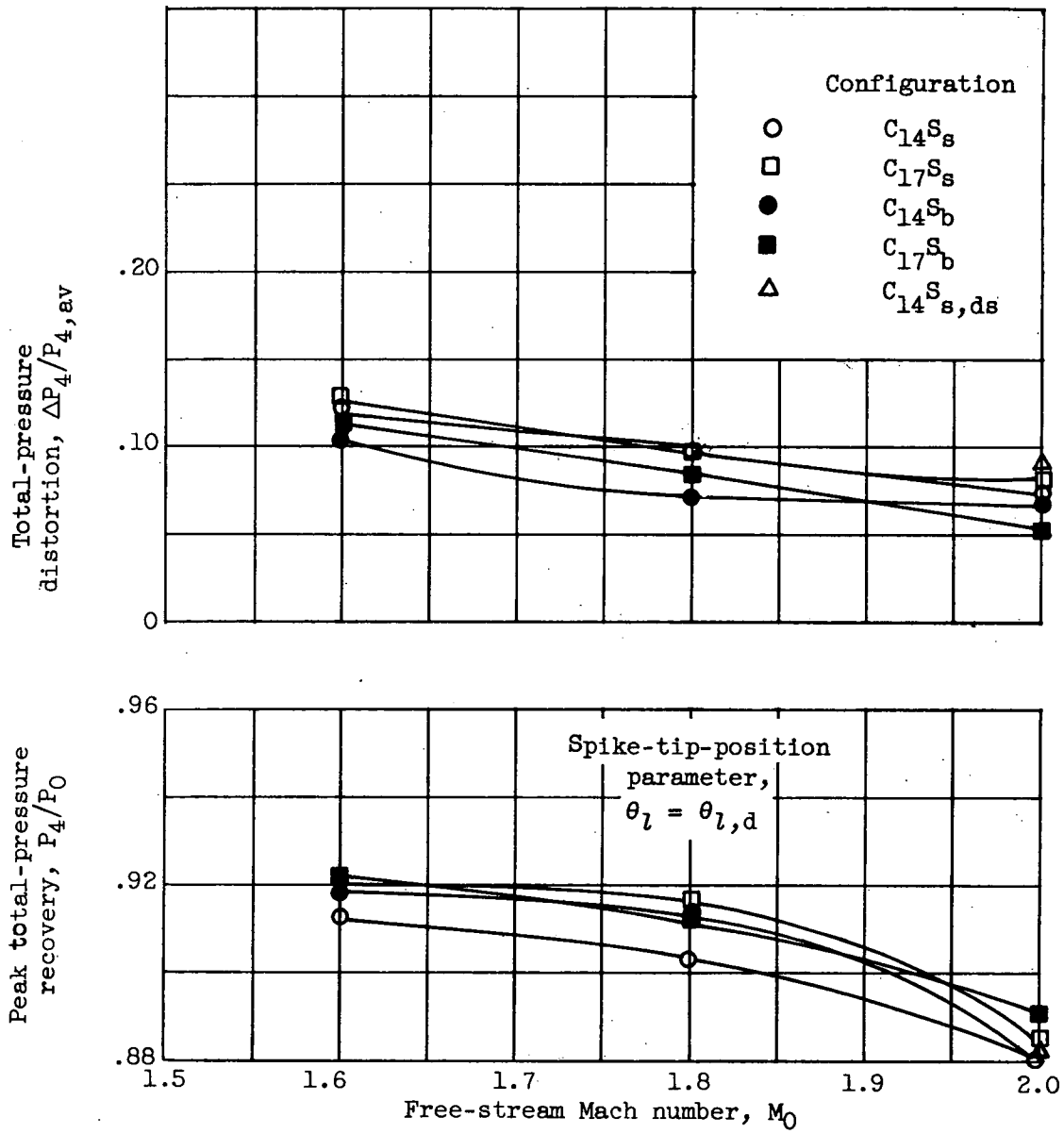
(a) Free-stream Mach number, 2.0.

Figure 11. - Performance comparison of various inlets at peak pressure recovery.

UNCLASSIFIED

5007

CR-5 back



(b) Angle of attack, 0°.

Figure 11. - Concluded. Performance comparison of various inlets at peak pressure recovery.

UNCLASSIFIED

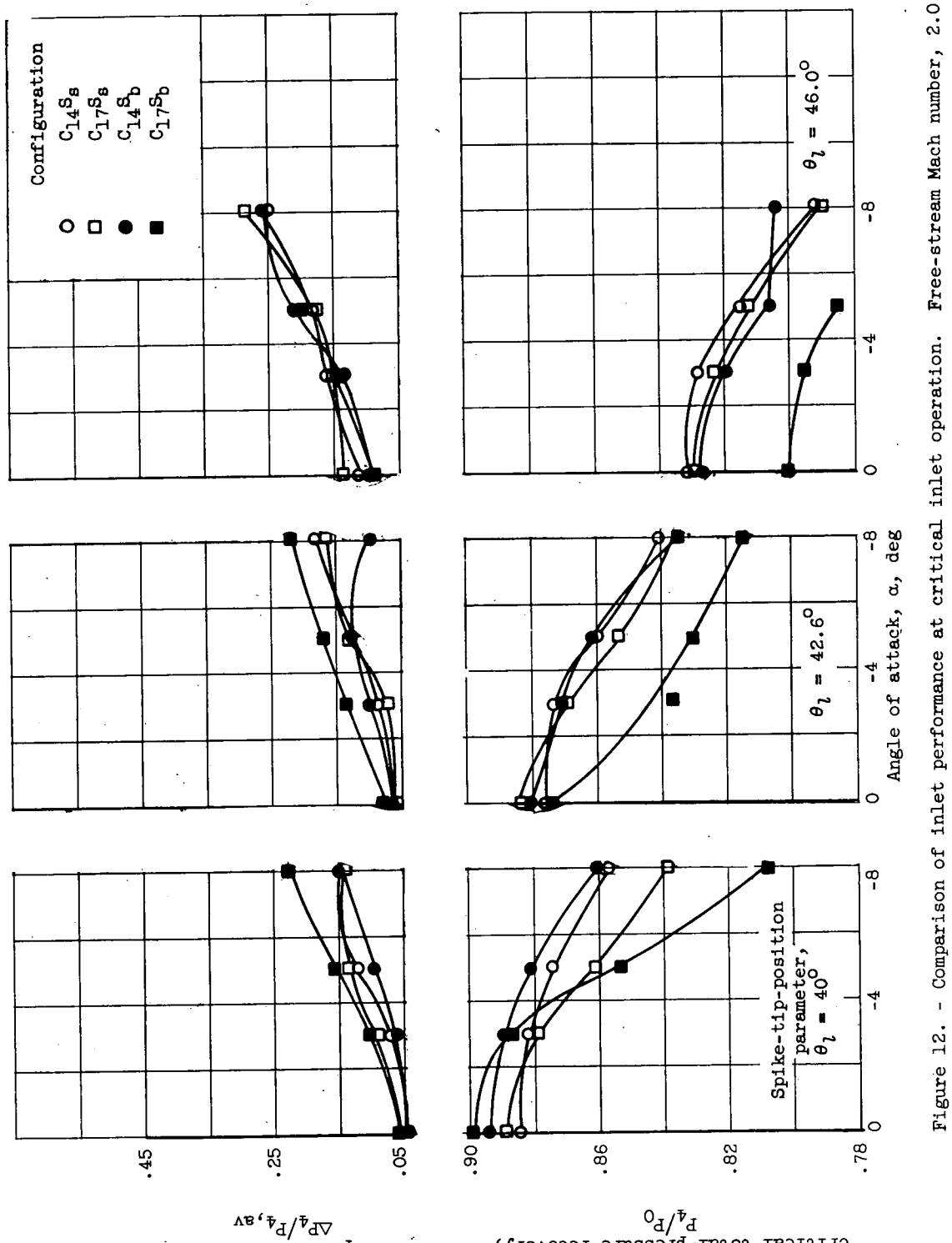
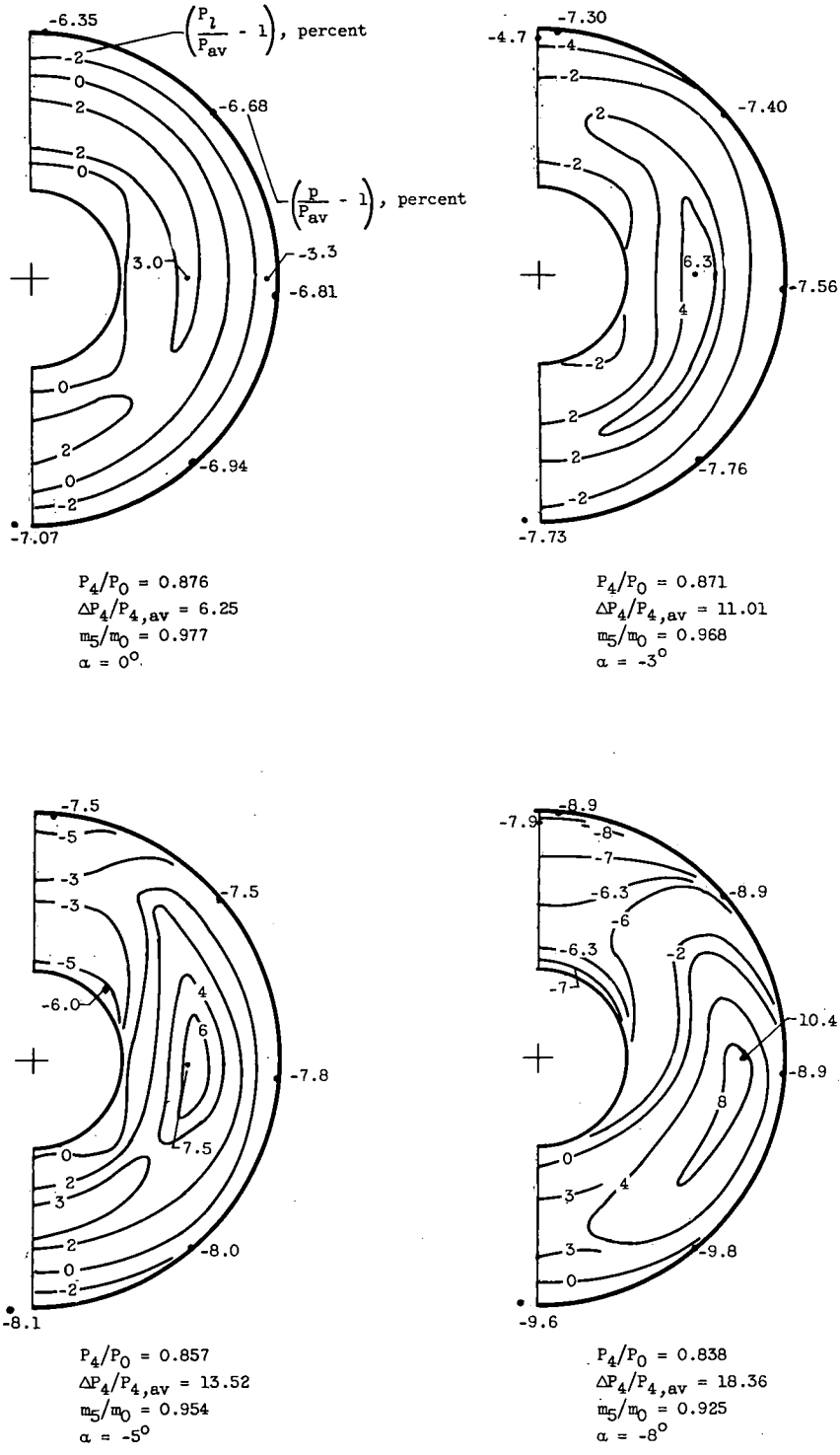


Figure 12. - Comparison of inlet performance at critical inlet operation. Free-stream Mach number, 2.0.

5007

UNCLASSIFIED

5007

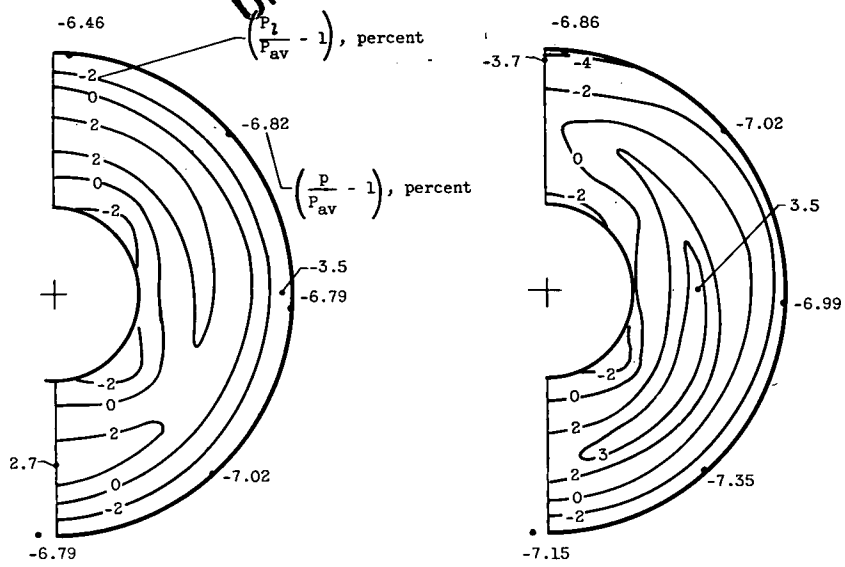


(a) Inlet $C_{14}S_s$.

Figure 13. - Total-pressure contours at station 58. Critical operation; spike-tip-position parameter, 42.6°; free-stream Mach number, 2.0.

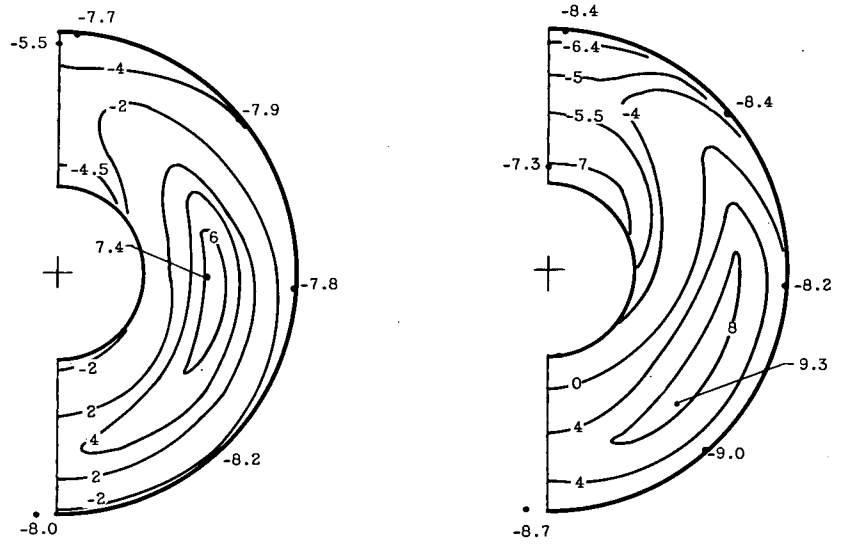
UNCLASSIFIED

5007



$P_4/P_0 = 0.884$
$\Delta P_4/P_{4,av} = 6.20$
$m_5/m_0 = 0.974$
$\alpha = 0^\circ$

$P_4/P_0 = 0.869$
$\Delta P_4/P_{4,av} = 7.3$
$m_5/m_0 = 0.963$
$\alpha = -3^\circ$



$P_4/P_0 = 0.853$
$\Delta P_4/P_{4,av} = 12.9$
$m_5/m_0 = 0.938$
$\alpha = -5^\circ$

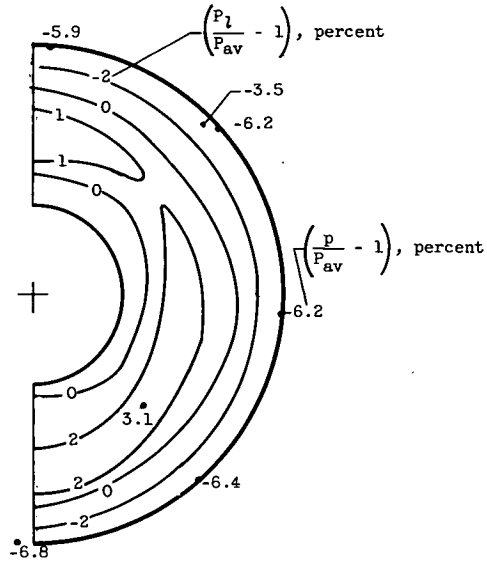
$P_4/P_0 = 0.835$
$\Delta P_4/P_{4,av} = 16.6$
$m_5/m_0 = 0.911$
$\alpha = -8^\circ$

(b) Inlet $C_{17}S_s$.

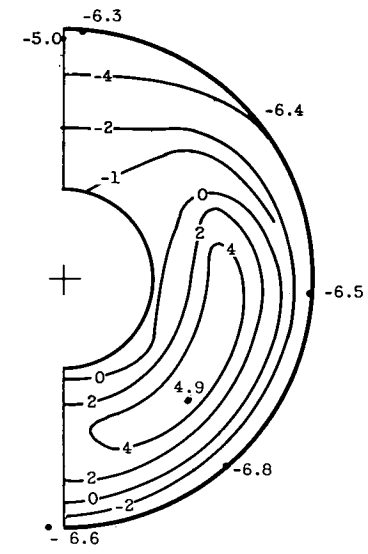
Figure 13. - Continued. Total-pressure contours at station 58. Critical operation; spike-tip-position parameter, 42.6°; free-stream Mach number, 2.0.

UNCLASSIFIED

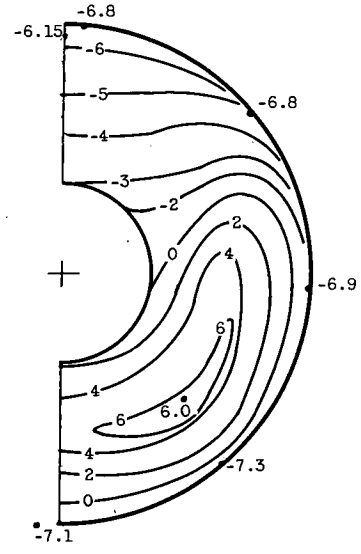
5007



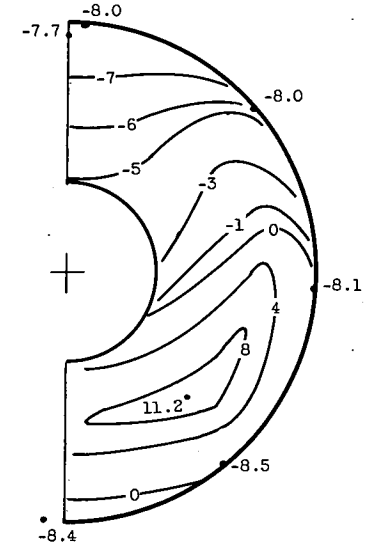
$P_4/P_0 = 0.881$
$\Delta P_4/P_{4,av} = 6.55$
$m_5/m_0 = 0.922$
$\alpha = 0^\circ$



$P_4/P_0 = 0.871$
$\Delta P_4/P_{4,av} = 9.94$
$m_5/m_0 = 0.894$
$\alpha = -3^\circ$



$P_4/P_0 = 0.861$
$\Delta P_4/P_{4,av} = 12.51$
$m_5/m_0 = 0.877$
$\alpha = -5^\circ$

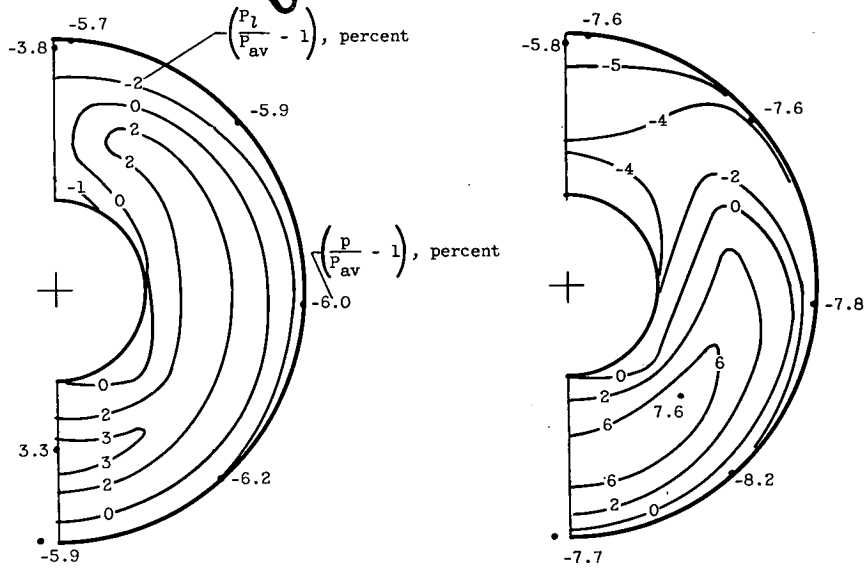


$P_4/P_0 = 0.845$
$\Delta P_4/P_{4,av} = 18.80$
$m_5/m_0 = 0.869$
$\alpha = -8^\circ$

(c) Inlet $C_{14}S_b$ with maximum bleed flow.

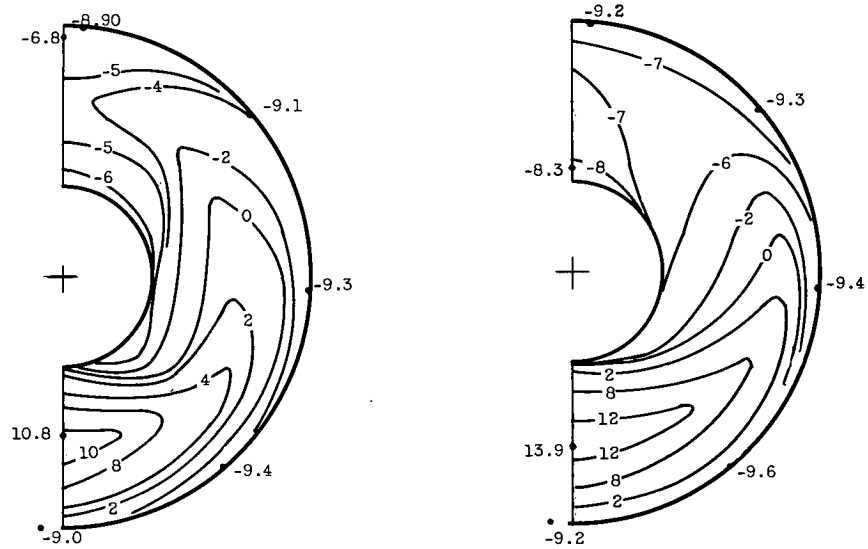
Figure 13. - Continued. Total-pressure contours at station 58. Critical operation; spike-tip-position parameter, 42.6°; free-stream Mach number, 2.0.

UNCLASSIFIED



$P_4/P_0 = 0.874$
$\Delta P_4/P_{4,av} = 7.12$
$m_5/m_0 = 0.898$
$\alpha = 0^\circ$

$P_4/P_0 = 0.836$
$\Delta P_4/P_{4,av} = 13.37$
$m_5/m_0 = 0.912$
$\alpha = -3^\circ$



$P_4/P_0 = 0.821$
$\Delta P_4/P_{4,av} = 17.55$
$m_5/m_0 = 0.930$
$\alpha = -5^\circ$

$P_4/P_0 = 0.813$
$\Delta P_4/P_{4,av} = 22.15$
$m_5/m_0 = 0.892$
$\alpha = -8^\circ$

(d) Inlet $C_{17}S_b$.

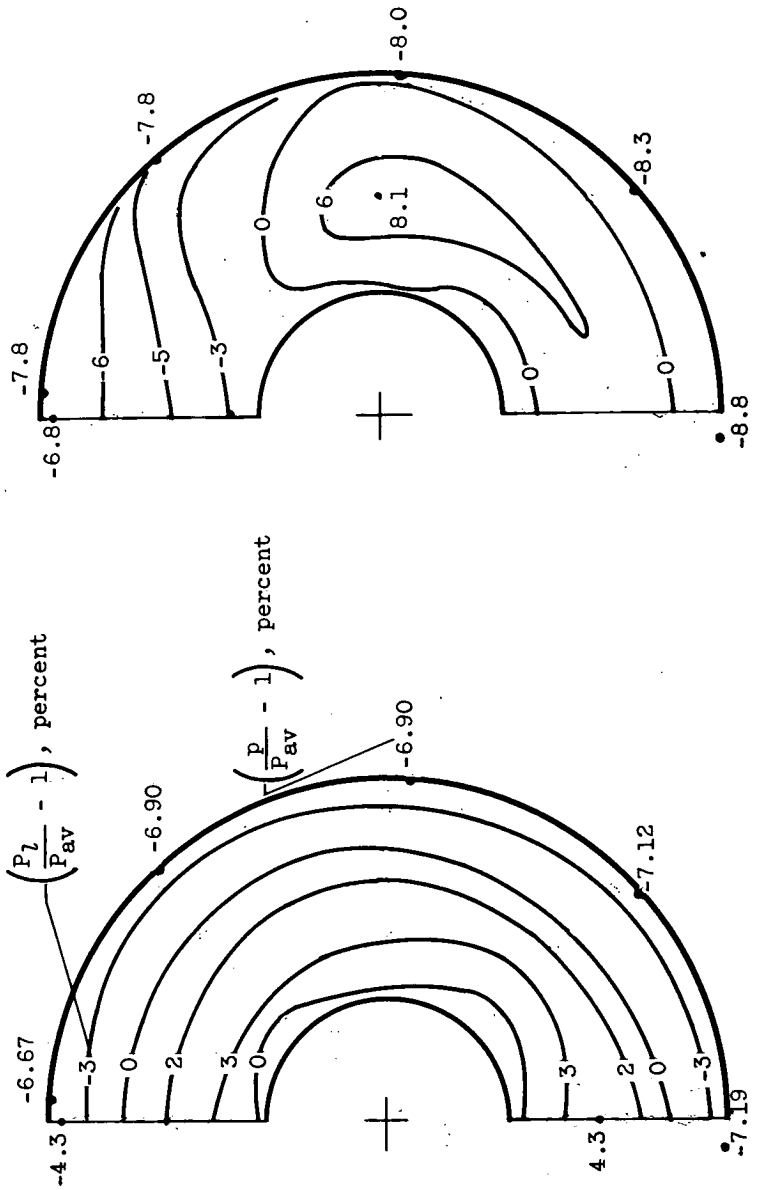
Figure 13. - Continued. Total-pressure contours at station 58. Critical operation; spike-tip-position parameter, 42.6°; free-stream Mach number, 2.0.

5007

UNCLASSIFIED

5007

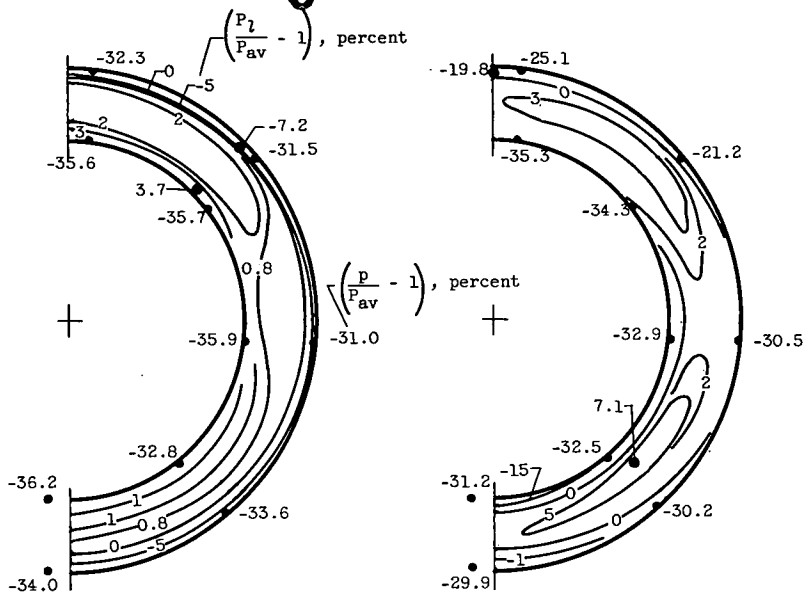
CR-6



(e) Inlet $C_{14}S_{s,ds}$.

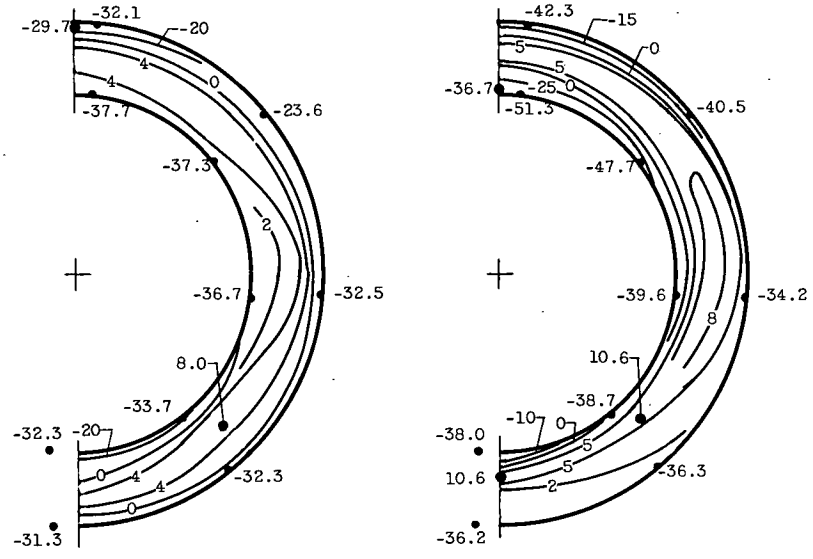
Figure 13. - Concluded. Total-pressure contours at station 58. Critical operation; spike-tip-position parameter, 42.6°; free-stream Mach number, 2.0.

UNCLASSIFIED



$P_l/P_0 = 0.910$
$\Delta P_l/P_{l,av} = 10.9$
$m_5/m_0 = 0.977$
$\alpha = 0^\circ$

$P_l/P_0 = 0.903$
$\Delta P_l/P_{l,av} = 26.9$
$m_5/m_0 = 0.965$
$\alpha = -3^\circ$



$P_l/P_0 = 0.895$
$\Delta P_l/P_{l,av} = 37.7$
$m_5/m_0 = 0.950$
$\alpha = -5^\circ$

$P_l/P_0 = 0.875$
$\Delta P_l/P_{l,av} = 47.3$
$m_5/m_0 = 0.918$
$\alpha = -8^\circ$

(a) Inlet $C_{14}S_s$. Spike-tip-position parameter, 42.6°.

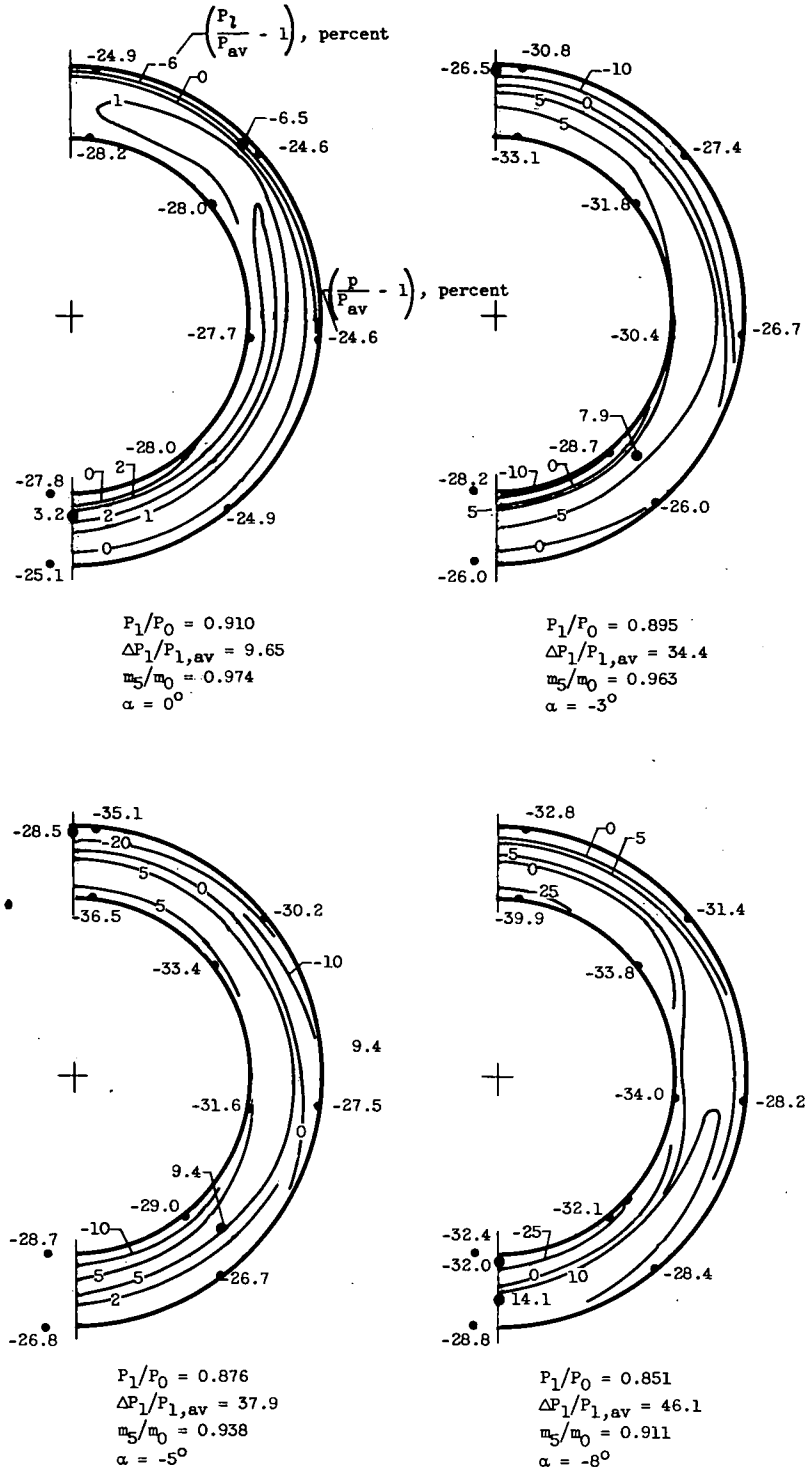
Figure 14. - Total-pressure contours at station 7.0. Free-stream Mach number, 2.0.

5007

UNCLASSIFIED

5007

CR-6 back



$P_l/P_0 = 0.910$
$\Delta P_l/P_{l,av} = 9.65$
$m_5/m_0 = 0.974$
$\alpha = 0^\circ$

$P_l/P_0 = 0.895$
$\Delta P_l/P_{l,av} = 34.4$
$m_5/m_0 = 0.963$
$\alpha = -3^\circ$

$P_l/P_0 = 0.876$
$\Delta P_l/P_{l,av} = 37.9$
$m_5/m_0 = 0.938$
$\alpha = -5^\circ$

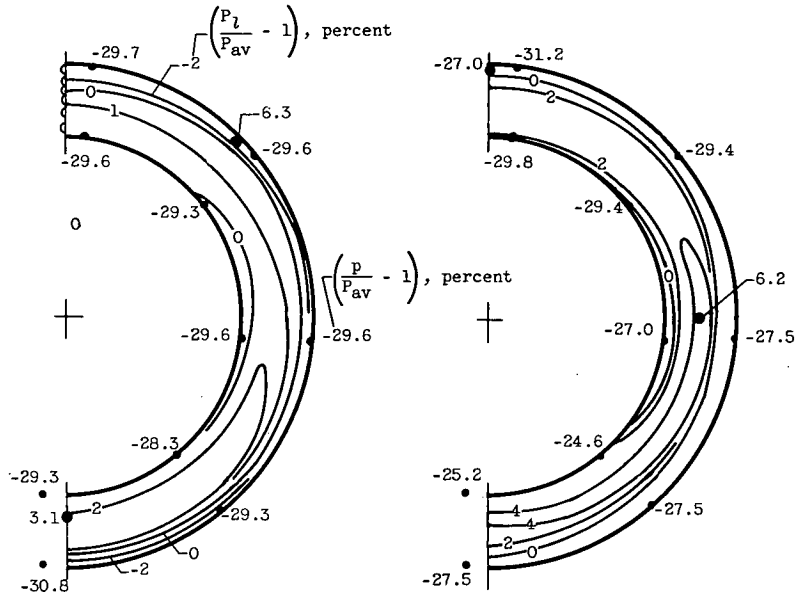
$P_l/P_0 = 0.851$
$\Delta P_l/P_{l,av} = 46.1$
$m_5/m_0 = 0.911$
$\alpha = -8^\circ$

(b) Inlet $C_{17}S_8$. Spike-tip-position parameter, 42.6°.

Figure 14. - Continued. Total-pressure contours at station 7.0. Free-stream Mach number, 2.0.

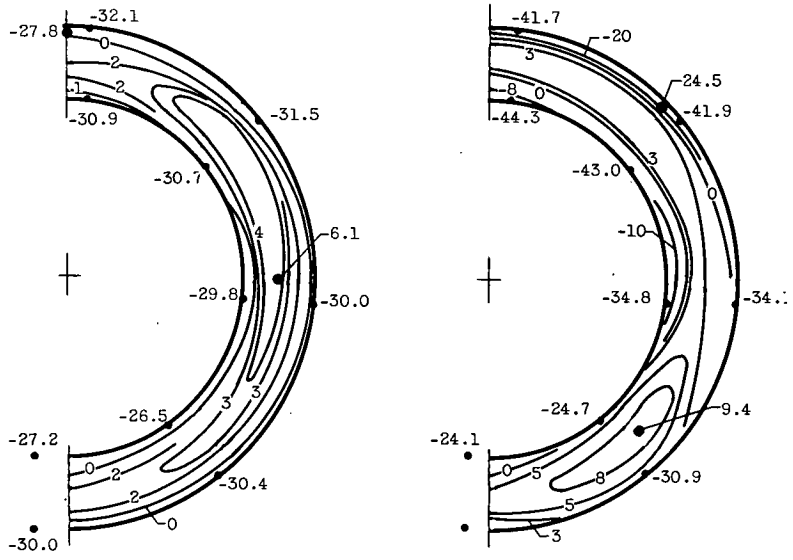
UNCLASSIFIED

5007



$P_l/P_0 = 0.912$
$\Delta P_l/P_{l,av} = 9.32$
$m_5/m_0 = 0.922$
$\alpha = 0^\circ$

$P_l/P_0 = 0.888$
$\Delta P_l/P_{l,av} = 33.5$
$m_5/m_0 = 0.894$
$\alpha = -3^\circ$



$P_l/P_0 = 0.887$
$\Delta P_l/P_{l,av} = 33.9$
$m_5/m_0 = 0.877$
$\alpha = -5^\circ$

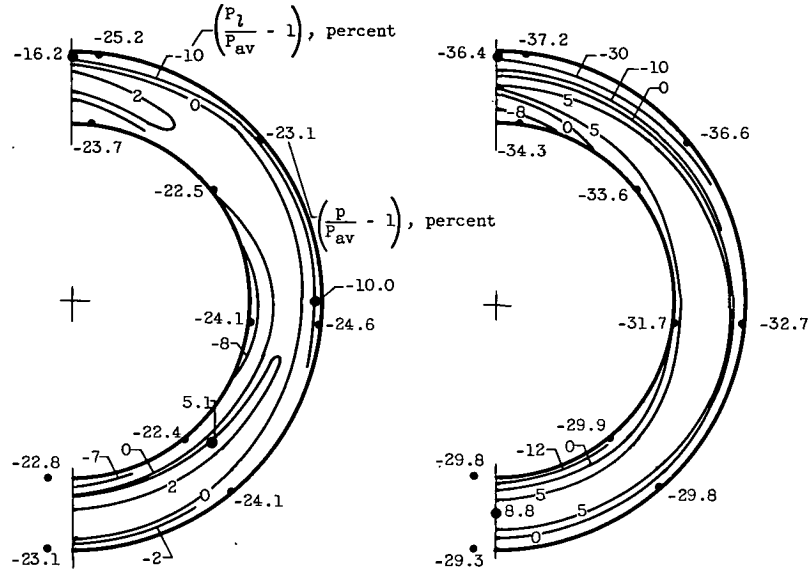
$P_l/P_0 = 0.871$
$\Delta P_l/P_{l,av} = 34.9$
$m_5/m_0 = 0.885$
$\alpha = -8^\circ$

(c) Inlet $C_{14}S_b$. Spike-tip-position parameter, 42.6°.

Figure 14. - Continued. Total-pressure contours at station 7.0. Free-stream Mach number, 2.0.

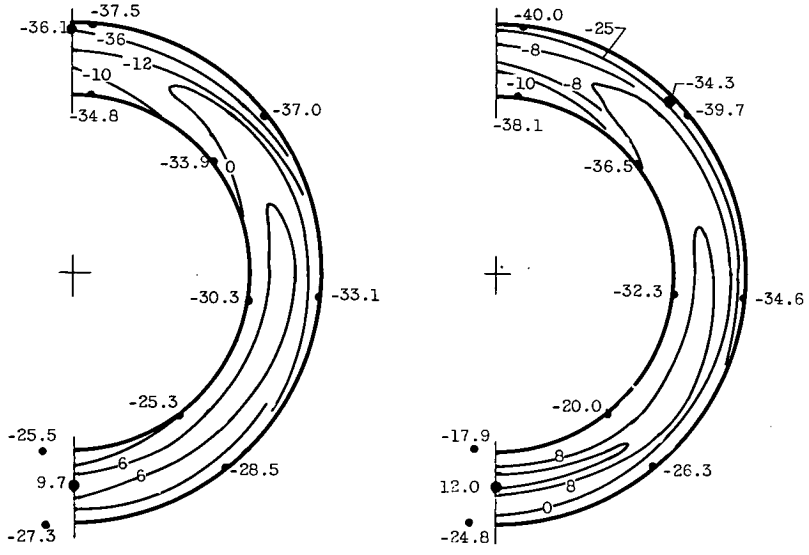
UNCLASSIFIED

5007



$P_l/P_0 = 0.914$
$\Delta P_l/P_{l,av} = 21.3$
$m_5/m_0 = 0.898$
$\alpha = 0^\circ$

$P_l/P_0 = 0.873$
$\Delta P_l/P_{l,av} = 45.2$
$m_5/m_0 = 0.912$
$\alpha = -3^\circ$



$P_l/P_0 = 0.877$
$\Delta P_l/P_{l,av} = 45.8$
$m_5/m_0 = 0.908$
$\alpha = -5^\circ$

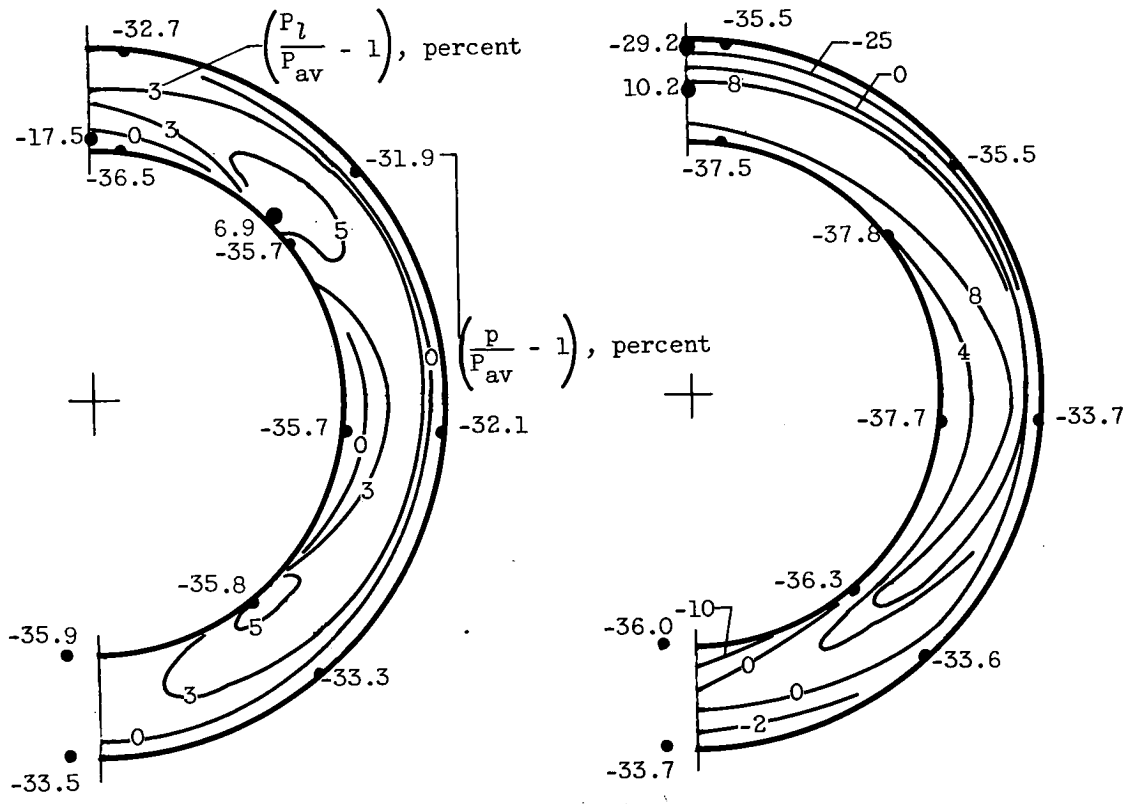
$P_l/P_0 = 0.862$
$\Delta P_l/P_{l,av} = 46.9$
$m_5/m_0 = 0.892$
$\alpha = -8^\circ$

(d) Inlet $C_{17}S_b$. Spike-tip-position parameter, 42.6°.

Figure 14. - Continued. Total-pressure contours at station 7.0. Free-stream Mach number, 2.0.

UNCLASSIFIED

5007



$P_1/P_0 = 0.910$
$\Delta P_1/P_{1,av} = 24.4$
$m_5/m_0 = 0.977$
$\alpha = 0^\circ$

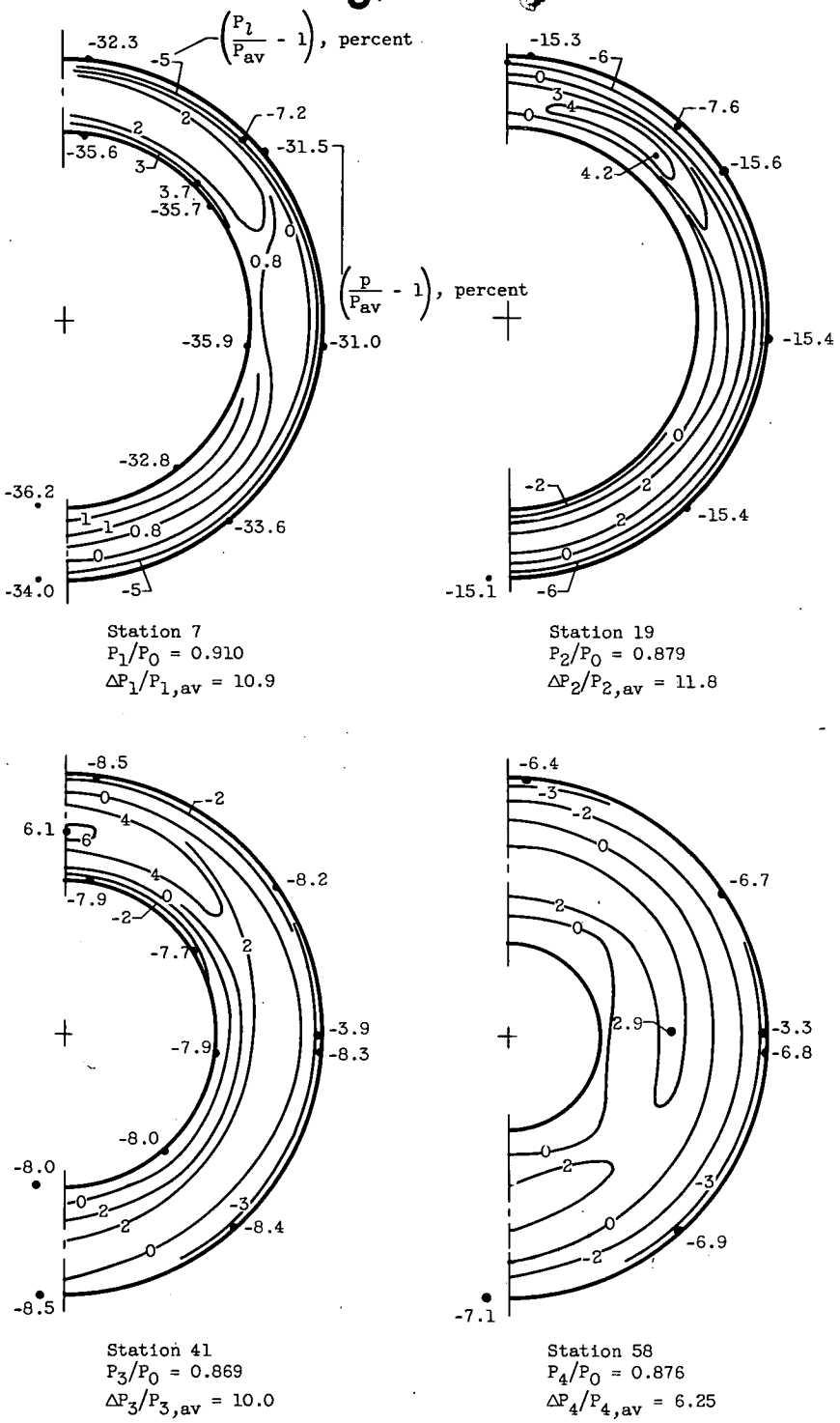
$P_1/P_0 = 0.892$
$\Delta P_1/P_{1,av} = 39.4$
$m_5/m_0 = 0.953$
$\alpha = -5^\circ$

(e) Inlet $C_{14}S_{s,ds}$. Spike-tip-position parameter, 33.8°.

Figure 14. - Concluded. Total-pressure contours at station 7.0. Free-stream Mach number, 2.0.

UNCLASSIFIED

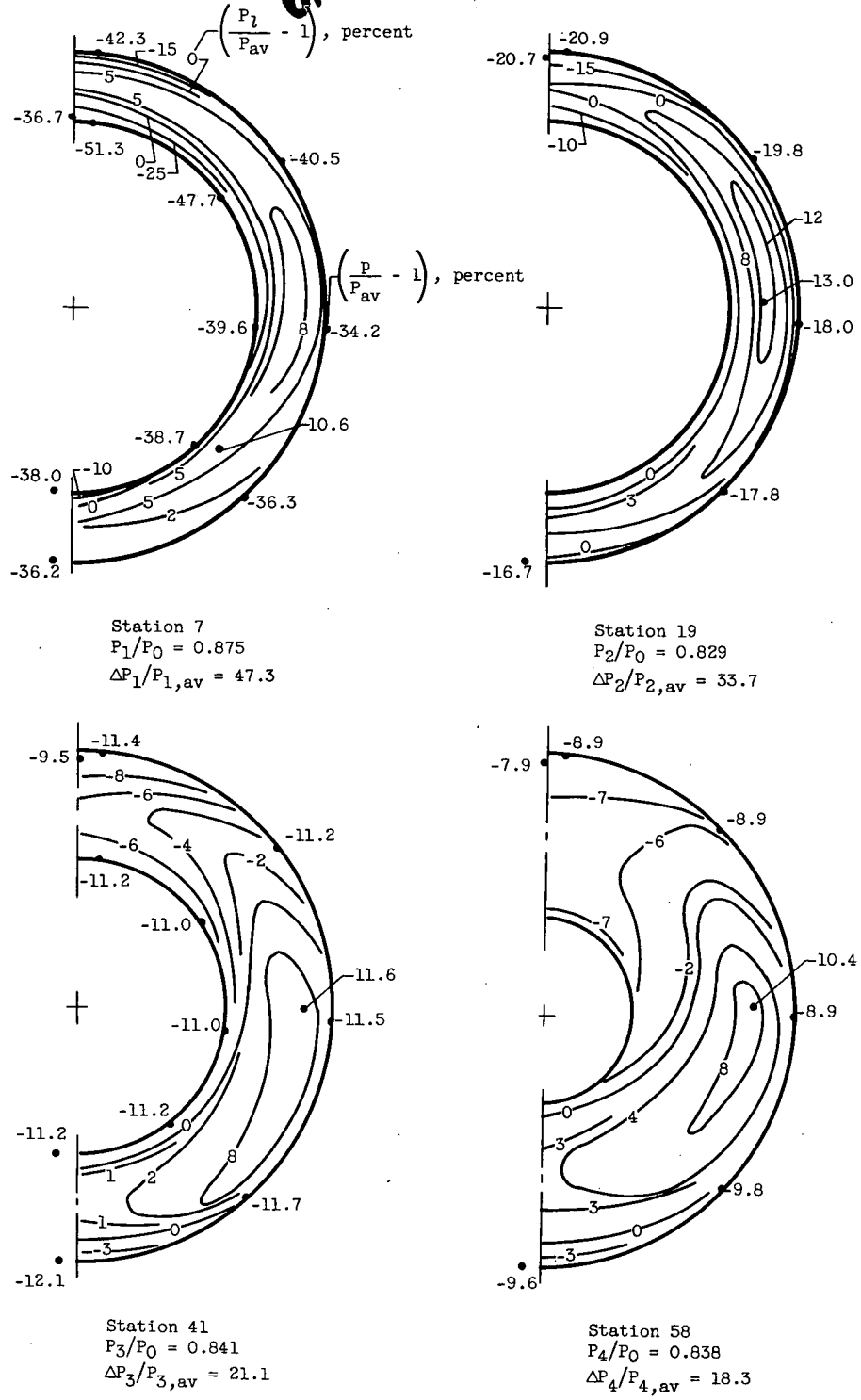
5007



(a) Inlet $C_{14}S_8$. Free-stream Mach number, 2.0; angle of attack, 0°; mass-flow ratio, 0.977.

Figure 15. - Total-pressure contour development.

UNCLASSIFIED



Station 7
$P_1/P_0 = 0.875$
$\Delta P_1/P_{1,av} = 47.3$

Station 19
$P_2/P_0 = 0.829$
$\Delta P_2/P_{2,av} = 33.7$

Station 41
$P_3/P_0 = 0.841$
$\Delta P_3/P_{3,av} = 21.1$

Station 58
$P_4/P_0 = 0.838$
$\Delta P_4/P_{4,av} = 18.3$

(b) Inlet $C_{14}S_8$. Free-stream Mach number, 2.0; angle of attack, -8°; mass-flow ratio, 0.918.

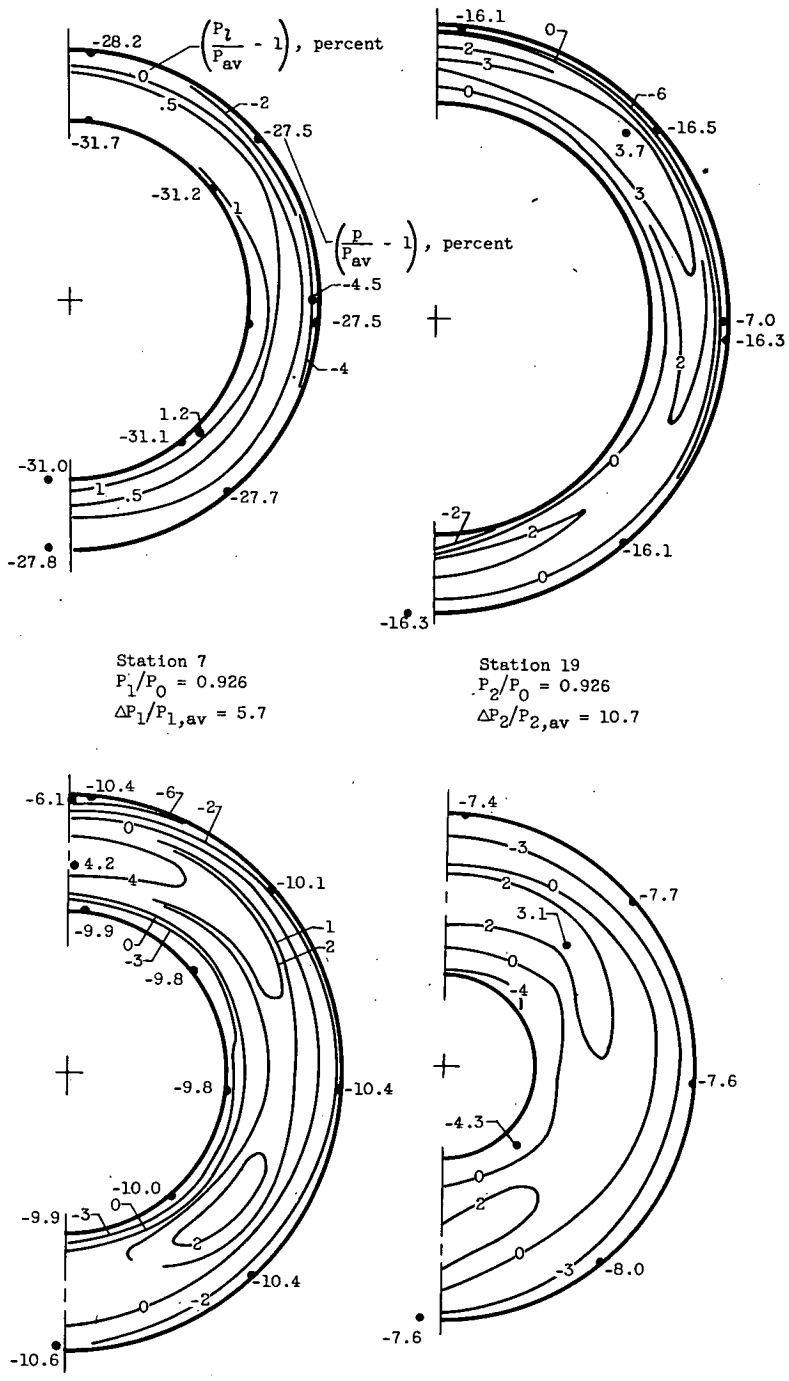
Figure 15. - Continued. Total-pressure contour development.

5007

UNCLASSIFIED

5007

CR-7



Station 7
$P_1/P_0 = 0.926$
$\Delta P_1/P_{1,av} = 5.7$

Station 19
$P_2/P_0 = 0.926$
$\Delta P_2/P_{2,av} = 10.7$

Station 41
$P_3/P_0 = 0.924$
$\Delta P_3/P_{3,av} = 10.3$

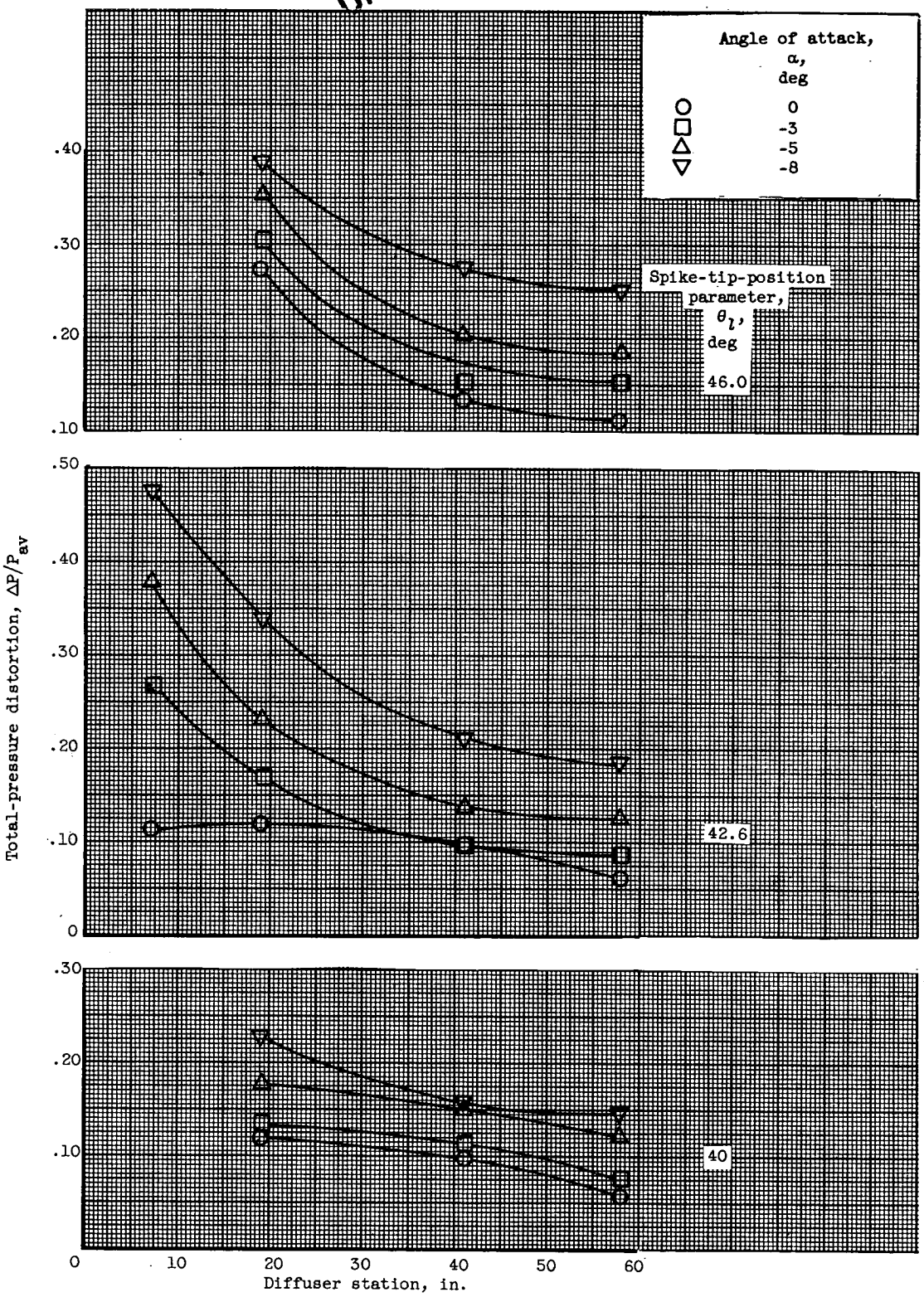
Station 58
$P_4/P_0 = 0.930$
$\Delta P_4/P_{4,av} = 7.4$

(c) Inlet $C_{17}S_8$. Free-stream Mach number, 1.8; angle of attack, 0°; mass-flow ratio, 0.974.

Figure 15. - Concluded. Total-pressure contour development.

UNCLASSIFIED

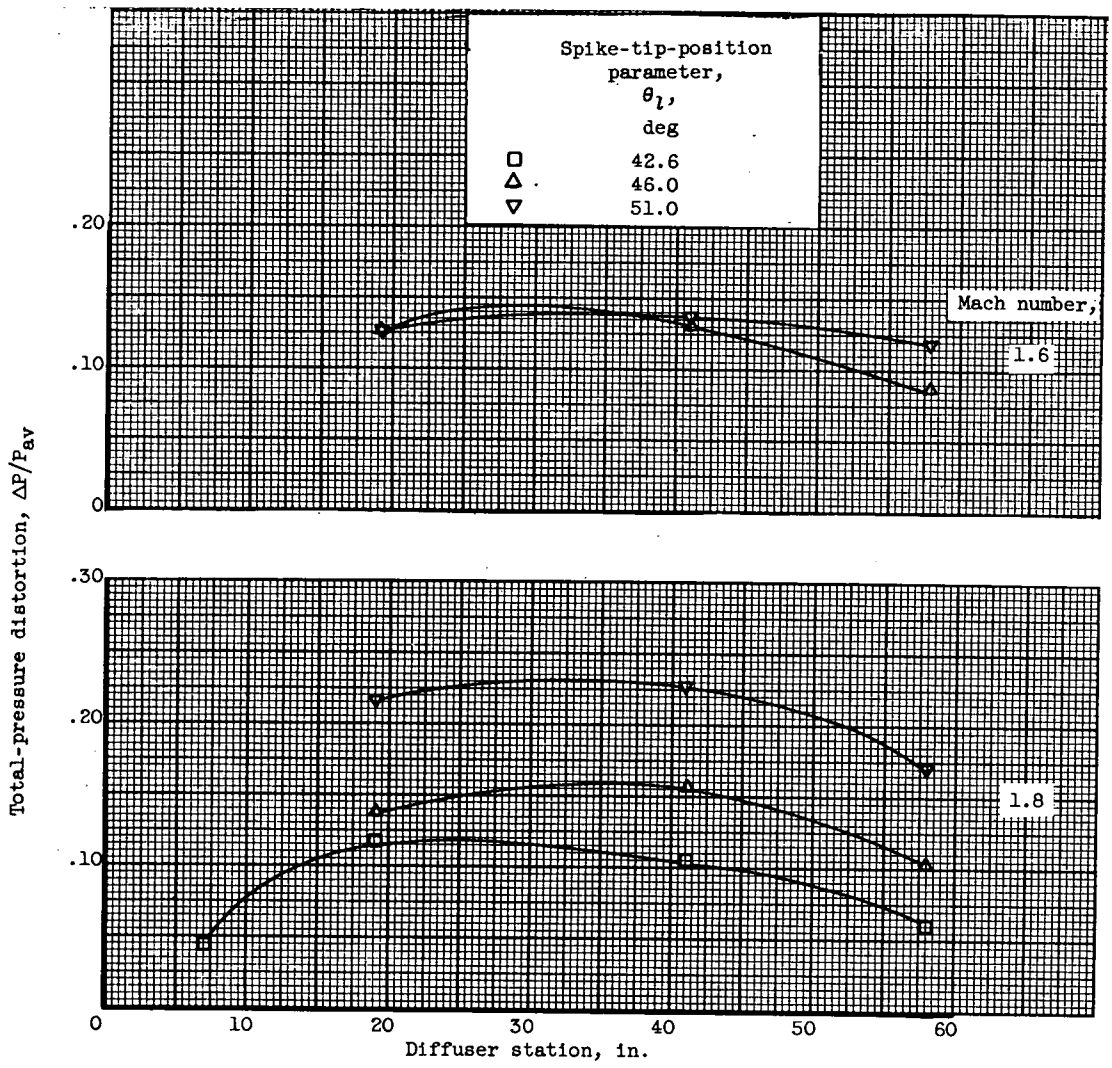
5007



(a) Mach number, 2.0.

Figure 16. - Distortion in diffuser duct of inlet $C_{14}S_s$ for critical inlet operation.

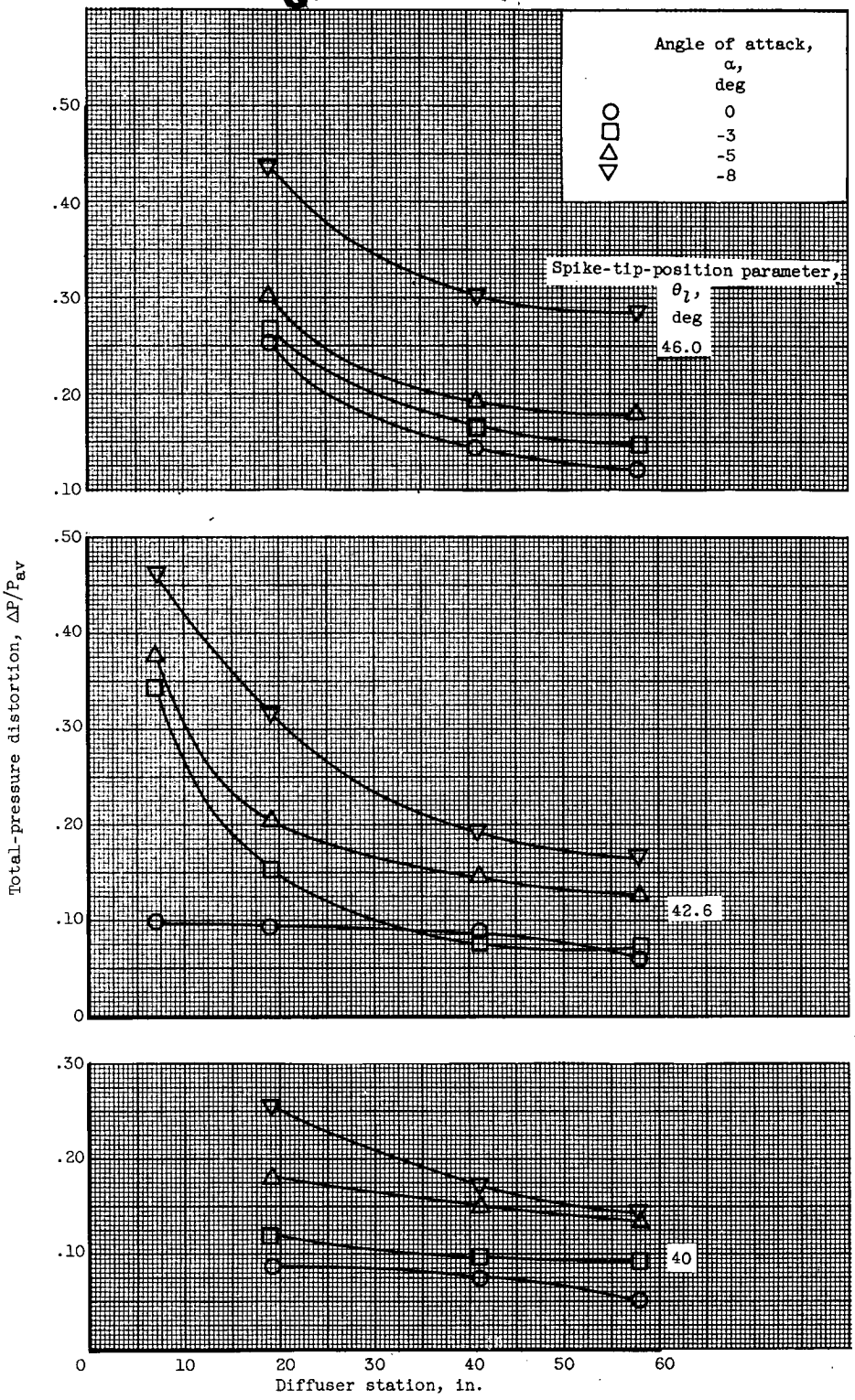
UNCLASSIFIED



(b) Reduced Mach number; angle of attack, 0°.

Figure 16. - Concluded. Distortion in diffuser duct of inlet $C_{14}S_s$ for critical inlet operation.

UNCLASSIFIED



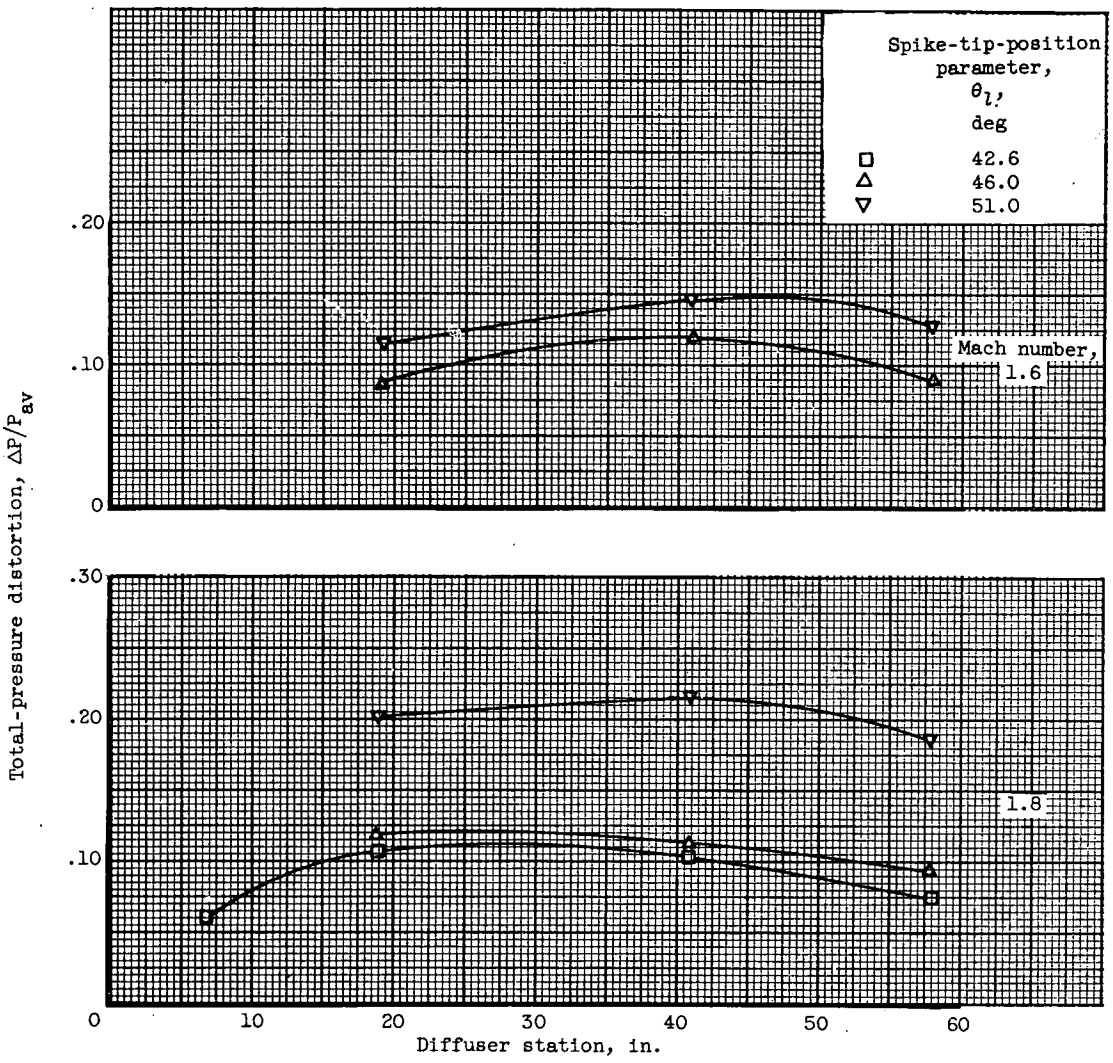
(a) Mach number, 2.0.

Figure 17. - Distortion in diffuser duct of inlet $C_{17}S_8$ for critical inlet operation.

5007

UNCLASSIFIED

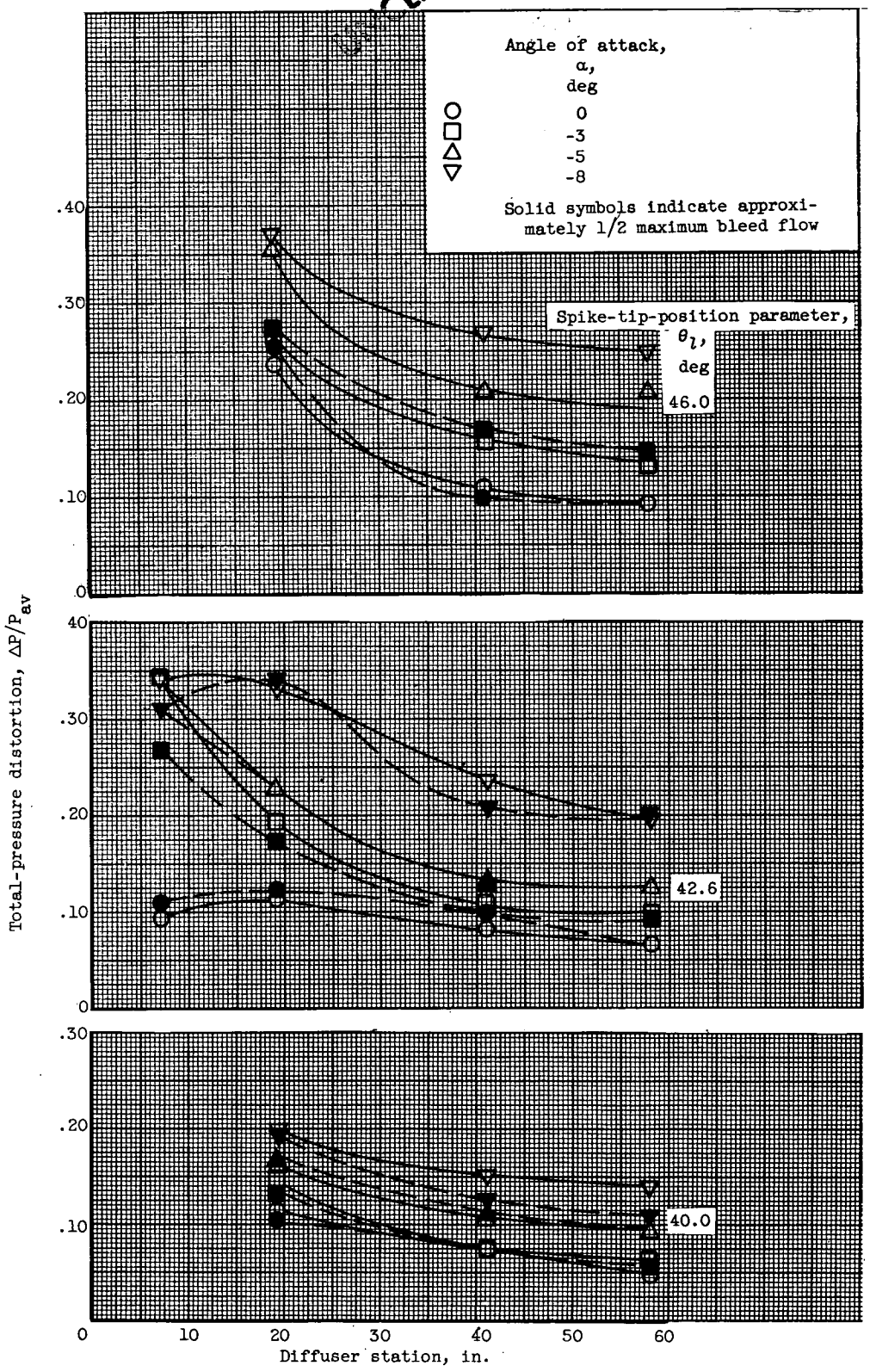
5007



(b) Reduced Mach number; angle of attack, 0°.

Figure 17. - Concluded. Distortion in diffuser duct of $C_{17}S_8$ inlet for critical inlet operation.

CLASSIFIED



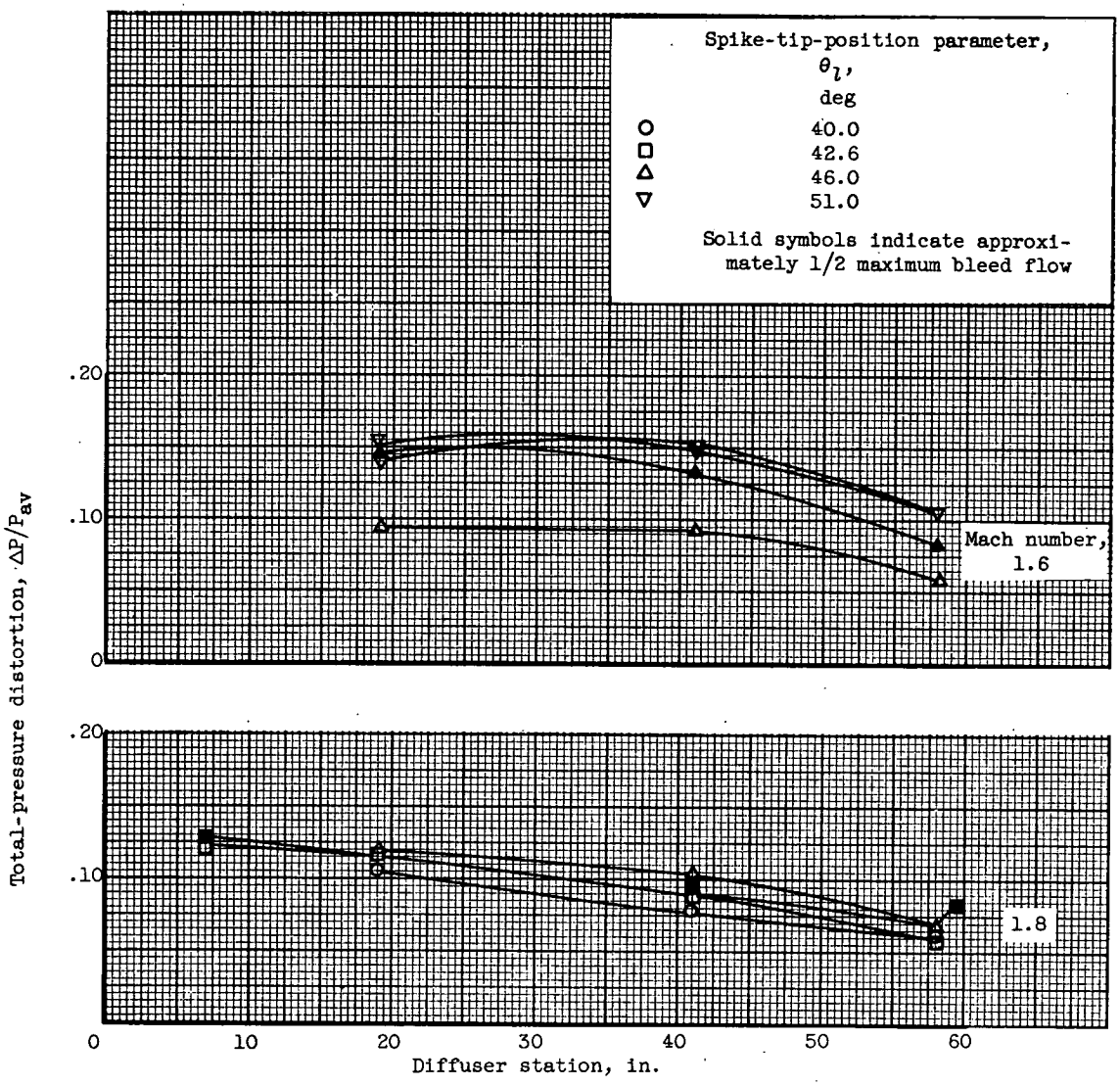
(a) Mach number, 2.0.

Figure 18. - Distortion in diffuser duct of inlet $C_{14}S_b$ for critical inlet operation.

5007

UNCLASSIFIED

5007

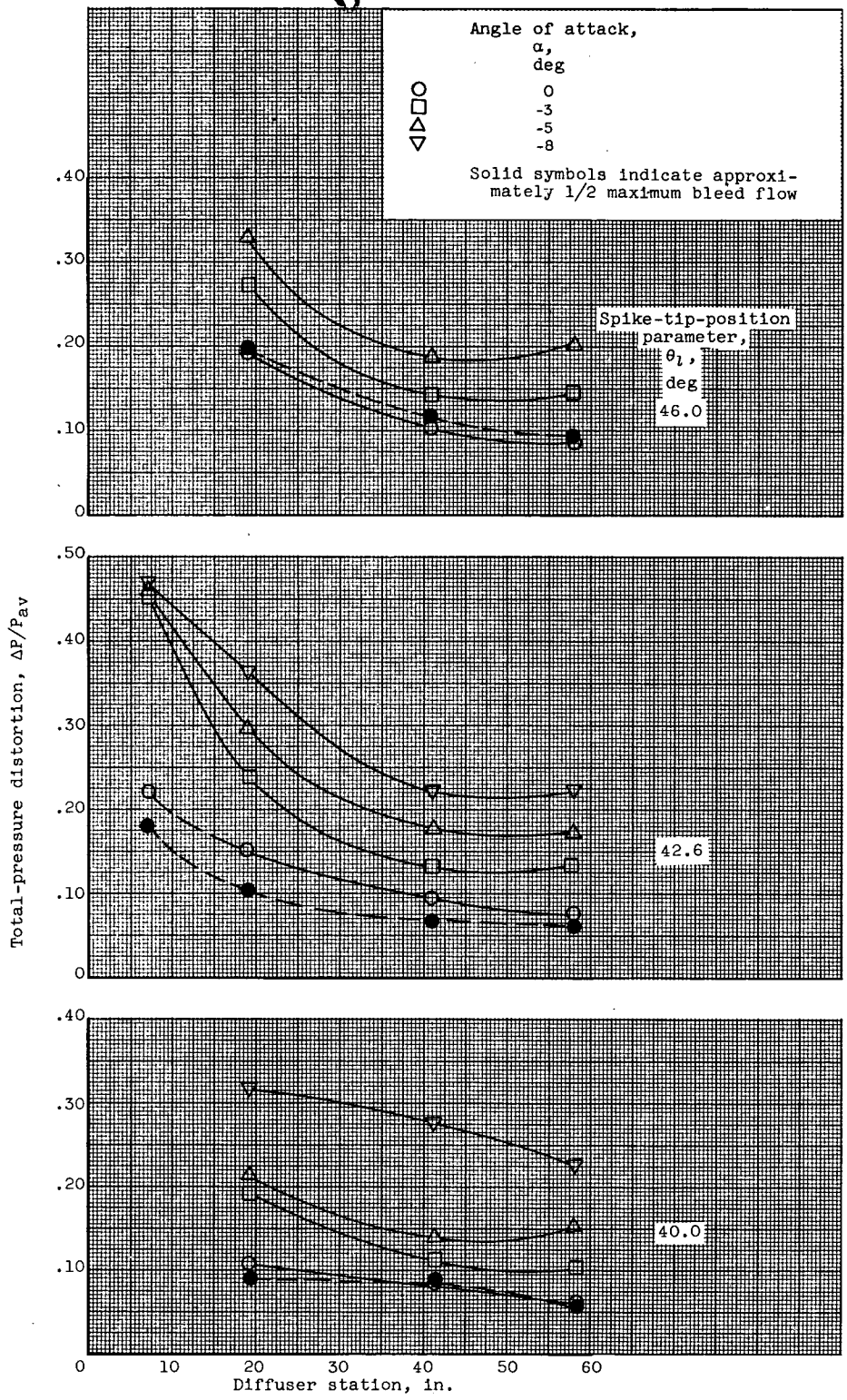


(b) Reduced Mach number; angle of attack, 0°.

Figure 18. - Concluded. Distortion in diffuser duct of inlet $C_{14}S_b$ for critical inlet operation.

UNCLASSIFIED

5007



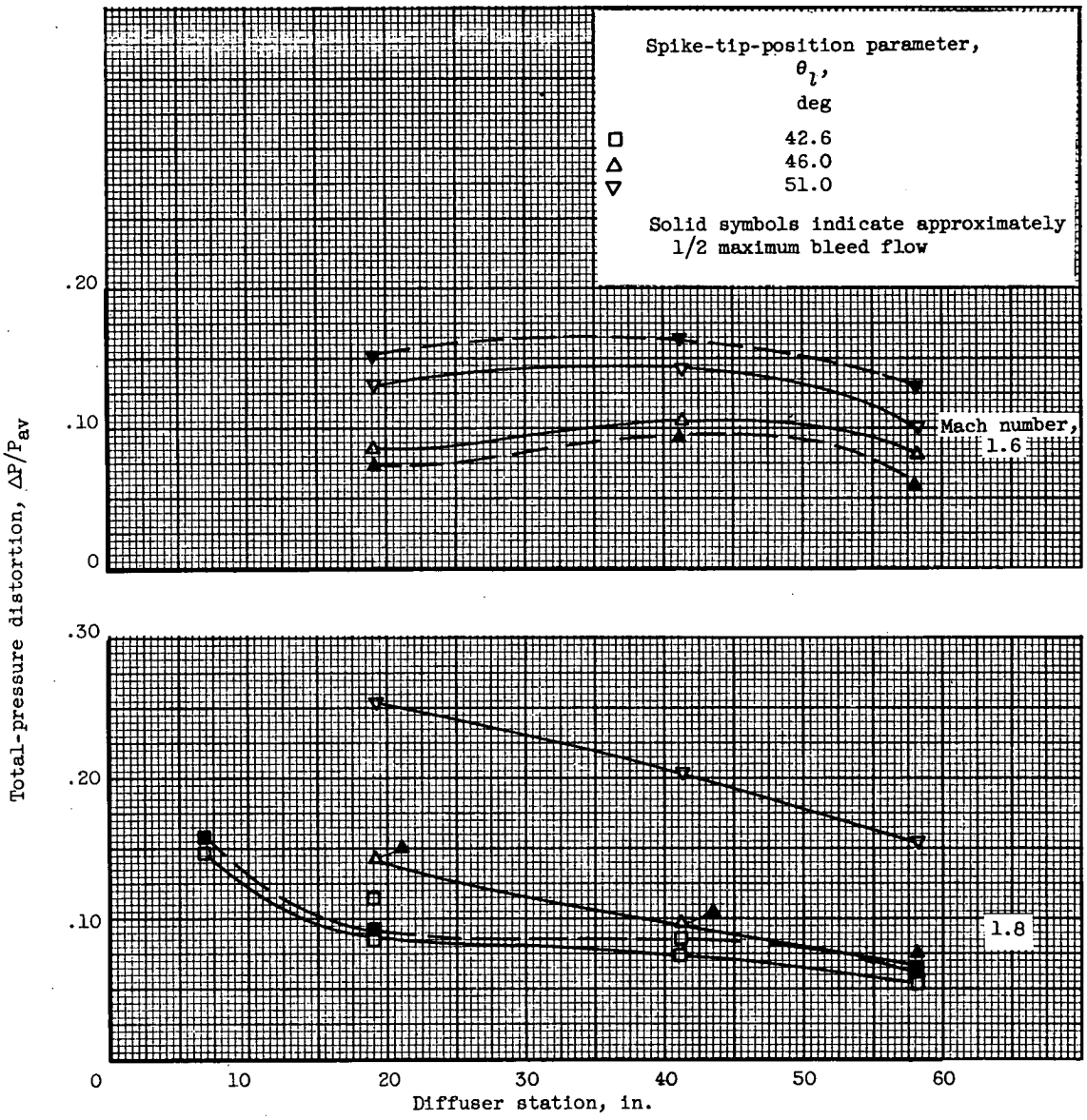
(a) Mach number, 2.0.

Figure 19. - Distortion in diffuser duct of inlet $C_{17}S_b$ for critical inlet operation.

UNCLASSIFIED

5007

CR-8



(b) Reduced Mach number; angle of attack, 0°.

Figure 19. - Concluded. Distortion in diffuser duct of inlet $C_{17}S_b$ for critical inlet operation.

UNCLASSIFIED

5007

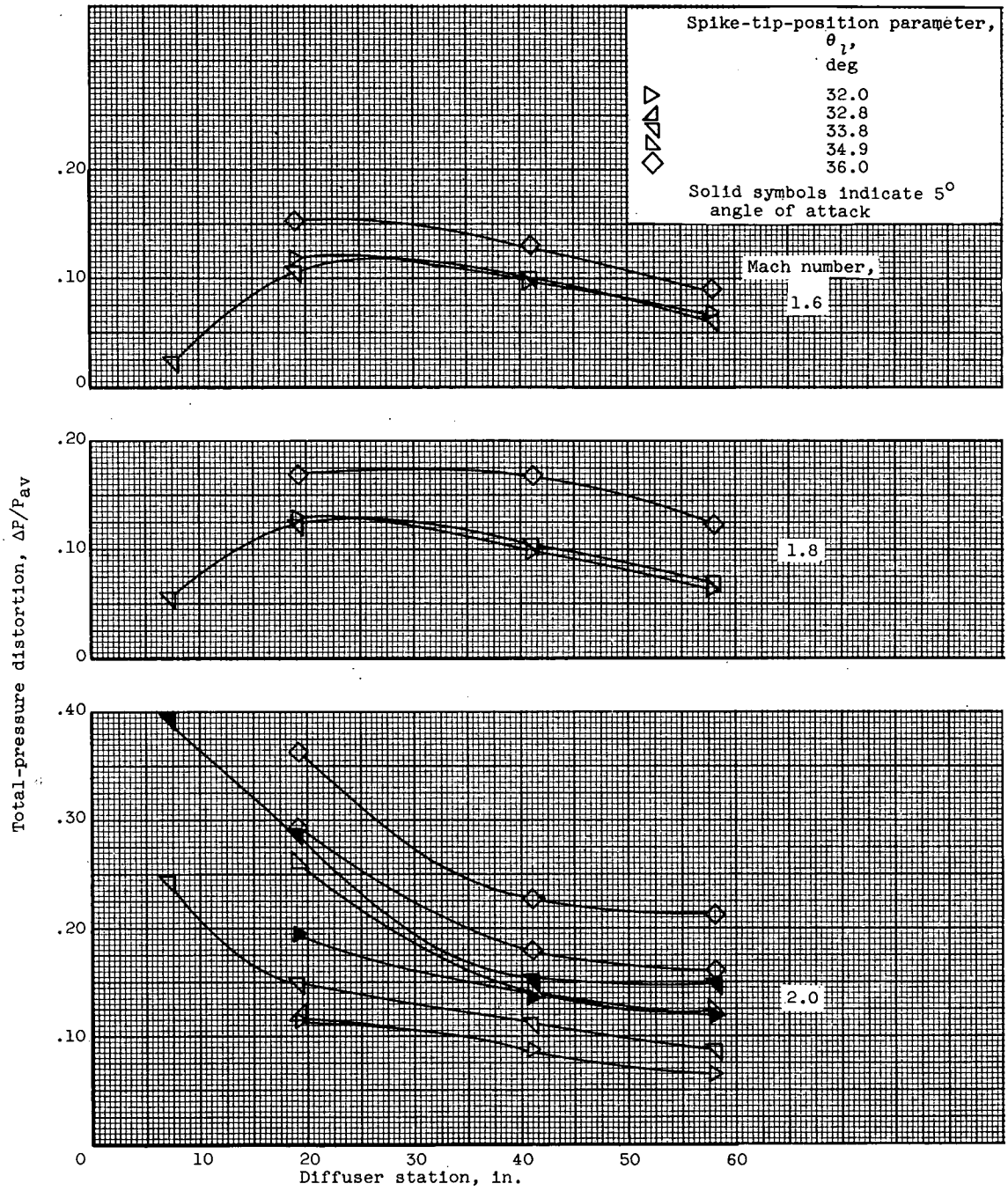


Figure 20. - Distortion in diffuser duct of inlet $C_{14}S_{8,ds}$ for critical inlet operation.

UNCLASSIFIED

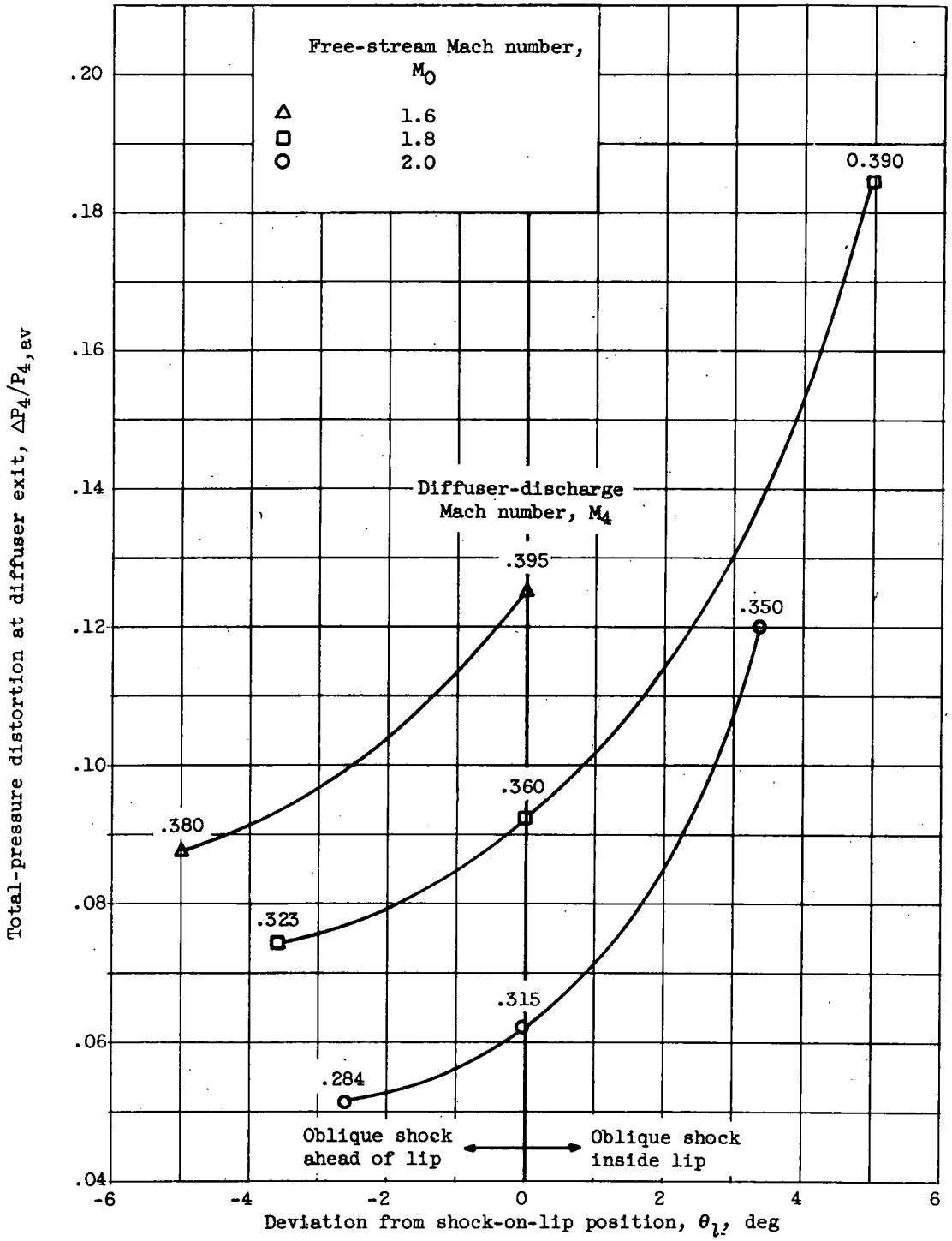


Figure 21. - Effect of oblique-shock location on distortion at diffuser exit. Inlet $C_{17}S_8$; angle of attack, 0°.

UNCLASSIFIED

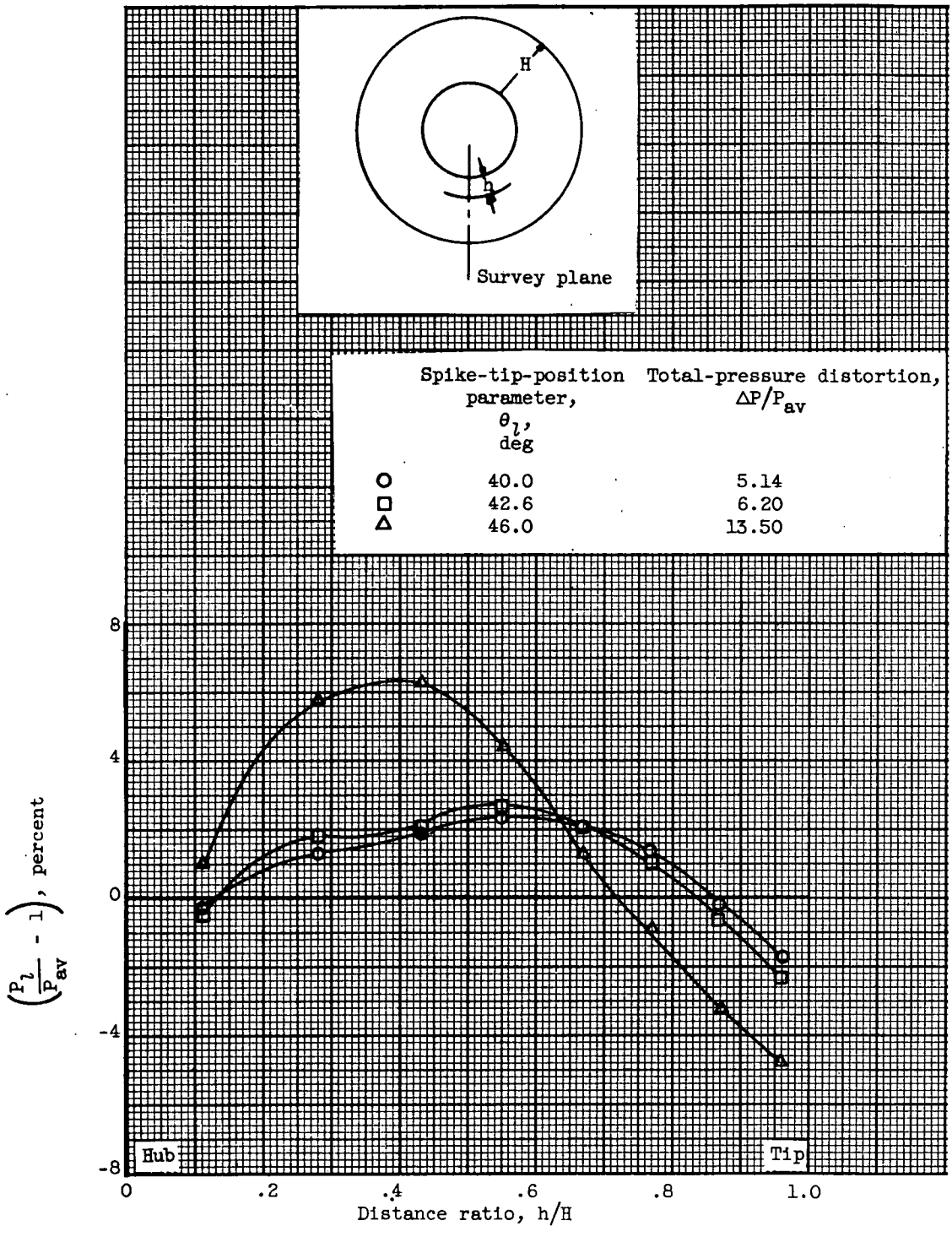
(a) Inlet $C_{17}S_b$; station 7; free-stream Mach number, 2.0; angle of attack, 0°.

Figure 22. - Effect of oblique-shock location on total-pressure profiles.

5007

UNCLASSIFIED

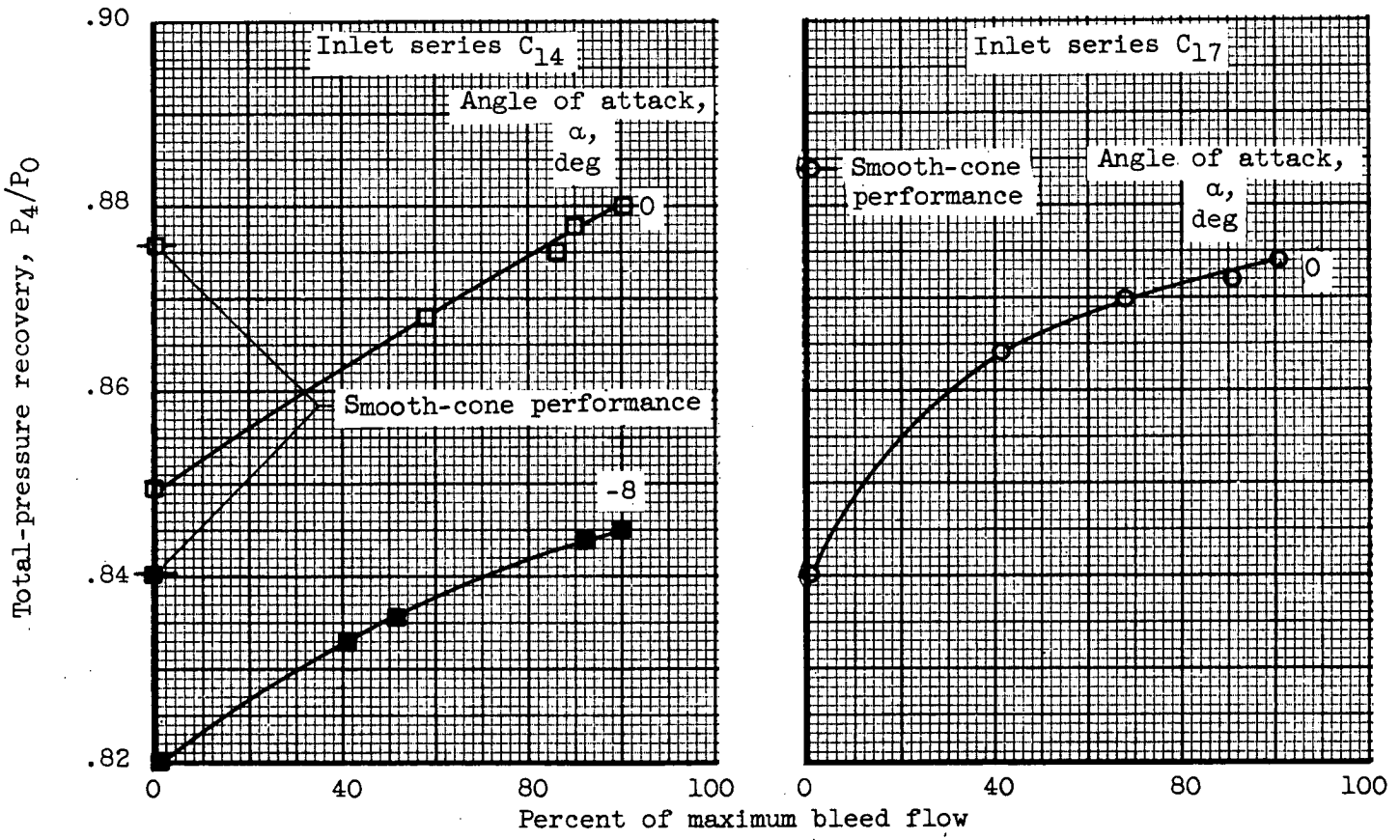
5007



(b) Inlet $C_{17}S_8$; station 58. Free-stream Mach number, 2.0; angle of attack, 0°.

Figure 22. - Concluded. Effect of oblique-shock location on total-pressure profiles.

CONFIDENTIAL



(a) Total-pressure recovery.

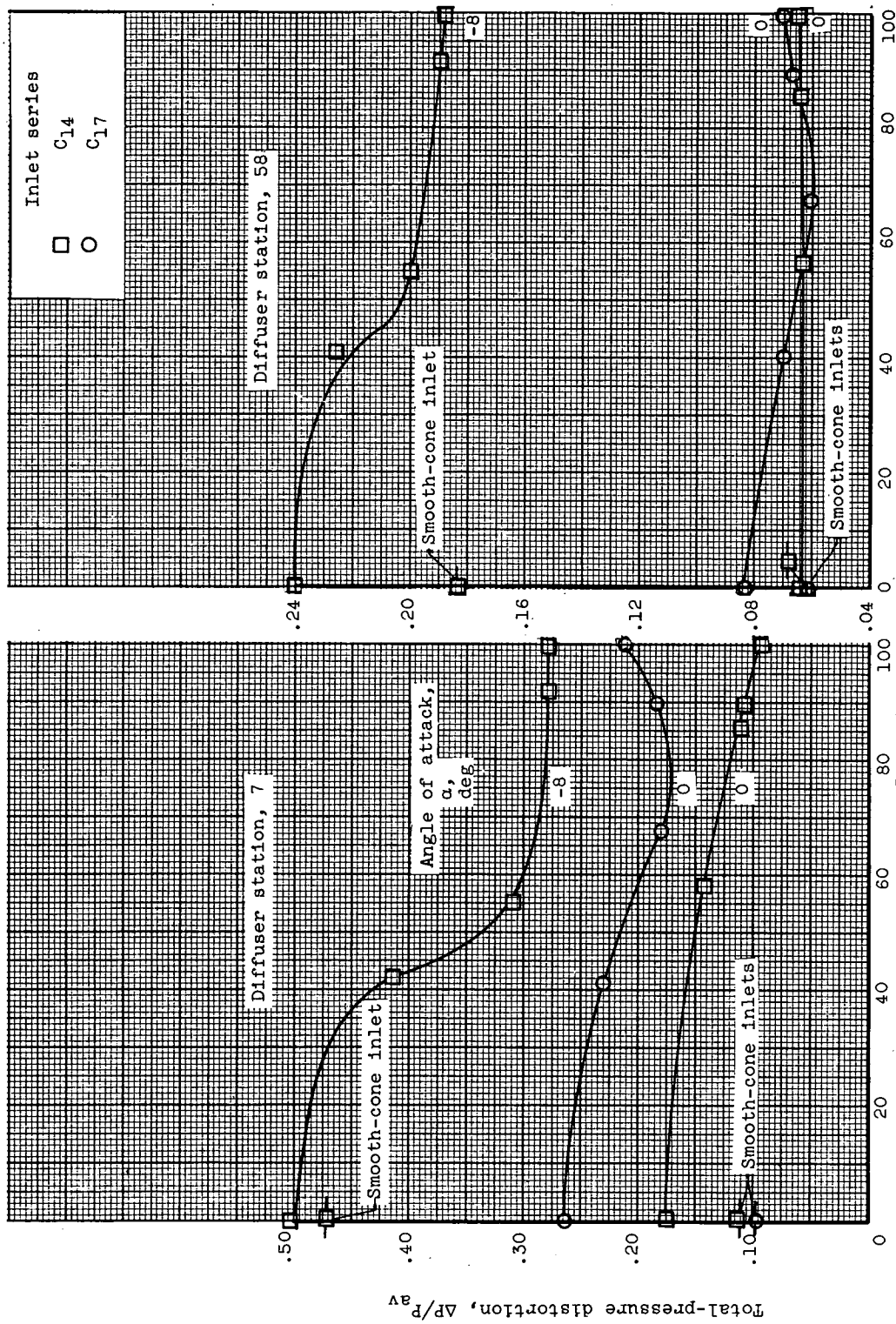
Figure 23. - Effect of bleed at critical inlet operation. Spike-tip-position parameter, 42.6°.

UNCLASSIFIED
CONFIDENTIAL

CONFIDENTIAL

UNCLASSIFIED

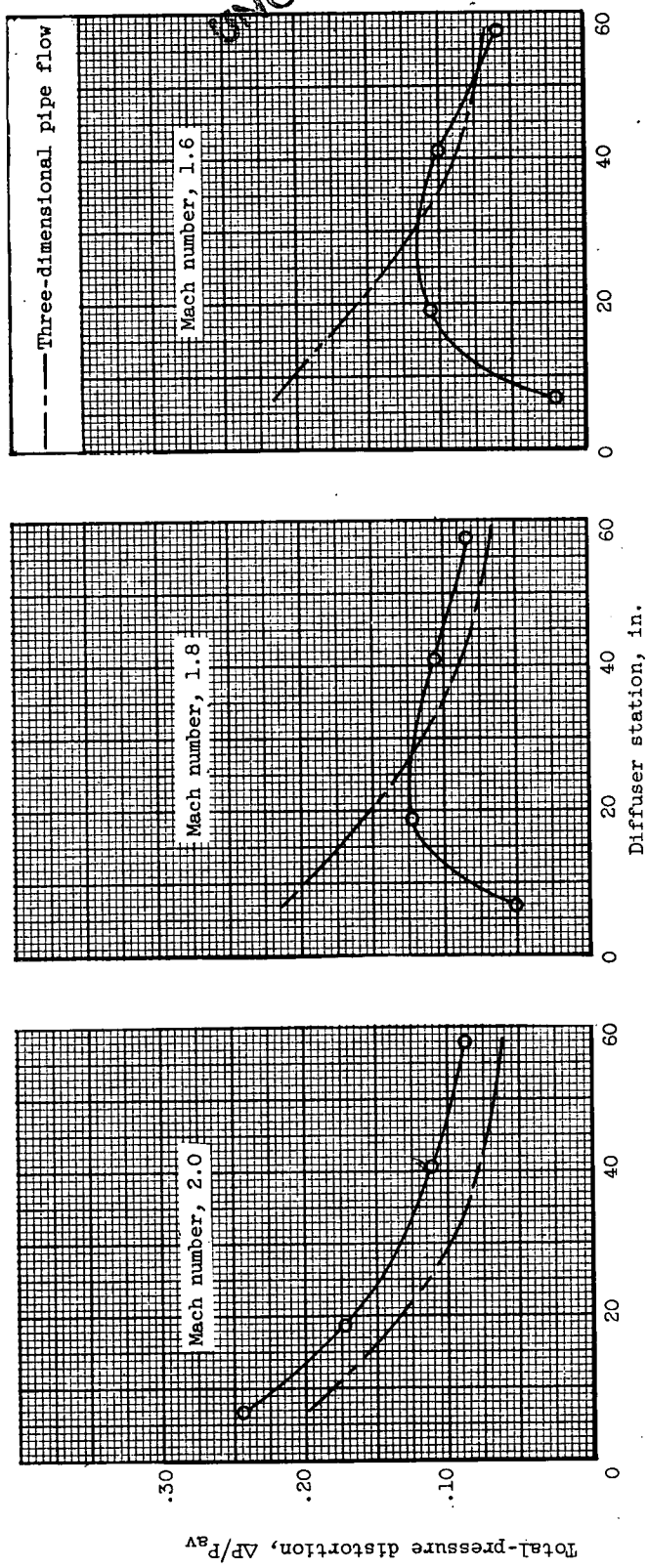
5007



(b) Total-pressure distortion.

Figure 23. - Concluded. Effect of bleed at critical inlet operation. Spike-tip-position parameter, 42.6°.

UNCLASSIFIED

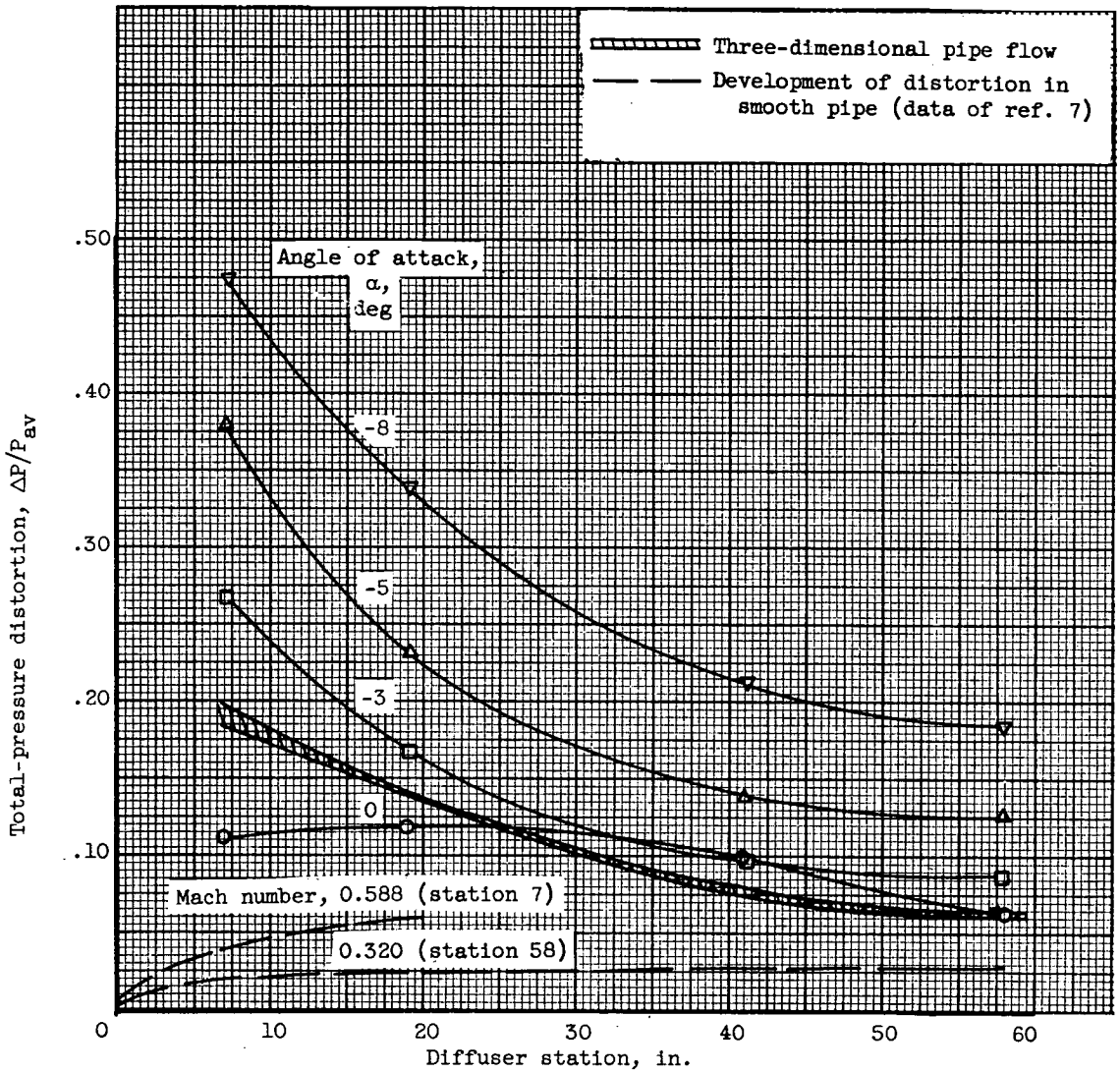


(a) Inlet $C_{14}S_{8,ds}$; angle of attack, 0°; spike-tip-position parameter, 33.8°.

Figure 24. - Mixing in subsonic diffuser.

5007

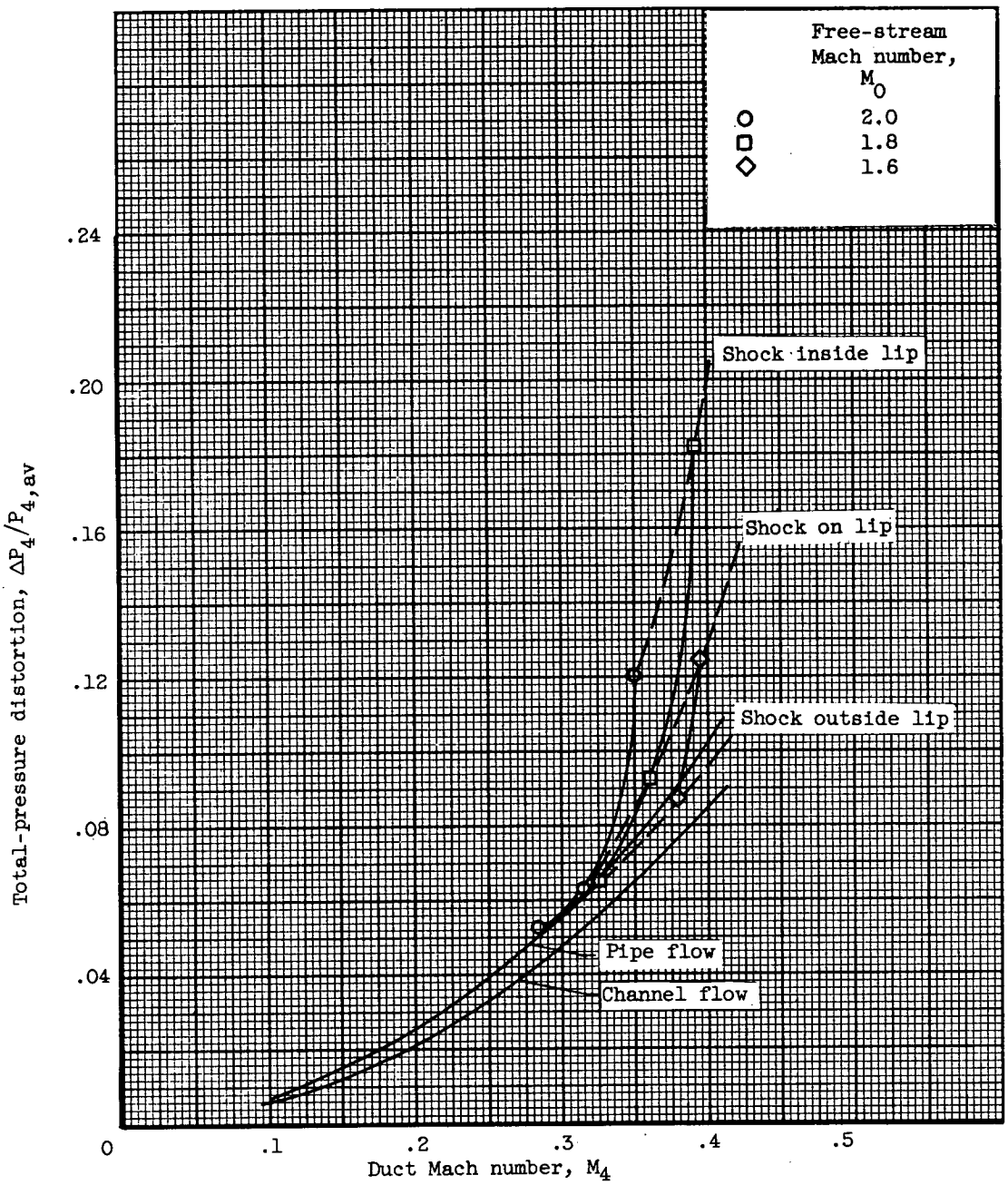
UNCLASSIFIED



(b) Inlet $C_{14}S_8$. Free-station Mach number, 2.0; spike-tip-position parameter, 42.6.

Figure 24. - Concluded. Mixing in subsonic diffuser. 5007

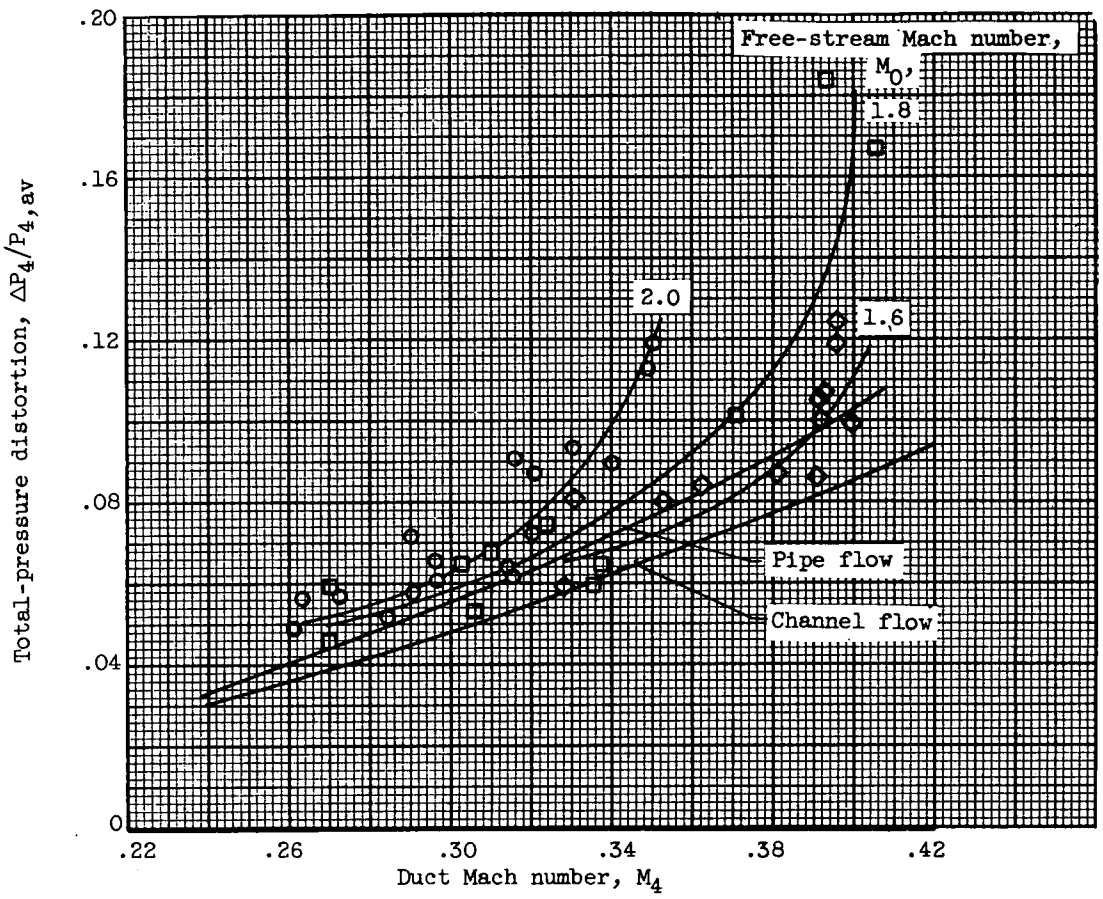
UNCLASSIFIED



(a) Inlet $C_{17}S_8$; angle of attack, 0^o.

Figure 25. - Comparison of exit distortion with fully developed turbulent values.

UNCLASSIFIED



(b) Summary for all configurations.

Figure 25. - Concluded. Comparison of exit distortion with fully developed turbulent values.

NACA - Langley Field, Va.

CONFIDENTIAL
UNCLASSIFIED

RECEIVED
OCT 25 1956
RESEARCH

Classification Changed
To UNCLASSIFIED
By Authority of O.A. #11 Date 12-1-59

CONFIDENTIAL
UNCLASSIFIED